Effect of Carrier Fluid Properties on the Self-Lubricated Flow of Bitumen Froth

by

Mubarak Adedamola Gbadamosi

A thesis submitted in partial fulfillment of the requirements for the degree of

Master of Science

in

Chemical Engineering

Department of Chemical and Materials Engineering

University of Alberta

Abstract

Bitumen froth is produced from mined oil sands using the water-based extraction process. The froth is very viscous and contains roughly 60% bitumen, 30% water, and 10% fine solids (by mass). The mixture of water, fine solids, and dissolved ions in the froth is usually called carrier fluid. The carrier fluid properties vary significantly depending on the process water chemistry and the concentration of fines in the bitumen froth. After extraction, the bitumen froth is transported to treatment and upgrading facilities using the self-lubricated flow technique. The self-lubricated flow occurs due to the migration of some of the carrier fluid in the froth to the high-shear region near the pipe wall. This results in the formation of a thin lubricating water layer around the bitumen-continuous core, thereby lowering the pump energy required to transport the bitumen froth. Despite the strong dependence of self-lubricated flow on the lubricating layer produced by the carrier fluid, there is no information in the literature on how the properties of the carrier fluid impact the flow. Therefore, the objective of this work is to investigate the effect of carrier fluid properties, specifically pH, salt concentration, and fines concentration, on the self-lubricated froth flow.

Previous studies have shown that the parameters affecting self-lubricated froth flow in pipeline transport can be studied using a Couette cell device. This can be achieved by subjecting the bitumen froth to shear inside the Couette cell and measuring the torque exerted by the bitumen-continuous froth on the spindle over time. Using the Couette cell device to study the self-lubricated flow mechanism has numerous advantages; these includes cost-effectiveness, simpler experimental design, and the requirement of smaller froth quantities for conducting experiments. Hence, the parameters affecting the self-lubricated flow mechanism were studied in this work using a Couette cell device. Preliminary experiments were conducted to investigate the effects of

water concentration on self-lubricated flow using a water-in-oil emulsion as a bitumen froth analog. The concentration of the dispersed phase was varied between 10 to 30 wt.%. The results showed that increased water concentration reduces the spindle speed required to produce a self-lubricated flow. At higher water concentrations, more water droplets will be available to form the lubricating layer. This observation is consistent with the previous study conducted by Bello using the same geometry.

The main experiments were conducted using bitumen froth samples. The first phase of the experiments examined the effect of temperature on self-lubricated flow. The tests were conducted at 50, 55, and 60 ℃. The results showed that the increase in temperature increases the shear rate required to maintain a stable self-lubricated flow. This observation can be attributed to the reduction in the viscosity ratio of the continuous phase to the dispersed phase. The result agrees with the experiments conducted by Bello using water-in-oil emulsions as a bitumen froth analog. The second phase of the project was designed to examine the effect of carrier fluid pH, salts concentration, and fines concentration on self-lubricated flow. The salts concentration refers to the concentration of sodium chloride in the carrier fluid. Studies on the effect of carrier fluid pH on self-lubricated flow were performed at pH values of 8.5, 9, 9.5, and 10. Notably, above the pH 9, the shear rate required to produce the self-lubricated flow increased. Further experiments were conducted to examine the effect of carrier fluid NaCl concentration on the self-lubricated froth flow. The tests were performed at 1205 ppm, 2000 ppm, and 3000 ppm. It was observed that above 2000 ppm, a higher spindle speed was required to produce a self-lubricated flow. The increase in the shear rate required to produce a self-lubricated flow with an increase in pH and salt concentration is due to the reduction in bitumen-water interfacial tension. As the interfacial tension decreases, the dispersed droplets in the froth will have lesser resistance to deformation.

Consequently, a high shear rate will be required to facilitate the droplet migration to produce a lubricating layer. The final phase of this project investigated the effects of carrier fluid fines concentration on the self-lubricated flow. The concentration of fines in the carrier fluid was varied between 0 to 6.3 vol.% by adding kaolinite clay. The result shows that the increase in the yield stress of the carrier fluid increases the stability of the self-lubricated flow. This observation can be attributed to the increased resistance of the lubricating water layer against deformation, allowing it to remain stable within the annulus. This is beneficial to minimize bitumen fouling of the pipe wall and reduce friction losses associated with self-lubricated froth transport.

The result from this study shows that self-lubricated flow is strongly dependent on water concentration, spindle speed, temperature, and carrier fluid properties. Future research should focus on studying the effect of carrier fluid properties on the self-lubrication mechanism in pipelines.

To my parents

For their support and sacrifices to ensure that I have a good life

Acknowledgments

I want to express my profound gratitude to Dr. Sean Sanders for his patience, guidance, support, and technical contribution during my program.

I am grateful to Dr. Marcio Machado and Aref Fozooni for their contributions and recommendations while executing this project. I am also thankful to Terry Runyon for her administrative support throughout my project. My heartfelt appreciation goes to Dr. Seun Adedeji for his selflessness and kind support during my program.

I am grateful to the Natural Sciences and Engineering Research Council (NSERC), Syncrude, Suncor, and Canadian Natural Resources for funding my research.

I am thankful for the invaluable support of my parents, Dr. Gbadamosi and Mrs. Gbadamosi. I would like to thank my siblings Saheed Olalekan, Afeeze Olayinka, and Barakat Abimbola for their timely contributions and unwavering kindness.

Finally, I thank the Department of Chemical and Materials Engineering for providing excellent facilities and a conducive learning environment. Many thanks to my friends Muhammed Jamiu, Temitayo Giwa, Yusuf Abul-Razak, Oyinkanola Timileyin, Tasnim Olatoke and Oluyele Adekanye for their timely support. Thanks so much, Khadeejah, for your support and patience during my program.

Table of Contents

List of Tables

List of Figures

List of Symbols

Roman Symbols	Description	Unit
Ca	Capillary number	-
C_f	Fines volume fraction	-
d_{Nl}	Number mean diameter	µm
d_{32}	Sauter mean diameter	µm
L	Length of spindle	mm
M_f	Mass of fines	kg
N	Spindle speed	rpm
R_1	Spindle radius	mm
R_2	Cup radius	mm
t	time	s
T	Torque	Nm
V_{aq}	Volume of aqueous phase	mL
V_w	Volume of water	mL

Greek Symbols	Description	Unit
$\dot{\gamma}$	Shear rate	s^{-1}
µ	Viscosity	Pa. s
μ_d	Dispersed phase viscosity	Pa. s
μ_m	mixture viscosity	Pa. s
μ_o	Continuous phase viscosity	Pa. s
μ_p	Plastic viscosity	Pa. s
ρ_f	Density of fines	kg/m^3
σ	Interfacial tension	N/m
τ_y	Yield stress	Pa
ω	Angular velocity	rad/s

Chapter 1 Introduction

1.1 Background

Oil sands, often referred to as bituminous sands, are a type of unconventional petroleum deposit [1,2]. They consist of a mixture of coarse sand grains, clay, minerals, water, and bitumen [3]. Bitumen is a type of heavy crude oil with high heavy metal concentrations and relatively low hydrogen content [4]. Once extracted, it must undergo extensive treatment to be converted to lighter and more valuable products, such as heating oils, gasoline, diesel, and jet fuels [4,5]. Canada's oil sands resources account for approximately 10% of the world's confirmed oil reserves, positioning it as the third-largest global oil reserve [6,7]. Most of these reserves, about 97%, are in the oil sands deposits in Alberta [7]. Alberta oil sands contain 6−16 wt.%, 1−8wt.% water, and 80−87 wt% mineral matter (silt, sand, and clay) [8].

With the increase in the global demand for petroleum, much attention has been given to exploiting bitumen from oil sand ores [9,10]. The bitumen from oil sands deposits is recovered using two principal methods depending on the deposit characteristics: surface mining or in situ production (e.g., steam-assisted gravity drainage, SAGD) [11]. The choice of production technique is dependent on the depth of the bituminous sands. Surface mining technology is used when the oil sands deposit is close to the surface, while SAGD is used for deeper oil sands deposits [6,12]. The SAGD operation involves drilling wells and injecting steam into the bitumen to reduce its viscosity so that it can be pumped to the surface [4,13].

In the extraction of bitumen from oil sands using the surface mining technique, a water-based extraction process is used to separate the bitumen from the sand particles [14]. Figure 1.1 presents schematically the key steps of the water-based bitumen extraction process. To recover bitumen from oil sands using water-based extraction processes, oil sand ore is mixed with hot water and process aids such as sodium hydroxide to form an oil sand slurry. The dense slurry is conveyed through a hydrotransport pipeline from the mine to the extraction facilities [15]. Afterward, the bitumen is partially separated from other oil sands constituents (clay, sand, and water) in a primary separation vessel [15–17]. The intermediate product obtained from the primary separation vessel is known as bitumen froth.

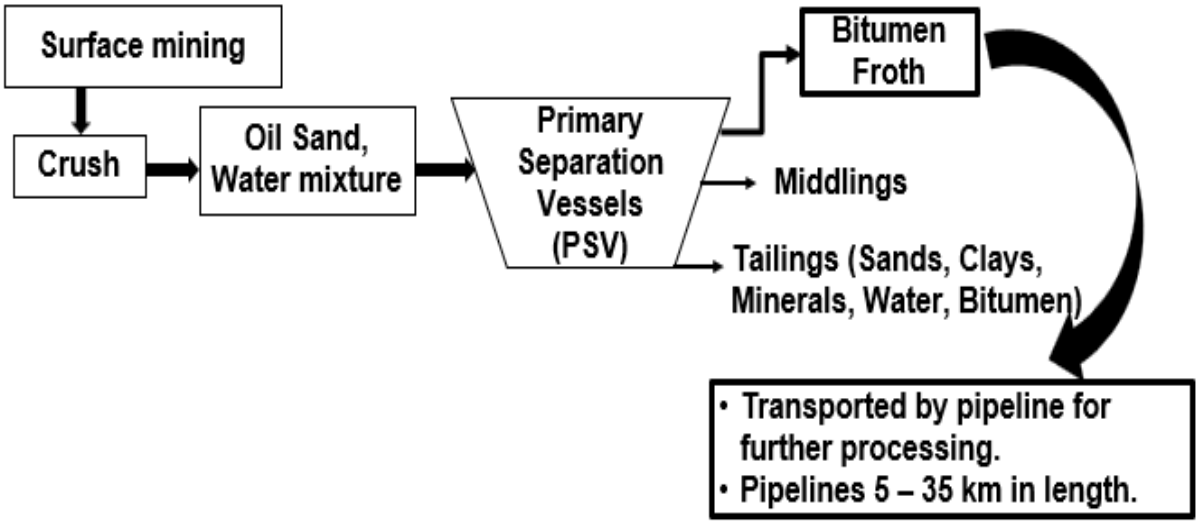

Figure 1.1: Schematic description of the bitumen production process. Adapted from Rao and Liu [2].

The bitumen froth contains about 60 wt.% bitumen, 30 wt.% water, and 10 wt.% solids on average [2,15,18,19]. After the extraction process, the bitumen froth has to be transported to a froth treatment plant through a pipeline. The transportation of the highly viscous bitumen froth over a long distance is a complex operation and remains a major challenge in the oil sands industry [15,17]. Under a wide range of conditions, a specific flow regime, known as Lubricated Pipe Flow (LPF), can be used to transport bitumen froth over a long distance [15,20–25]. The two main types of lubricated pipe flows are self-lubricated flow and core-annular flow. Core annular flow involves the injection of water to lubricate a viscous oil in a pipe flow. The present study is focused on self-lubricated froth flow, also known as Natural Froth Lubricity, which occurs under certain conditions in the pipeline where dispersed water droplets in the bitumen froth migrate to the high shear region near the pipe wall, as shown in Figure 1.2 [17,18]. This results in the formation of a lubricating water layer around the bitumen-continuous froth. Unlike core annular flow, there is no need for the injection of external water in the pipeline for self-lubricated flows. The presence of the water layer near the pipe wall reduces the resistance between the oil and the pipe wall during flow. Consequently, a lower pumping energy is required for the transport compared to the transport of the bitumen alone, or as a water-in-bitumen emulsion [17]. The pipeline friction losses in self-

lubricated froth are orders of magnitude lower than those predicted based on the bitumen viscosity [15].

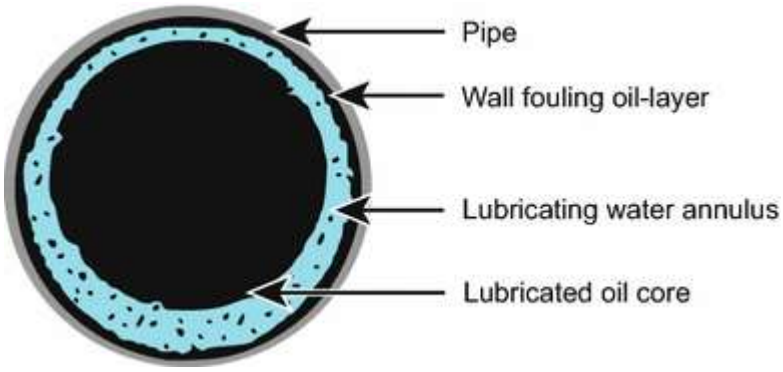

Figure 1.2: Hypothetical representation of lubricated pipe flow [26].

Numerous industrial-scale applications of lubricated pipe flow (LPF) have been reported in the literature since its discovery. For example, Shell operated a 15 cm diameter and 38.9 km long lubricated pipeline for oil transport from the North Midway Sunset near Bakersfield, California, for more than 12 years at flow rates up to 24,000 barrels per day [27,28]. Similarly, Syncrude Canada Ltd currently makes use of self-lubricated flow for the transportation of bitumen froth from the Aurora mine to its froth treatment and upgrading facilities at Mildred Lake, which is a distance of about 35km [29]. At Lake Maracaibo in Venezuela, lubricated pipe flow is used for the transportation of heavy oil from the well clusters to the process facilities [17,24].

Previous studies have shown that the parameters affecting self-lubricated froth flow in pipeline transport can be studied using a Couette cell device. This type of device is used to create a Couette flow, in which a fluid flows between a rotating inner and stationary outer cylinder [30]. The rotation of the inner cylinder creates a shear flow between the cylinders, and the torque exerted by the fluid on the spindle is measured by the device. The onset of self-lubricated flow in Couette flow experiments is characterized by the drastic reduction in the initially high measured torque, which is very similar to the drastic reduction in pressure drop observed in the self-lubricated flow experiments in pipelines [17–19]. This makes it possible to study the self-lubrication mechanism using a Couette cell device. The use of the Couette cell device for studying the self-lubricated flow mechanism has numerous advantages; these include cost-effectiveness, simpler experimental design, and the requirement of smaller froth quantities for conducting experiments.

Bello [17] conducted experiments to investigate some of the factors that influence the mechanism of self-lubrication using a Couette flow device. The tests were conducted by using a water-in-oil emulsion as an analog for bitumen froth. The Author concluded that the ability to produce a self-lubricating flow is strongly dependent on water concentration, temperature, oil viscosity, and spindle speed [17]. However, the experiments conducted by Bello [17] were performed using a water-in-oil emulsion and not a bitumen froth. Further work is required to determine to what extent the Author's observations using an analogous system represent the self-lubricated flow characteristics of bitumen froth. The present work is a continuation of the previous research conducted by Bello [17]. Additionally, the effect of the properties of bitumen froth carrier fluid, which is a water-continuous mixture of dissolved ions and fine particles present in the froth, on the self-lubricated flow phenomenon will be studied. Experiments will be conducted under a broader set of conditions to understand the effects of carrier fluid pH, salts concentration, and fines concentration on the self-lubrication process using a concentric cylinder viscometer.

1.2 Problem Statement

The self-lubricated flow occurs due to the migration of some of the dispersed carrier fluid in the bitumen froth to the high-shear region near the pipe wall. The properties of the carrier fluid vary significantly depending on the process water chemistry and the concentration of fines in the bitumen froth [31,32]. Despite the strong dependence of the self-lubricated flow mechanism on the lubricating layer produced by the carrier fluid, there is no information in the literature on how the properties of the carrier fluid impact the flow. This aspect is very important because the accumulation of electrolytes in the process water due to repeated recycling will significantly impact the bitumen froth interfacial properties and will most likely influence the self-lubricated mechanism. Additionally, bitumen froth contains a significant quantity of fine solids. The increase in the concentration of fines can change the rheological behavior of the carrier fluid from a Newtonian fluid to a non-Newtonian fluid with a yield stress. This will significantly impact the stability of the self-lubricated froth flow because the lubricating water layer will have more resistance to deformation. With increased resistance of the lubricating water layer to deformation, it will be easier to maintain the layer near the pipe wall where it provides the lubricating effect. Consequently, this will prevent contact between the bitumen and the pipe wall and reduce bitumen fouling and friction losses associated with self-lubricated froth transport. To fill this research gap,

this study will extend on the previous work conducted by Bello [17] on the mechanism of self-lubrication. Specifically, this study will examine the effects of carrier fluid pH, salt concentration, and fines concentration on the self-lubricated froth flow phenomenon.

1.3 Research Objectives

This study investigates the effects of carrier fluid properties on self-lubricated froth flow using a Couette cell device.

The main objective of this project is to investigate the effect of the carrier fluid pH, salts concentration, and fines concentration on the self-lubrication of bitumen froth. To achieve this objective, the activities of this study are:

- To prepare a stable and reproducible water-in-oil emulsion using the procedure described by Bello [17].
- To conduct a preliminary set of experiments to examine the effect of water concentration on self-lubricated flow using water-in-oil emulsion as a model bitumen froth.
- To investigate the effect of temperature on self-lubricated froth flow in the Couette cell device and compare the results with those obtained by Bello [17] using a water-in-oil emulsion as a model bitumen froth.
- To investigate the reversibility of the self-lubricated froth flow.
- To develop an experimental procedure to study the effect of pH, salt concentrations, and fines concentration on self-lubricated froth flow.

1.4 Thesis Outline

Chapter 1 of this thesis provides the general background of the bitumen extraction process, the challenges of bitumen froth transport, benefits of lubricated pipe flow and describes some of the most relevant work done by others on self-lubricated flow. It also introduces the areas that need to be further investigated to improve the understanding of self-lubricated froth flow.

Chapter 2 provides a literature review of previous work related to this study that is relevant to the understanding of the present work. The research gaps that are relevant to this work are identified in the chapter.

Chapter 3 describes the experimental method, i.e., the information on the materials, equipment, and procedures followed in order to conduct the experiments.

In Chapter 4, the preliminary experimental results are presented and discussed. This includes results obtained from the calibration tests, emulsion preparation, and experiments conducted to examine the effect of water concentration on self-lubricated flow using water-in-oil emulsion as an analogous froth.

Chapter 5 presents the results of the main set of experiments conducted using bitumen froth. The first part of the chapter describes the tests performed to examine the effect of temperature on self-lubricated froth flow. The second part presents the results obtained from the experiments conducted to investigate the effect of carrier fluid properties (pH, salt concentration, and fines concentration) on the mechanism of self-lubrication of bitumen froth.

Chapter 6 summarizes the conclusions, recommendations, presents the novel contributions of this study, and highlights some industrial implications.

1.5 Author's Contributions

The Author of this work has designed the experimental plan for this project through the technical contributions of Dr. Sean Sanders, Dr. Marcio Machado, and Aref Fozooni. This includes material selection and defining the test conditions. The Author studied the effect of water concentration on self-lubricated flow in a Couette cell and classified the various flow conditions observed in the experiments. The Author also conducted experiments to investigate the effect of temperature and carrier fluid properties (pH, salt concentration, and fines concentration) on the self-lubrication of bitumen froth. The safe work procedures for the emulsion preparation, emulsion microscopy, bitumen froth premixing, and the Couette flow tests were written by the Author. Dr. Sean Sanders, Dr. Marcio Machado, and Aref Fozooni contributed immensely to this project by providing recommendations, reviews, and technical inputs to improve the experiment procedure and experiment plan throughout the course of this project. Their invaluable inputs were used to develop the experimental matrix. The following list provides the details of the contribution of each person involved in this project based on Elsevier Contributor Roles Taxonomy (CRediT) author statement:

- Dr. Sean Sanders (Project Supervisor): project conceptualization, development of experiment matrix, experimental procedure recommendations, review of project methodology and experiment procedure, review of safe work procedure, review of experiment plan, review of thesis structure, review and editing of the thesis, supervision, funding acquisition, resources (laboratory space, materials, and equipment).
- Dr. Marcio Machado (Research associate): Review of safe work procedures for experiments, material coordination, review of experiment plan, thesis review and editing, experimental procedure recommendations (froth heating/mixing), and review of experiment procedures.
- Aref Fozooni (Research assistant): Review of safe work procedures for experiments, review of experiment plan and method, thesis review and editing, software and equipment training, experimental procedure recommendations, and review of experiment procedures.
- Mubarak Gbadamosi (MSc student): Developed safe work procedures, developed experiment plans and methods, material coordination, performed experiments, experimental results analysis, and thesis writing.

Chapter 2 Literature Review

2.1 Introduction

Several methods are currently being used to reduce friction losses and improve the transportation of heavy and extra-heavy oils in pipelines. These include partial upgrading, dilution, heating, and lubricated flow [15,33,34]. In the partial upgrading method, heavy oil is sent to a field refinery, where it is converted to a high-quality and low density product through the removal of carbonaceous solid material (coke) to make the oil more suitable for pipeline transportation [4]. Dilution involves the reduction of the viscosity of heavy oil through the addition of hydrocarbon diluents such as condensates from natural gas production and naphtha [35]. The heating technique requires preheating the crude oil to reduce the viscosity, with subsequent pipeline heating. Each of these methods has merits and deficits that are process specific. For example, the field refinery required for partial upgrading is associated with high investment costs [15,35]. Also, diluent addition requires the construction of twin pipelines and recovery facilities to separate the valuable solvents from the viscous oil. The challenges of the heating method include high capital costs, high energy requirements, and heat losses along the pipelines [15,35].

Lubricated pipelining, however, is different from other techniques and is considered as one of the most effective ways for heavy oil transportation because of its low operating cost [19,22]. This is a type of flow condition in which a water layer lubricates an oil-continuous phase in a pipe flow. This reduces the wall shear stresses, and consequently, the pressure loss in pipeline transportation using this technique is significantly reduced compared to the case where the viscous oil alone is transported as a single phase under the same conditions.

The two most popular methods used to create water lubrication of oils are Core-annular flows (CAF) and Self-lubricating flow (SLF) [17,22]. In core-annular flow, water is injected around the oil continuous phase in a pipe flow to produce a lubricating effect near the pipe wall. In self-lubricated flows, the lubricating water layer is formed through the migration of dispersed water droplets in the oil continuous phase to the high shear region near the pipe wall [15,17,18,36]. In other words, the self-lubricated flow condition does not require the injection of external water to produce the lubricating water layer. This method is applicable for transporting bitumen froth and water-in-oil emulsion in pipelines. The pressure losses using the self-lubricated flow technique are orders of magnitude lower than those obtained in transporting water-in-oil emulsion or bitumen

froth without using this technique. Rushd [22] reported that the pressure drop under the self-lubricated flow condition is comparable to those obtained for the single water phase under the same operating condition. Below the critical velocity, a high-pressure drop was recorded. The critical velocity represents the lowest flow velocity required to produce a self-lubricated flow [15,22]. Figure 2.1 presents the pressure gradient in pipe flow under different flow conditions. The result shows that once the critical flow velocity is attained, the water droplets in the water-in-bitumen emulsion migrate near the pipe wall and produce a lubricating effect that reduces the friction between the bitumen-continuous phase and the wall. Consequently, the pressure gradient is significantly reduced. This result demonstrates how the flow parameters impact the self-lubricated flow phenomenon. Additionally, it shows that water-in-oil emulsion is a good model system for studying the flow parameters affecting self-lubricated pipeline transport of bitumen froth.

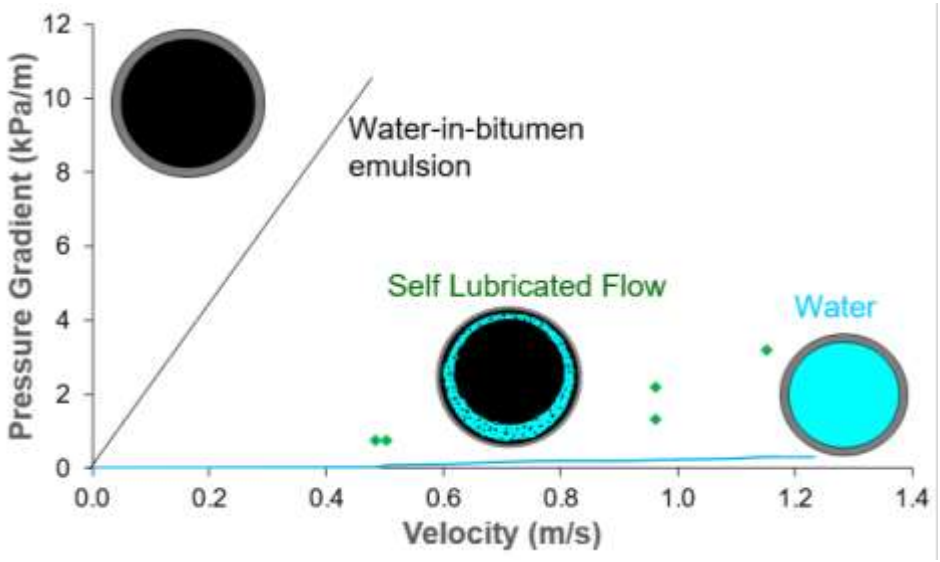

Figure 2.1: Pressure drop in pipe flow under different flow conditions.[22]

2.2 Bitumen Froth Carrier Fluid

The carrier fluid is a mixture of process water, dissolved ions, and fine solids [31,32]. About 50% of the solids are predominantly fines, which are particles smaller than 44 µm [37]. They are hydrophilic and usually found in the dispersed water present in the bitumen froth after the extraction process. Joseph et al. [18] confirmed the presence of a milky water layer during the self-

lubricated flow tests conducted in a pipe flow loop. They ascribed the milky color of the water to the presence of colloidal clay particles. However, they did not provide any information on how the concentration of fines in the carrier fluid could impact the self-lubricated flow mechanism. The increase in the concentration of fines in the bitumen froth can alter the rheological behavior of the carrier fluid from a Newtonian fluid to a non-Newtonian fluid with a yield stress. This is because, at high concentrations, the clay particle interaction would increase, requiring a higher force to break down. While Newtonian fluids deform easily when subjected to shear, yield stress fluids are more stable against deformation [38]. Allouche et al. [39] modelled the instability mechanism of the displacement of Bingham yield stress fluid by a low-viscosity Newtonian fluid using direct numerical simulations. The authors predicted a lower film thickness for the Newtonian fluid compared to the non-Newtonian fluid. Consequently, the yield stress fluid was more stable against deformation. These findings show that the rheological properties of the carrier fluid in the annulus will significantly impact self-lubricated froth flow. Specifically, an increase in the concentration of fines in the carrier fluid will increase its yield stress and resistance to deformation due to hydrodynamic forces. Consequently, a more stable self-lubricated flow will be produced. In pipe flow, a stable self-lubricated flow is one in which the water droplets in the lubricating layer are stable against deformation and maintain their position in the high shear region, thus effectively lubricating the oil core. This will minimize the contact between the bitumen continuous core and the pipe wall [22].

Process water chemistry strongly influences the bitumen carrier fluid properties [4,32]. Smith [31] conducted Ion chromatography tests on different samples of carrier fluid to determine their water chemistry. The Author reported a significant variation in the pH of the carrier fluid samples, ranging between 8.5 and 9.5. This observed variation can be attributed to differing ore types and chemical additive dosages [40]. Rocha et al. [41] reported that oil sands extraction process water has a significantly high salt concentration. Salt concentrations up to 3000 ppm have been reported in industrial process water [42,43]. It is therefore desirable to understand how the change in the properties of the carrier fluid associated with the water chemistry and fines concentration can impact the self-lubricated froth flow.

2.3 Effect of Carrier Fluid Properties on Self-Lubricated Flow

Bitumen froth consists of a bitumen continuous phase comprising approximately 60 wt.%, with a dispersed water phase comprising about 30 wt.% water and 10 wt.% solids. This means that the bitumen froth is predominantly a water-in-oil emulsion. Previous studies have shown that water-in-oil emulsions can be used as an analog to understand the factors affecting self-lubricated froth flow [17,20,44]. However, the effect of interfacial properties on the self-lubricated flow mechanism has generally been ignored. Relevant studies on how the carrier fluid properties can influence the self-lubricated froth flow phenomenon will be discussed. Specifically, the possible impacts of pH, salt concentration, and fines concentration will be discussed.

Wang et al. [45] investigated the effects of pH on bitumen-water interfacial tension. In their experiments, sodium hydroxide was used to vary the pH of the aqueous phase between the range of 4-12 [45]. Above pH 8.5, they noted a significant reduction in bitumen-water interfacial tension. Their observation was attributed to the migration of surface-active components from the bulk bitumen phase to the bitumen-water interface [45]. The migration is such that the hydrophilic head moves to the aqueous phase while the hydrophobic tail stays in the bitumen phase [4]. Thus, an increase in the pH of the aqueous phase facilitates the ionization of the carboxylic group (-COOH) of the surface-active molecules to carboxylate (-COO-), thereby decreasing the bitumen-water interfacial tension [45]. A similar observation was made in the studies conducted by Poteau et al. [46] and Kelesogle et al. [47]. The authors noted that the migration of natural surfactants to the water/oil interface and the reduction in interfacial tension strongly depend on the pH of the aqueous phase. These studies highlight the possible effect of carrier fluid pH on the bitumen froth interfacial properties, which have generally been ignored in self-lubricated froth flow experiments. This is important because the recycled process water used in bitumen production usually contains a significant concentration of dissolved ions, and, as mentioned earlier, the pH can vary from 8.5 to 9.5 [31]. Wang et al. [37] observed a significant reduction in the bitumen-water interfacial tension within this pH range. Based on this understanding of interfacial properties of the water-in-oil emulsion, the change in carrier fluid pH will most likely have a significant impact on the self-lubricated flow because of the alteration in the interfacial properties of the bitumen froth.

Bello [17] conducted some experiments to investigate the reversibility of self-lubricated flow in a concentric cylinder viscometer using water-in-oil emulsion as a model bitumen froth. This

was done by gradually increasing the spindle speed until the self-lubricated flow is produced, then decreasing the spindle speed stepwise. The Author noted that the critical spindle speed remains unchanged under both conditions. The critical spindle speed is the lowest spindle speed required to produce a self-lubricated flow. Additionally, Bello visually observed the migration of some elongated droplets during the shearing experiments. Under the self-lubricating flow condition, there was a continuous layer of elongated droplets orbiting around the spindle, while very few droplets were observed for the non-lubricating flow condition [17]. Bello's findings suggest that the self-lubricated flow is predominantly driven by droplet migration rather than the coalescence of the dispersed droplets to form a continuous layer, as previously reported by Joseph et al. [18]. Bello, however, did not examine how the oil-water interfacial properties impact droplet migration to produce the lubricating layer.

Dispersed droplets in emulsions often have a spherical shape. Generally, spherically shaped droplets have more resistance to hydrodynamic forces compared to deformed droplets [48]. The understanding of droplet resistance to deformation can be used to explain how the interfacial properties could impact droplet migration in bitumen froth. The reduction in the interfacial tension will reduce the thickness of the interfacial film and make the dispersed droplets in the bitumen froth less rigid or spherical. Consequently, the droplets will have less resistance to deformation by hydrodynamic forces and require a higher shear rate to facilitate their migration to form the lubricating water layer. This would significantly affect the free water fraction released from the froth to produce the lubricating layer. The free water is the percentage of water present in the bitumen froth released to form the lubricating water layer [15]. Sanders et al. [15] reported a drastic increase in pressure gradient when the free water fraction was reduced in their pipe flow experiments. Hence, the increase in carrier fluid pH will likely increase the droplet deformation and reduce the free water fraction released to form the lubricating layer. In addition to the impact of interfacial tension on droplet migration to form the lubricating layer, a low bitumen-water interfacial tension will also impact the stability of the self-lubricated flow. In pipe flow, a stable self-lubricated flow is one in which the water droplets in the lubricating layer are stable against deformation and maintain their position in the high shear region, thus effectively lubricating the oil core. At a sufficiently low interfacial tension, some of the droplets in the lubricating layer can be reabsorbed by the bitumen-continuous core, leading to an unstable self-lubricated flow. This

condition is undesirable in operating a self-lubricated pipeline because it increases contact between the bitumen and the pipe wall, thereby increasing wall fouling and frictional pressure loss.

Rocha et al. [41] investigated the effect of salt concentration on bitumen-water interfacial tension. The concentration of salt in the aqueous phase was adjusted from 0 to 10,000 ppm using NaCl. They reported a direct relationship between the increase in salt concentration and a reduction in the bitumen-water interfacial tension. They also observed a significant increase in water-oil-emulsion stability at 2000 ppm salt concentration. The observation was attributed to the increase in the mass coverage of asphaltenes. Asphaltenes act like weak ionic surfactants; thus, the salt concentration increase will facilitate the ionization of the polar group in the bitumen, thereby reducing the bitumen-water interfacial tension [41]. A similar observation was made in the studies conducted by Amal et al. [49]. Although the studies of Rocha et al. and Amal et al. [49] were performed using water-in-oil emulsions, their findings highlight how the salt concentration in the carrier fluid could affect the interfacial properties of the bitumen froth and influence the self-lubricated flow phenomenon. As discussed earlier in this section, a decreased bitumen-water interfacial tension will reduce the resistance of the droplets to deformation. Consequently, an increase in salt concentration will likely increase the flow velocity or spindle speed required to produce a stable self-lubricated flow.

As mentioned earlier, bitumen froth contains roughly 10 wt.% solids [4]. About 50% of the solids are predominantly fines [37], i.e., solid particles smaller than 44μm. The fines, usually hydrophilic, are mostly found in the dispersed water present in the bitumen froth after the extraction process. Despite the presence of fine particles in the bitumen froth, their contribution towards the self-lubricating flow phenomenon has always been ignored in the literature. The increase in the concentration of fines in the bitumen froth can be expected to produce a yield stress in the carrier fluid, which will likely impact the self-lubricated flow mechanism. Gabard and Hulin [50] experimentally investigated the displacement of Newtonian and yield stress fluids. They noted that the yield stress fluids are more hydrodynamically stable compared to the Newtonian fluids. A similar observation was made in the study conducted by Zare et al. [38]. Their findings demonstrate that the increase in the yield stress of the carrier fluid will increase the resistance of the dispersed droplets to deformation. Consequently, a lower flow velocity should be required to facilitate the migration of the droplets to produce a self-lubricated flow. Additionally, the lubricating layer produced will be more stable against deformation, making it easier for the

droplets to remain stationary in the region near the pipe wall. This is beneficial to minimize bitumen fouling of the pipe wall and reduce friction losses associated with self-lubricated froth transport.

2.4 Self-Lubricated Flow Test Geometries

2.4.1 Pipe Flow

As previously discussed, bitumen froth is usually transported through a pipeline from the extraction site to the froth treatment plant using the self-lubricated flow technique. Researchers commonly use pipe flows to examine the factors affecting the self-lubricated froth flow [15,18]. This involves pumping bitumen froth in a flow loop at different conditions and observing the pressure drop [15,18,22]. The pipe flow experiments are very valuable, as they provide important information that is directly applicable to industrial applications. A critical prerequisite to producing a self-lubricated flow in pipe flow experiments is that the flow velocity must be sufficient to allow the dispersed water droplets to form the lubricating water layer. This criterion is similar to the condition necessary to produce a self-lubricated flow in Couette flow tests, where the spindle speed must be sufficient to facilitate the migration of the droplets to form a lubricating layer. Additionally, the drastic reduction in pressure gradient attributed to the self-lubrication mechanism in pipe flow experiments is very similar to the drastic decrease in the measured torque in the Couette flow tests when self-lubricated flow is produced [17,18]. Both effects are due to the migration of dispersed droplets to form a lubricating water layer near the high-shear region. The similarities in flow behavior of the two geometries highlight that the Couette flow device can be used to study the parameters affecting the self-lubricated froth flow in pipelines.

2.4.2 Couette Flow Device

Concentric cylinder viscometers are often used to determine the viscosity of single-phase fluids like oil and water or the rheology of more complex multiphase systems such as suspension. In this device, the fluid sample is sheared in the gap between two concentric cylinders. The shear rate is controlled by adjusting the rotating speed of the inner cylinder. The schematic of the geometry of the concentric viscometer used for this work is shown in Figure 2.2. Here, R_2 and R_1 are the radii of the cup and the spindle, respectively. T is the torque, L is the length of the spindle, and ω is the angular velocity.

Bello [17] developed an experimental procedure to investigate some of the factors affecting self-lubricated flow in the Couette apparatus. The Author concluded that the factors affecting self-lubricated flow in pipelines can be investigated using the Couette flow device. Hence, the VT 550 viscometer will be used to conduct experiments to investigate some of the factors affecting self-lubricated froth flow in this study.

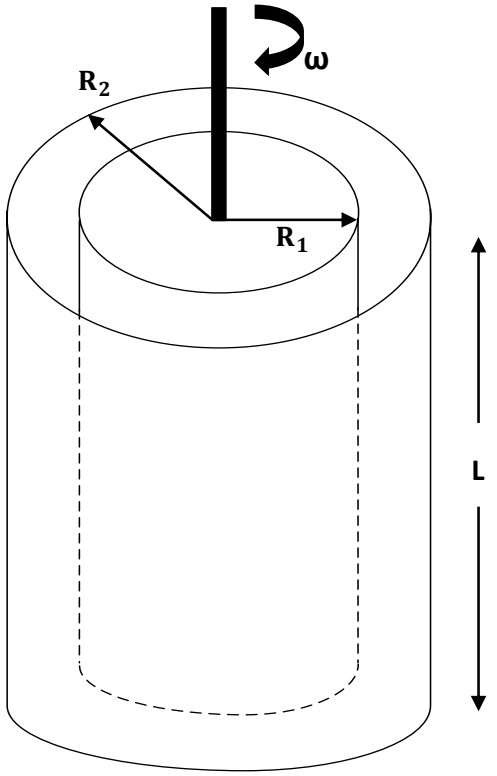

Figure 2.2: Schematic illustration of the concentric cylinders of a Couette flow viscometer.

2.5 Factors Affecting Self-Lubricated Flow

Numerous studies have been conducted to understand the mechanism of self-lubricated flow both in a pipe flow loop and in a concentric cylinder device [15,17,18,22]. Joseph et al. [18] studied the self-lubricated froth flow in pipelines of different diameters (25, 50, and 600 mm). The froth was recirculated in the flow loops at different flow velocities. It was observed that the measured pressure gradients of the froth are orders of magnitude lower than would be predicted based on the viscosity of the froth. The authors concluded that the self-lubrication mechanism depends on flow velocity and water concentration [18]. However, the Authors did not provide any information

about the properties of the bitumen froth carrier fluid used in their experiments. Joseph [51] highlighted some of the criteria that are critical to the self-lubricated flow phenomenon; for example, that the dispersed water droplets will migrate to the wall if the oil-continuous core viscosity is greater than 500 mPa.s. The Author also noted that drag reductions of the order of the viscosity ratio are possible when the oil-water viscosity ratio is equal to 10^5. Sanders et al. [15] conducted further experiments on self-lubricated froth flow in a 25 mm diameter pipeline. They examined the relationship between the free water content and the total concentration of water in the froth, and also studied the effect of water concentration on friction losses. The Authors reported a direct relationship between the free water content and pressure gradient. The increase in free water fraction decreased the pressure gradient significantly. However, the Authors did not provide information on how the properties of the carrier fluid impact the fraction of water present in the froth released to form the lubricating water layer.

Rushd [22] investigated the hydrodynamic effects produced by the wall fouling layer on the frictional pressure losses using a 25.4 mm flow loop. The fouling layer is a coating film of viscous oil formed due to the contact between the oil-continuous phase and the pipe wall during transportation [29]. It was observed that the frictional pressure losses in a fouled pipe are significantly higher than those obtained in an unfouled pipe under a similar condition [22]. This observation was attributed primarily to the roughness of the fouling layer. Rushd developed a new model for the prediction of pressure losses considering the impact of the fouling layer. The model considers the contributions of reduction in the pipe flow area due to wall fouling and the hydrodynamic roughness produced by the fouling layer. These findings provide valuable insights to improve the design of pipeline systems for lubricated pipe flows to consider the contribution of the viscous-coating layer. However, Rushd's experiments were not conducted using a bitumen froth. Both the experimental studies and numerical approach did not consider the impact of the oil-water interfacial properties and fine solids on the pressure losses. Hence, further work is required to understand how the properties of the dispersed phase could impact the wall fouling and self-lubricated flow stability. This is important because a more stable lubricating water layer will reduce the wall fouling produced through frequent contact between the bitumen continuous core and the pipe wall. Bannwart [52] investigated how interfacial tension impacts the stability of the oil-water core-annular flow. The Author concluded that a high interfacial tension is favorable to

maintaining a core-annular flow configuration. This observation demonstrates that the oil-water interfacial tension will significantly impact the self-lubricated froth flow.

In a separate study, Bello [17] conducted experiments to investigate some of the factors that influence the mechanism of self-lubrication using a Couette flow device. The experiments were conducted using a water-in-oil emulsion as a model bitumen froth. The experiment involves pouring the samples inside the viscometer cup and shearing it by gradually increasing the spindle speed until a self-lubricated flow is attained. The onset of self-lubricated flow in the Couette flow experiment is characterized by a drastic reduction in the initially observed high torque. The drastic reduction in the initially high torque is very similar to the drastic reduction in pressure drop observed in the bitumen froth self-lubricated flow experiments conducted in the pipeline [17,18,22]. These similarities show that the critical spindle speed required to produce a self-lubricated flow in a Couette cell is analogous to the flow velocity required to produce a self-lubricated flow in a pipeline.

Bello concluded that the critical spindle speed required to attain self-lubrication decreases with the increase in water concentration. The result demonstrates that increased water concentration will reduce the flow velocity required to produce a self-lubricated flow in a pipeline because more water droplets will be available to form the lubricating water layer. Bello also noted that the increase in temperature increases the spindle speed required to achieve a self-lubricated flow. This observation was ascribed to the reduction in the oil-water viscosity ratio when the temperature is increased. This observation is consistent with the result obtained in studies conducted by Rhoheth [53]. The Author noted that a high oil-water viscosity ratio is desirable to maintain a core-annular flow configuration in a pipe flow.

The findings of Bello [17] provide a valuable contribution to establishing the possibility of conducting self-lubricated flow experiments in a concentric cylinder viscometer and comparing the observations to the self-lubricated flow characteristics in pipelines. However, the experiments conducted by Bello [17] were performed using a water-in-oil emulsion and not a bitumen froth. Further work is required to determine to what extent Bello's observations using an analogous system represent the self-lubricated flow characteristics of bitumen froth. This work builds on the previous experiment conducted by Bello [17] to further investigate the conditions required to produce a self-lubricated froth flow. From the experiments conducted by Bello, a stable self-

lubricated flow is one in which, once the lubricating water layer is formed, there is no significant fluctuation in the corresponding low torque associated with the flow. In other words, the droplets migrate to form the lubricating layer, maintain their position, and are not reabsorbed by the oil core. A stable self-lubricated flow would reduce the pressure losses associated with operating a self-lubricated pipline.

2.6 Summary

The findings of the previous studies established a connection between the experiments conducted in pipe flow and Couette flow devices and highlighted that water-in-oil emulsions can be used as a model system to study the self-lubricating flow of bitumen froth. Some of the conditions that are crucial for the formation of lubricated flow have also been identified. The self-lubricating flow regime is found to be strongly dependent on water concentration, flow velocity, temperature, and continuous phase viscosity [15,22,54].

The literature review conducted for this study highlights some of the areas that need further investigation:

- The previous study conducted to investigate the factors affecting the self-lubricated flow in a Couette cell was conducted using an analogous water-in-oil emulsion rather than an actual bitumen froth.
- The effect of carrier fluid properties (salt concentration, fines concentration, and pH) has been ignored in self-lubricated flow experiments. There has been no attempt to understand how these factors contribute to the formation and stability of self-lubricated froth flow.

2.7 Project Objectives and Hypotheses

2.7.1 Project Objectives

The objective of this project is to study the effect of carrier fluid properties (salt concentration, fines concentration, and pH on the mechanism of self-lubrication of bitumen froth.

To achieve this objective, the activities of this study are:

- To conduct a preliminary experiment to examine the effect of water concentration on self-lubricated flow using the procedure described by Bello [17].

- To examine the effect of temperature on self-lubricated froth flow using the couette flow device.
- To investigate the effect of carrier fluid properties (pH, salt concentration, and fines concentration) on the stability of bitumen froth self-lubricated flow.
- To investigate the reversibility of the self-lubricated froth flow.
- To characterize the self-lubrication flow phenomenon using a dimensionless number.

2.7.2 Hypotheses

The hypotheses of this project are as follows:

- It is known that an increase in pH reduces bitumen-water interfacial tension [55]. It is expected, therefore, that an increase in carrier fluid pH will reduce the rigidity of the droplets and the stability of the lubricating layer. Consequently, a higher spindle speed or pipeline velocity will be required to produce a self-lubricated flow.
- It is known that an increase in salt concentration decreases the bitumen-water interfacial tension [41]. It is expected, therefore, that an increase in carrier fluid salt concentration will make the droplets easily deformable and increase the shear conditions required to produce self-lubricated flow.
- The increase in the concentration of fines in the carrier fluid will increase its yield stress and enhance the stability of the self-lubricated flow, meaning that self-lubricated flow should occur at lower spindle speeds or pipeline velocities.
- It is expected that the self-lubricated froth flow will exhibit reversibility. This is because below the critical speed, the droplets will not be able to overcome the hydrodynamic forces, resulting in the loss of the self-lubricated flow regime.

Chapter 3 Methodology

3.1 Materials

This section provides a detailed description of the materials used for conducting the experiments.

Model Oil

Meropa 460 oil (Model #: 277213) procured from Chris Page and Associates was used in conducting all the preliminary experiments as the model oil. The oil has a kinematic viscosity of 460 mm^2/s at 40 ℃. The density of the model oil measured at 25 ℃ using the pycnometer is 892.4 kg/m^3. The density was obtained according to the methodology described in Section 3.4.1.

Bitumen Froth

The main experiments were conducted using bitumen froth collected from Suncor Canada. Two froth samples were used for the main experiments. The first sample contains 77 wt% bitumen and 23 wt% water, according to the Karl Fisher test. The concentration of solids in the sample was not measured. This sample was used for the experiment to study the effect of temperature on self-lubricated flow and will be referred to as Bitumen froth A. The second sample contains 69% bitumen, 25% water, and 6% solids by mass, according to Dean Stark's Analysis. This sample was used to conduct experiments to study the effect of carrier fluid on self-lubrication. Additional water was added to the froth to increase the water concentration to 30 wt.% to adjust the properties of the carrier fluid. The second sample will be referred to as Bitumen froth B.

Deionized Water

All the emulsions prepared in this work were prepared using the deionized water produced from the Elix Advantage 5 Water Purification System.

Kaolin

The Kaolin used in the work was procured from Plainsman Pottery, Edmonton, Canada. The average particle diameter of the kaolinite clay is around 1 – 1.2 microns, and the density is about 2696 $kg/m^{3,}$ according to Saskatchewan Research Council (SRC) database [56]. The Kaolin was used to examine the effect of fines concentration on bitumen froth lubrication.

3.2 Equipment

Homogenizer and Probe

The VWR 250 homogenizer was used for the preparation of water-in-oil emulsion. It has a speed range of 10,000 – 30,000 RPM. The VWR Saw- Tooth probe with dimensions, 11.5 x 1 cm was selected for the entire mixing process.

Microscope

All the photomicrographs of the emulsion droplets were obtained using the ZEISS Axioscope-40 Microscope. The 10X objective lens was used to view the emulsion droplets and capture the photomicrographs. The sample images were further processed using MATLAB code script to obtain the droplet size distribution. This MATLAB code is provided in Appendix D.

Concentric Cylinder Viscometer

All the lubricating flow experiments in this work were conducted with the concentric cylinder viscometer (HAAKE VT550, Thermo Fisher Scientific, Waltham, MA, USA). The viscometer was also used for the rheology measurement of the Meropa 460 oil, bitumen froth, and concentrated kaolin suspension. The operating temperature of the viscometer was adjusted with the temperature control unit. This was achieved by pouring deionized water into the water bath and allowing it to circulate inside the temperature control vessel. The specification of the viscometer is provided in Table 3.1.

Table 3.1: VT550 viscometer technical specifications

Sensor System	**MV1**	**MV2**	**MV3**
Rotor R_i (mm)	20.04	18.4	15.2
Cup R_0 (mm)	21.0	21.0	21.0
Height L (mm)	60.0	60.0	60.0
Gap width (mm)	0.96	2.6	5.8
Sample volume V (cm^3)	34	46	66
Maximum Torque (Nm)	0.03		

Rheometer

The rheological measurements of the low-concentration kaolin suspension (up to 8 vol% fines concentration) were performed with the ARG2 rheometer. The spindle speed was controlled, and the torque response was measured by the equipment. The Aluminium DIN spindle was used for all the tests conducted. The rheometer has a torque range of 0.1 mNm - 200 mNm and a resolution of 0.1 nNm. The temperature of the device is controlled by re-circulating deionized water inside the fluid bath. The specification of this measuring device is given in Table 3.2.

Table 3.2: AR-G2 rheometer technical specifications

System sensor	**Aluminium DIN**
Cup diameter(mm)	30.40
Spindle diameter(mm)	28.00
Rotor length(mm)	40.03
Operating gap(mm)	0.010
Sample size(mL)	22.42

Ethylene Glycol Temperature Bath

The preheating of the bitumen froth was done inside the ethylene glycol (ETG) bath. The froth is usually heated to 70 ℃ inside the bath.

Electric Mixer

The IKA RW-20 overhead stirrer was used for the froth premixing. The Bitumen froth used for the shearing experiments was poured inside 1L aluminum cans. The froth is usually kept in the fume hood a day before the experiment is conducted to allow the sample to prewarm to room temperature. The 45° Pitched blade impeller with a 6 cm diameter is attached to the mixer after heating the froth to 70 ℃. The froth was mixed at a speed of 1000 rpm for 15 minutes.

Other Equipment

The other equipment used for the experiments conducted in this work include:

- **Magnetic stirrer:** The IKA RCT stirrer was used to prepare the additional aqueous phase by mixing the additives with deionized water inside the beaker using the magnetic stir bar.
- **pH Meter:** Mettler Toledo Seven Multi system pH-meter was used for the measurement of pH during the experiments.
- **Microscope slides and coverslips:** Emulsion droplets were placed on Fisherbrand microscope slides (25mm x 75mm x 1mm) and covered with coverslips (24mm x 50mm x 0.13mm) before placing the samples under the microscope.
- **Mass Scale:** FX 3000 Electronic balance (0.01 grams accuracy) was used to measure the Di-water, oil, and fines used during the experiments.
- **Pipette:** A 3 ml Cole-Parmer plastic pipette was used to slowly add water to the Meropa oil during the emulsion preparation.
- **Digital thermometer:** The Fisherbrand thermometer was used to measure the froth temperature at intervals during the froth preheating procedure.
- **Burrete:** 25 mL Eisco Glass Burette was used for the titration analysis to adjust the overall pH of the bitumen froth carrier fluid.

3.3 Oil Characterization

3.3.1 Density Measurement

The density of the Meropa oil was determined with the use of a pycnometer. The procedure used in the experiment consists of the following steps:

1. Measure the mass of an empty pycnometer using the weighing scale.
2. Fill the pycnometer with water and close it with the cap. Measure the mass of the pycnometer and the water.
3. Calculate the volume of water required to fill the pycnometer using the mass of water in Step 2 and the reference density of water at 25 ℃ using

$$\rho = \frac{m}{V} \tag{3.1}$$

Where m is the mass of the water, ρ is the density of water, and V is the volume of the fluid in the pycnometer.

4. Turn on the water bath and set it to the desired temperature (25 ℃ and 40 ℃).
5. Pour 100 mL water inside a glass jar and place the glass jar inside the water bath. Use a thermometer to check the sample temperature at intervals until the desired temperature is reached.
6. Remove the glass jar from the water bath and fill the pycnometer with the preheated water.
7. Measure the total mass of the pycnometer and the water using the weighing scale.
8. Determine the mass of water by subtracting the total mass from the mass of the pycnometer measured in step (1).
9. Determine the density of the water at the selected temperature by dividing the mass of water in the pycnometer by the volume of water.
10. Repeat the same procedure for Meropa 460 lubricating oil to determine the density.

3.3.2 Oil Viscosity Measurement

The viscosity of the Meropa oil was measured with the concentric cylinder viscometer. The procedure for the viscosity measurement involves the following steps:

1. Turn on the water bath and set it to the desired temperature for the experiment.
2. Pour the oil sample inside the cup of the viscometer. Check the cylinder level to ensure that the volume of oil poured touches the datum line for the selected spindle (MV3) inside the cup.
3. Carefully attach the spindle and the cup to the viscometer. Check the connection to ensure that the spindle is well-tightened to the viscometer rotor.
4. Set the spindle speed of the viscometer using the RheoWin Job Manager software.
5. Allow the oil to attain thermal equilibrium by shearing the oil sample at a low rotating speed (2 rpm) for 30 minutes. This duration is sufficient to ensure that the torque remains constant with time.
6. Increase the rotational spindle speed in a stepwise manner and measure the torque.

3.3.2 Bitumen Froth Viscosity Measurement

The procedure was used to measure the viscosity of the bitumen froth:

1. Turn on the water bath and set it to the desired temperature for the experiment.
2. Pour the preheated froth sample inside the cup of the viscometer. Check the cylinder level to ensure that the volume of the sample poured touches the datum line for the selected spindle (MV3) inside the cup.
3. Carefully attach the spindle and the cup to the viscometer. Check the connection to ensure that the spindle is well-tightened to the viscometer rotor.
4. Set the spindle speed of the viscometer using the RheoWin Job Manager software.
5. Allow the bitumen froth to attain thermal equilibrium by shearing the oil sample at a low rotating speed (2 rpm) for 45 minutes. This duration is sufficient to ensure that the torque remains constant with time.
6. Shear the sample by gradually increasing the spindle speed and measure the torque. The test was conducted within the spindle speed range of 2 to 10 rpm.

3.4 Emulsion Preparation and Characterization

Water-in-oil emulsions were prepared at 10 wt.%, 25 wt.%, and 30 wt.% water concentrations for the preliminary experiments. All the emulsions were prepared at room temperature. Figure 3.1 shows the image of the model oil before and after the emulsion was prepared.

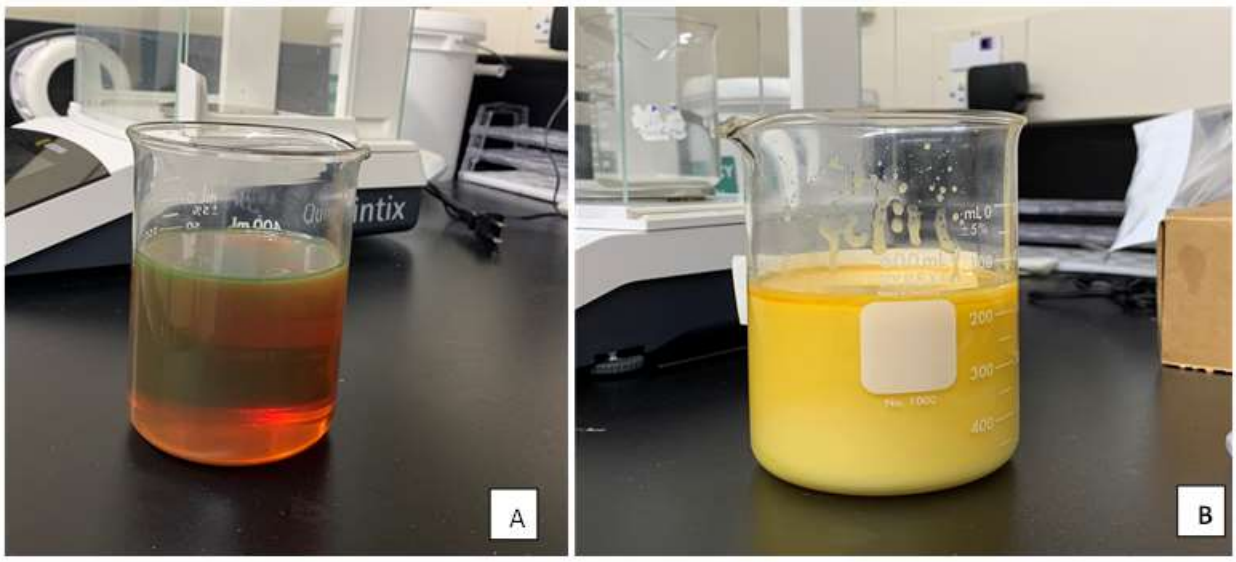

Figure 3.1: Meropa 460 Oil (A), and 30wt% water-in-Oil Emulsion (B)

3.4.1 Emulsion Preparation

The emulsion preparation procedure in this study consists of the following steps:

1. Take two beakers (600 mL and 250 mL), one for the oil sample, and the other for DI water.
2. Weigh the desired mass of oil and deionized water into the 600 mL and 250 mL beakers respectively using the electronic balance.
3. Place the beaker containing the oil sample (continuous phase) under the probe of the homogenizer inside the fume hood.
4. Place the mixing head of the homogenizer probe inside the oil beaker and completely immerse it inside the oil (continuous phase). The tip of the probe should be at 1/3 of the height of the oil in the beaker.
5. Connect the homogenizer to the power source and shear the oil at a mixing speed of 14,000 rpm.
6. Slowly add the deionized water (dispersed phase) to the oil continuous phase in a dropwise manner using the plastic transfer pipette to ensure adequate mixing.
7. Stir the mixture for about 5 minutes after the water phase has been added to ensure that the oil-water mixture is well homogenized and water droplets are properly dispersed through the oil.
8. Turn off the homogenizer, and carefully remove the mixing head from the beaker containing the emulsion prepared.
9. Cover the beaker with a Parafilm and store the emulsion inside the fume hood for droplet size analysis.

3.4.2 Droplet Size Analysis

All photomicrographs of the water-in-oil emulsion prepared were obtained with the ZIESS Axioscope -40 Microscope. The procedure used for conducting the microscopy of the water-in-oil emulsion is given below:

1. Dip the micropipette inside the emulsion to withdraw a small sample (10 μL) and put the sample on the microscope slide.
2. Place the coverslip on the emulsion drop and allow the sample to expand between the slides.
3. Place the sample on the microscope stage where the light will be transmitted through it.

4. Turn on the microscope and put it on the Free mode settings.
5. Use the 10X lens to observe the emulsion sample to be analyzed.
6. Adjust the lens to take a picture with high contrast by using the focusing drive screws of the microscope.
7. Once the satisfactory image is obtained, take a snapshot, and save the file into a folder for further processing.
8. Remove the prepared droplet sample under the microscope stage and turn off the device.
9. Use the MATLAB script (provided in the Appendices) written for analysis of droplet size to obtain the size distribution of the droplets from the saved image.

3.5 Carrier Fluid Extraction and Characterization

3.5.1 Carrier Fluid Extraction

The carrier fluid was extracted from the bitumen froth contained in three different 4L cans for titration analysis. Approximately 600 mL of the sample was extracted from the cans. The procedure used to take extract the carrier fluid from the froth is as follows:

1. Remove the bitumen froth from the refrigerator and allow it to prewarm at room temperature for 24 hrs inside the fume hood.
2. Dip the spatula inside the froth and stir slowly until the carrier fluid is visible from the bitumen continuous phase.
3. Remove the froth can from the bath and pour the carrier fluid inside a 600mL beaker.
4. Pour the carrier fluid inside a glass jar and store it in the fume hood.

After the carrier fluid was extracted, the pH was measured using the following procedure:

1) Pour about 50 mL carrier fluid inside a 100 mL beaker. This quantity is sufficient to fully cover the pH meter probe.
2) Turn on the pH meter and place the probe inside the beaker containing the carrier fluid, then press the “CAL” button.
3) Observe the pH reading of the sample on the pH meter display board.
4) Remove the probe from the beaker and clean it with DI water.

3.5.2 Carrier Fluid Dissolved Ions

A carrier fluid sample (100 mL) extracted from the bitumen froth can using the procedure described in Section 3.6.1 was sent to Sherritt Analytical Technologies for inductively coupled plasma (ICP) analysis to determine the dissolved ions. Table 3.3 shows the concentration of dissolved ions in the carrier fluid.

Table 3.3: Concentration of dissolved ions in the carrier fluid.

Element	Concentration (g/L)
Calcium	0.010
Magnesium	0.011
Potassium	0.009
Sodium	0.911
Sulphur	0.0558
Chloride	0.723

3.5.3 Carrier Fluid pH Adjustment Procedure

The measured pH of the bitumen froth carrier fluid used in this work is 8.5. The following procedure was used for the carrier fluid pH adjustment:

Important Definitions

Carrier fluid: The fluid extracted from the 4 L bitumen froth can. The carrier fluid used for the titration test was extracted using as described in section 3.5.1.

Aqueous phase: The 8.5 pH solution prepared using DI water and NaOH. The solution represents the 5wt.% additional aqueous phase that was used to adjust the water concentration in the froth which was initially 25 wt.% to 30 wt.%.

Final mixture: Mixture of the aqueous phase and the carrier fluid.

1. Prepare an aqueous solution with a pH of 8.5 using 0.1N NaOH solution and DI water.
2. Calculate the volume of water in the bitumen froth (V_A). This represents the initial volume of the carrier fluid in the froth.

3. Calculate the volume of additional aqueous phase required to increase the concentration of water in the froth from 25 wt.% to 30 wt.%. A sample calculation is provided in Appendix E.
4. Measure one-third of the volume of carrier fluid (V_A) calculated in step 2 using a graduated cylinder. The carrier fluid here was extracted from a bigger froth container from the same froth batch using the procedure described in section 3.6.1.
5. Measure one-third of the volume of the additional aqueous phase (V_{aq}) using the graduated cylinder. One-third of the samples are used in steps 4 and 5 because limited carrier fluid is available for the titration tests.
6. Pour the samples measured in steps 4 and 5 into a 200 mL beaker and stir the mixture with the magnetic stirrer.
7. Attach a burette firmly to the retort stand and close the stopcock.
8. Fill the burette above the zero mark with the 0.1N NaOH solution using the funnel.
9. Place the beaker containing the mixture under the burette.
10. Adjust the burette with the tip placed inside the beaker and note the initial volume of the NaOH inside the burette. Ensure that the tip of the burette is above the sample.
11. Slowly add the NaOH solution to the carrier fluid in a dropwise manner through the stopcock.
12. Stir the final mixture on the magnetic stirrer to ensure good mixing.
13. Close the stopcock and measure the pH of the carrier fluid using the pH meter and compare it with the desired pH value.
14. Repeat steps (11) to (13) until the desired carrier fluid pH (8.5, 9, 9.5, and 10) is reached.
15. Note the final volume of the NaOH solution in the burette at which the desired pH was achieved.
16. Determine the volume of NaOH required to adjust the carrier fluid pH to the desired value from the difference between the initial and final volume of the titrant in the burette.

3.5.4 Fines Concentration Adjustment Procedure

The procedures used to adjust the bitumen froth fines concentration are as follows:

1. Calculate the volume of water in the bitumen froth (V_A). This represents the initial volume of the carrier fluid in the froth.

2. Calculate the volume of the additional aqueous phase (V_{aq}) required to increase the concentration of water in the froth from 25 wt.% to 30 wt.%. Add the water to the froth in the can.
3. Determine the quantity of Kaolin needed to produce the desired volume fraction of Kaolin in the froth using

$$M_f = \frac{C_f V_t \rho_f}{(1 - C_f)} \tag{3.2}$$

Where C_f is the fines volume fraction, V_t is the total volume of the final water mixture ($V_A + V_{aq}$) in the froth and ρ_f is the density of the Kaolin. A sample calculation is provided in Appendix E.

4. Put the froth can inside the ETG bath and heat it to about 40 ℃ and then add the desired quantity of dry Kaolin to the bitumen froth.
5. Use the spatula to stir the froth and ensure adequate mixing of the dry Kaolin with the bitumen broth.
6. Allow the mixture to heat to 70 ℃ inside the ETG bath.

3.6 Bitumen Premixing Procedure

To homogenize the bitumen froth sample before the shearing experiments, the froth was preheated and premixed inside the ETG bath using the procedure described by Laplante [57]. Afterward, the froth sample was poured inside the glass jars for storage before conducting the shearing experiments. The procedure for the bitumen froth premixing is as follows:

1) Insert the bitumen froth can inside the can holder in the ETG bath and heat the froth to 70 ℃.
2) Adjust the height of the mixer so that the pitch blade impeller can be conveniently attached to the mixer.
3) Fit the can with a lid and the baffle and attach the pitched-blade impeller to the mixer. Ensure to maintain an off-bottom clearance of 1/3 the height of the container.
4) Mix the bitumen froth at 1000rpm for 15 minutes to homogenize the sample in the can.
5) Transfer the bitumen froth to the glass jars and store the samples inside the ETG bath for the shearing experiments.

3.7 Kaolin Suspension Rheology

3.7.1 Suspension Preparation

Kaolinite clay suspension rheology tests were conducted at different concentrations of fines to study the rheological behaviour of the carrier fluid. The aqueous phase used for the suspension preparation is 8.5 pH water containing 1205 ppm NaCl. This is to ensure that the suspension properties are similar to the properties of the bitumen froth carrier fluid. The procedure used for the suspension preparation was adapted from the work of Rahman [56].

The mass of fines required to prepare the suspension at different volume fractions is determined using equation (3.2). For example, the mass of fines required to prepare a 5 vol% kaolin suspension using 500 ml water as a basis can be calculated as follows:

$$M_f = \frac{0.05 \times 500 \times 2.696}{(1 - 0.05)} = 70.95\ g.$$

Table 3.4 provides the details of the kaolin suspension experiment condition.

Table 3.4: Kaolin suspension experiment conditions

Particle type	Fines volume fraction (C_f)
Kaolin	0.025
	0.05
	0.08
	0.11
	0.15
	0.17
	0.20

The procedure used for the preparation of the kaolin suspension is as follows:

1. Determine the quantity of Kaolin needed to produce the desired volume fraction of kaolin suspension using equation (3.2).
2. Measure the required quantity of aqueous phase for the target suspension inside the beaker.
3. Attach the impeller to the overhead mixer and place the impeller inside the beaker underneath it.

4. Turn on the mixer and start mixing the aqueous phase at about 250 RPM.
5. Slowly add the measured kaolin clay into the aqueous phase inside the beaker.
6. Allow the sample to mix for 30 minutes before commencing the rheology test.

3.7.2 Suspension Rheology Procedure

The procedure used for the rheology measurement of the kaolin suspension is provided in this section. The AR-G2 rheometer was used for the low suspension concentration tests due to its high torque sensitivity. The VT 550 viscometer was used for the high kaolin suspension concentration (>8 vol% fines concentration) rheology tests.

The procedure for the suspension rheology tests conducted with the AR-G2 rheometer is as follows:

1. Open the rheometer air supply valve and turn on the temperature control system.
2. Turn on the rheometer and the computer. Launch the instrument software to set the test conditions.
3. Perform calibration of the equipment on free geometry before attaching the spindle.
4. Attach the conical DIN spindle to the rheometer rotor and raise the device to the loading gap.
5. Click the experiment menu drop-down and define the test procedure for the sample (see Table 3.5)
6. Add 23 mL of the sample inside the cup of the rheometer and set the device to the geometry gap.

Table 3.5: Rheometer operating condition

Step 1	1. Flow – Peak Hold
Temperature	25 ℃
Controlled variable	Angular velocity (30 rad/s)
Duration	600 s
Step 2	Flow – Linear sweep
Controlled variable	Angular Velocity (5 – 30 rad/s)
Number of points	10
Averaging time	60 s
Equilibrating time	5 s
Step 3	Flow – Linear sweep
Controlled variable	Angular Velocity (30 – 5 rad/s)
Number of points	10
Averaging time	60 s
Equilibrating time	5 s

The procedure for the suspension rheology tests for the VT550 viscometer is as follows:

1. Turn on the viscometer and the water bath and attach the MV1 spindle to the rotor.
2. Set the operating conditions of the tests using the RheoWin software.
3. Pour 34 mL of the suspension sample inside the cup and attach the cup to the spindle.
4. Shear the sample by gradually increasing the spindle speed and measure the torque.

3.8 Lubricating Flow Experiment Procedure

The VT550 concentric cylinder viscometer was used to carry out all the lubricating flow experiments. The working principle of the viscometer has been discussed in Chapter 2. The procedure used for conducting the experiments involves the following steps:

1. Turn on the water bath of the viscometer and set it to the desired temperature.
2. Carefully attach the MV3 spindle to the rotor and ensure that the connection is tight.
3. Pour the prepared sample (water-in-Meropa Oil emulsion or bitumen froth depending on the test condition) inside the cup of the viscometer to reach the datum line of the MV3 spindle selected for the experiment.
4. Turn on the computer and launch the RheoWin job manager to set the operating speed of the viscometer.
5. Shear the sample at a low speed (2 rpm) for 45 min to allow it to attain thermal equilibrium with the water bath.
6. Shear the sample by gradually increasing the spindle speed in a stepwise manner (stepwise spindle speed procedure) and observe the torque at each speed for about 5 minutes. This should be done until the self-lubricating flow is obtained (a drastic reduction in measured torque).
7. Conduct subsequent experiments around the region in which the drastic torque reduction was observed to identify the critical spindle speed for the self-lubricated flow.

3.8.1 Experiment Matrix

Two sets of experiments were conducted, the preliminary experiment and the main experiment. The summary of the experiment condition in this work is as follows:

Preliminary experiment

The preliminary experiment was conducted to investigate the effects of water concentration on the mechanism of self-lubrication using the water -in -Meropa oil emulsion prepared in Section 3.4 as an analogous froth. The detail of the experiment condition is provided in Table 3.6.

Table 3.6: Preliminary experiment condition

Oil Sample	Meropa 460
Spindle type	MV3
Temperature (℃.)	25
Water Concentration (wt.%)	10, 25, 30

Effect of temperature on self-lubrication

The detail of the experiment condition for the effect of temperature on the mechanism of self-lubrication of bitumen froth is provided in Table 3.7.

Table 3.7: Experiment condition for the effect of temperature on self-lubricated flow

Sample	Bitumen froth A
Temperature (℃.)	50, 55, 60
Water Concentration (wt.%)	23
Spindle type	MV3

Effect of carrier fluid pH on self-lubricated flow

The detail of the experiment condition for the effect of the carrier fluid pH on the mechanism of self-lubrication of bitumen froth is provided in Table 3.8.

Table 3.8: Experiment condition for the effect of carrier fluid pH on self-lubricated flow

Sample	Bitumen froth B
Base	NaOH
pH	8.5, 9, 9.5, 10
Temperature (℃.)	55
Water Concentration (wt.%)	30

Effect of salt concentration on self-lubricated flow

The detail of the experiment condition for the effect of salt concentration on self-lubricated froth flow is provided in Table 3.9.

Table 3.9: Experiment condition for the effect of salt concentration on self-lubricated flow

Sample	Bitumen froth B
Salt type	NaCl
Salt concentration (PPM)	1205, 2000, 3000
Temperature (℃.)	55
Water Concentration (wt.%)	30

Effect of fines concentration on self-lubricated flow

The detail of the experiment condition for the effect of fine concentration on self-lubricated froth flow is provided in Table 3.10.

Table 3.10: Experiment condition for the effect of fines concentration on self-lubricated flow

Sample	Bitumen froth B
Particle type	Kaolin
Fines Concentration C_f (Vol%)	0, 4.1, 6.3
Temperature (℃.)	55
Water Concentration (wt.%)	30

Chapter 4 Preliminary Experiment Results

4.1 Viscometer Calibration and Viscosity Measurement

The VT550 viscometer was calibrated using Cannon S60 and Cannon S200 standard oils. Calibrating the equipment with standard oils of known properties helps to verify that the viscometer is operating appropriately and providing accurate measurements. After confirming the accuracy of the viscometer through calibration, viscosity measurements of the Meropa 460 lubricating oil were conducted. The experimental procedure involved subjecting the oil to different rotating speeds and measuring the torque exerted by the oil on the spindle. It is important to mention that the full-scale torque (FST) of the viscometer used in this work is 30,000 µNm. The full-scale torque value represents the maximum torque reading that the viscometer is capable of measuring. After the experiments, the measured torque was plotted against the angular velocity, as shown in Figure 4.1.

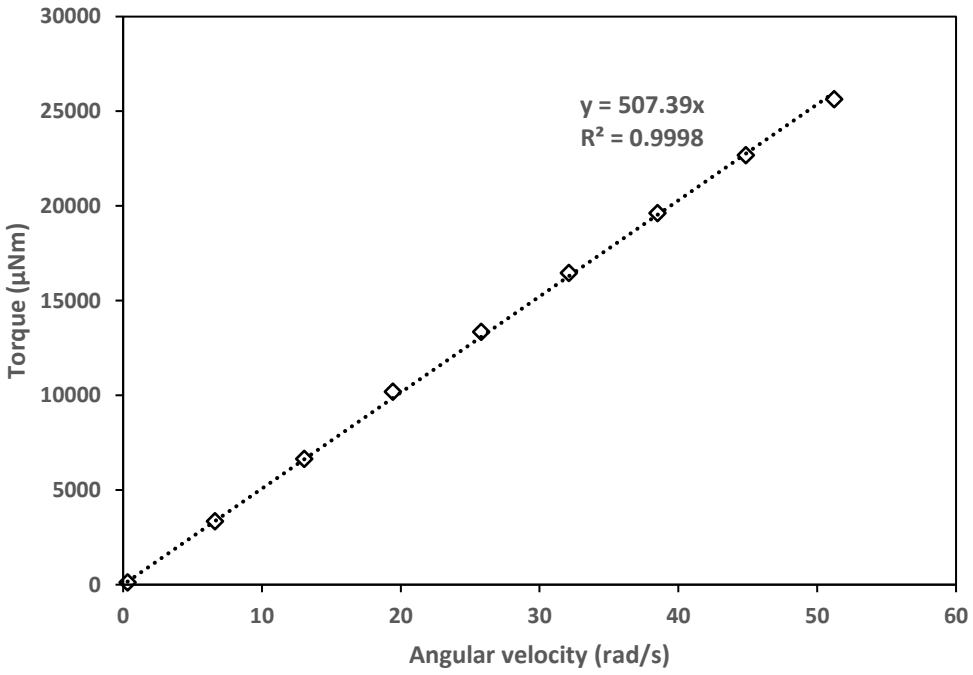

Figure 4.1: Cannon S60 standard oil viscosity measurement procedure. Full-scale torque (FST) = 30,000 µNm.

The viscosity of the oil sample was determined from the slope of the graph by using the Newtonian model equation for the concentric cylinder viscometer [58]:

$$T = \frac{4\pi L\mu}{\frac{1}{R_1^2} - \frac{1}{R_2^2}} . \omega \tag{4.1}$$

where R_2 and R_1 are the radii of the cup and the spindle, respectively, T is the torque in Nm, L is the length of the spindle, and ω is the angular velocity of the spindle.

The angular velocity ω is calculated using

$$\omega = \frac{2\pi n}{60} \tag{4.2}$$

where n represents the rotating spindle speed.

The viscometer calibration tests were performed at both low and high angular velocities to confirm the viscometer's accuracy across a wide torque range. Figure 4.1 shows that the oil sample exhibited a Newtonian behavior since the data is linear and passes through the origin, as expected for a typical viscometer standard oil. At 20 ℃, the measured viscosity of the Cannon S60 standard oil is 0.149 Pa.s, while the referenced viscosity is 0.139 Pa.s. An error of 7.19% was calculated using these values. For the calibration test conducted with Cannon S200 standard oil, the measured and referenced viscosities of the oil at 25 ℃ are 0.362 Pa.s and 0.342 Pa.s, respectively, with a percentage error of 5.85%. The slight difference observed in the measured viscosity in the calibration tests can be attributed to various factors, including the precision of the measuring device or the measurement procedure. Experimental measurements are inherently subject to some level of variability. However, the percentage errors obtained in the tests are believed to be acceptable to this experimental study.

Figure 4.2 presents the comparison of the measured torque with the predicted torque using the Newtonian model equation. The predicted torque is the torque value calculated by putting the measured viscosity value inside the Newtonian model equation. The strong agreement between the two sets of values further demonstrates the high level of accuracy of both the viscometer and the experimental procedure employed in this study.

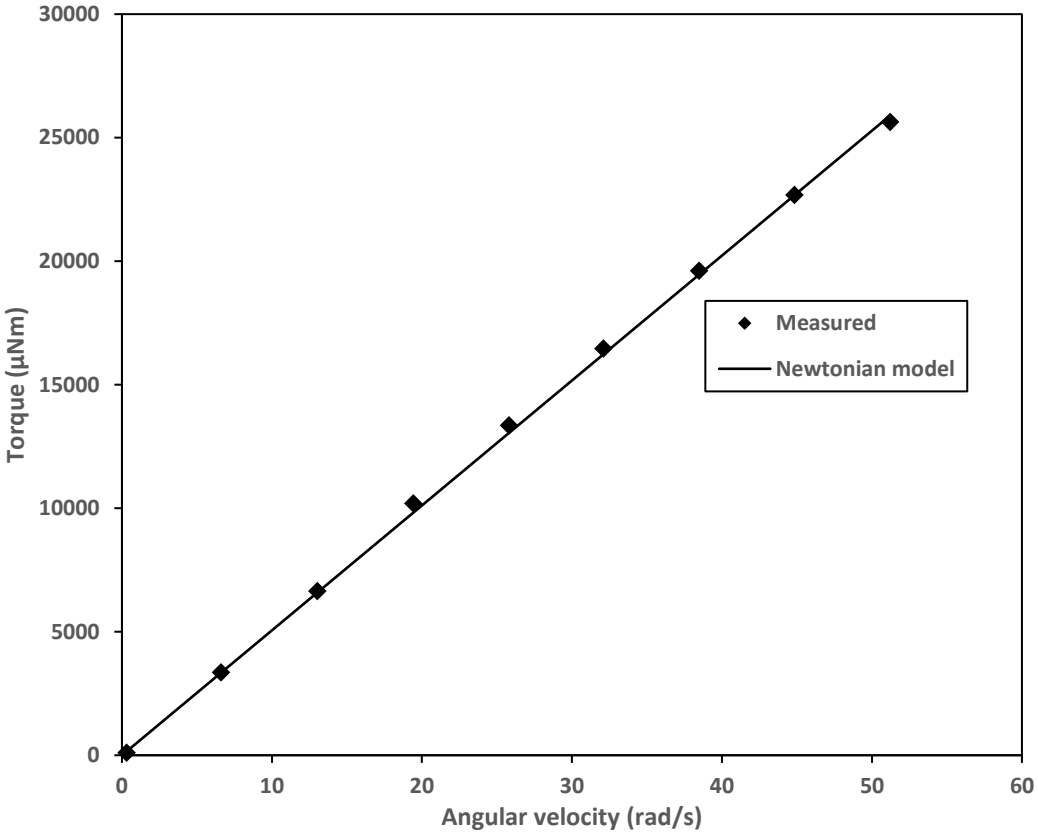

Figure 4.2: Newtonian model fit for measured torque and angular velocity data of Cannon S60 standard oil obtained using MV3 spindle.

After the calibration tests, the viscosity of the Meropa oil was measured using the same procedure that was used for the calibration. The measured viscosity of the oil at 25 ℃ is 1.210 Pa.s. A kinematic viscosity of 460 cSt at 40 ℃ was provided by the supplier. The measured oil density and dynamic viscosity at 40 ℃ were 887.8 kg/m^3 and 0.437 Pa.s, respectively. Using these values, the calculated kinematic viscosity at 40 ℃ is 492 cSt, which is 7% greater than the supplier's value. The slight difference observed might be attributed to the difference in the measurement procedure. However, this deviation falls within an acceptable range in industrial applications. Figure 4.3 compares the measured torque from the rheology tests of the Meropa 460 oil and predicted torque using Equation 4.1. The good agreement between these values further demonstrates the accuracy of test results.

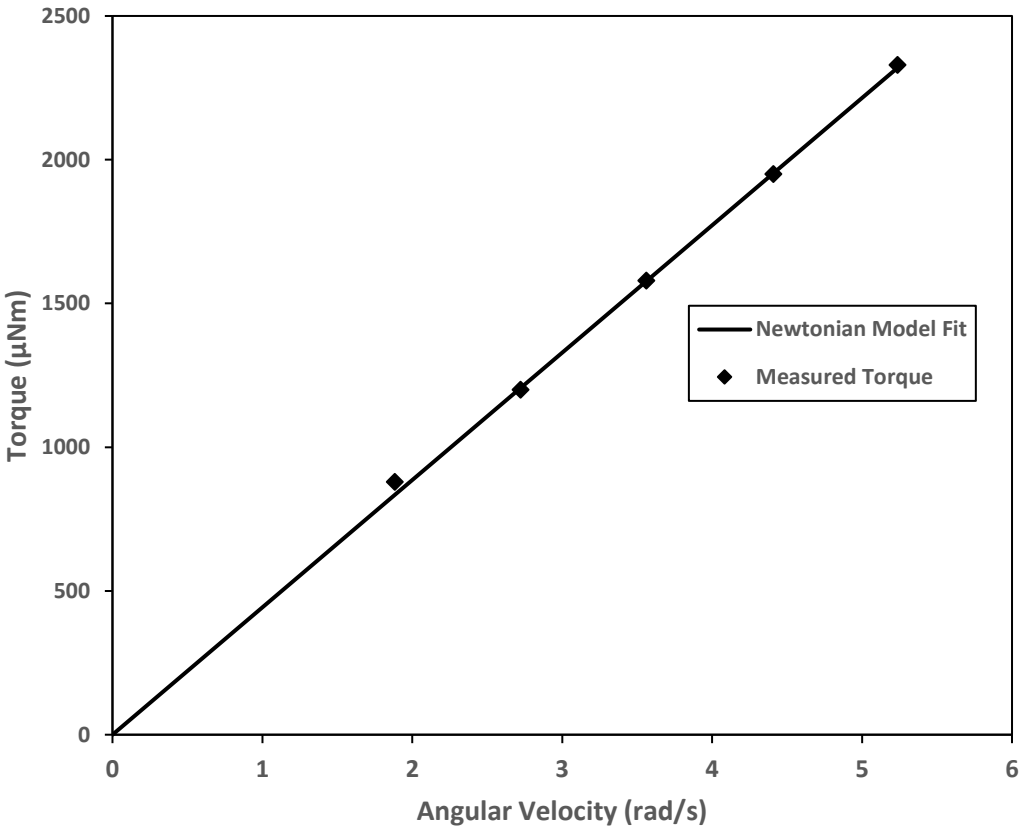

Figure 4.3: Newtonian model fit for measured torque and angular velocity data of Meropa oil obtained using MV3 spindle at 25 ℃.

4.2 Emulsion Stability and Reproducibility

4.2.1 Emulsion Stability

The emulsion stability test was conducted using a 10 wt.% water-in-Meropa oil emulsion. This emulsion was chosen to allow the proper assessment of the water droplets under the microscope. The water-in-oil emulsions prepared using 25 and 30 wt.% water concentration were difficult to observe under the microscope due to the overlapping of the droplets. As a result, the microscope could not take representative images of the emulsion droplets that could be analyzed appropriately. Nonetheless, previous studies on the stability of water-in-oil emulsions have demonstrated that the system maintains stability up to a water concentration of 30%. Yeuyin et al. [59] studied the effect of water concentration on emulsion stability. The Authors observed that there was no significant change in the droplet size range of the emulsion they studied up to 30%

water concentration for a duration of up to 6 hours. Similarly, Bello [17] reported that the water-in-oil emulsion remains stable up to 35 wt.% water concentration. The droplet size ranges from these studies are within the same order of magnitude as those obtained for the emulsions prepared in this work. This underscores the notion that the emulsions produced in this study would remain stable at 25% and 30 wt.% water concentrations within the test duration.

After the emulsion was prepared using the homogenizer, the emulsion samples were drawn immediately from the top and the bottom of the Pyrex beaker with the micropipette. Other samples were drawn after four hours. This time interval is sufficient to conduct a complete Couette flow shearing experiment. The samples taken immediately from the top and bottom of the beaker were designated samples A and B, respectively, while the samples taken at the top and bottom after four hours were designated samples C and D, respectively. The microscopy of all the samples was conducted using a 10X magnification objective lens, and the size distribution was obtained using a MATLAB script. The photomicrograph of the droplets before and after the image was processed is shown in Figure 4.4 and Figure 4.5, respectively. The rest of the images are presented in Appendix B.

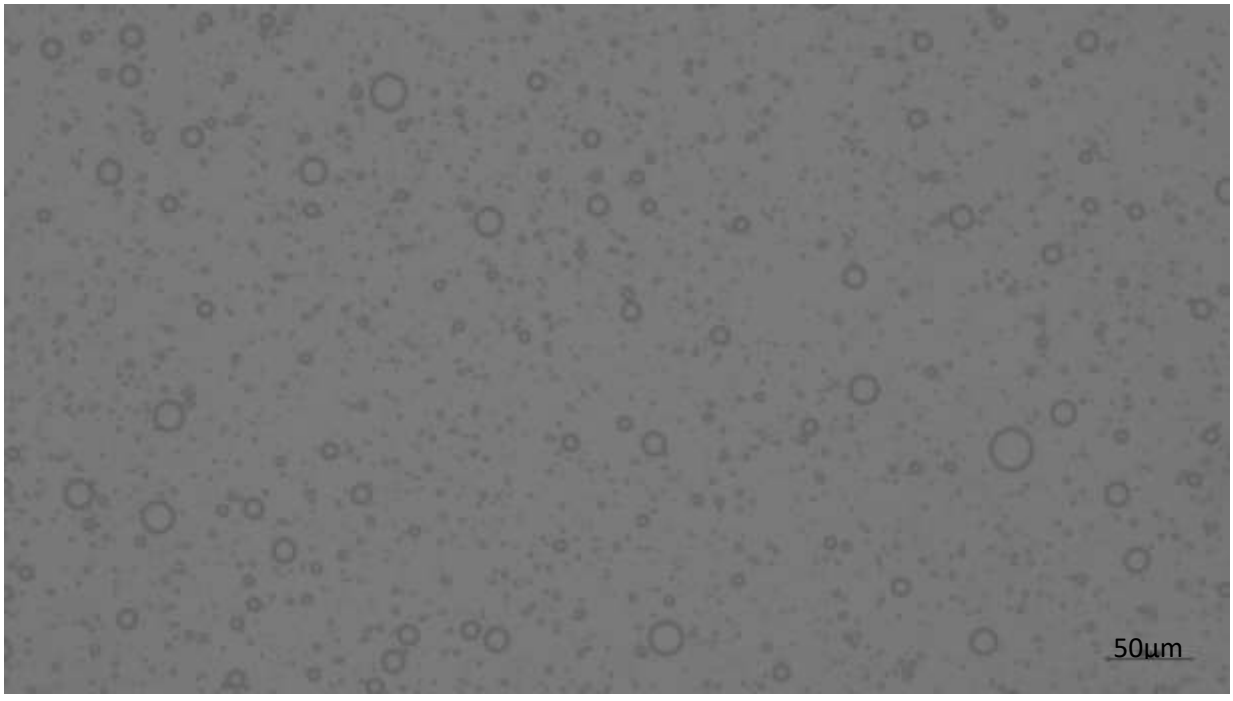

Figure 4.4: Photomicrograph of 10wt% water-in-Meropa oil emulsion prepared in this study.

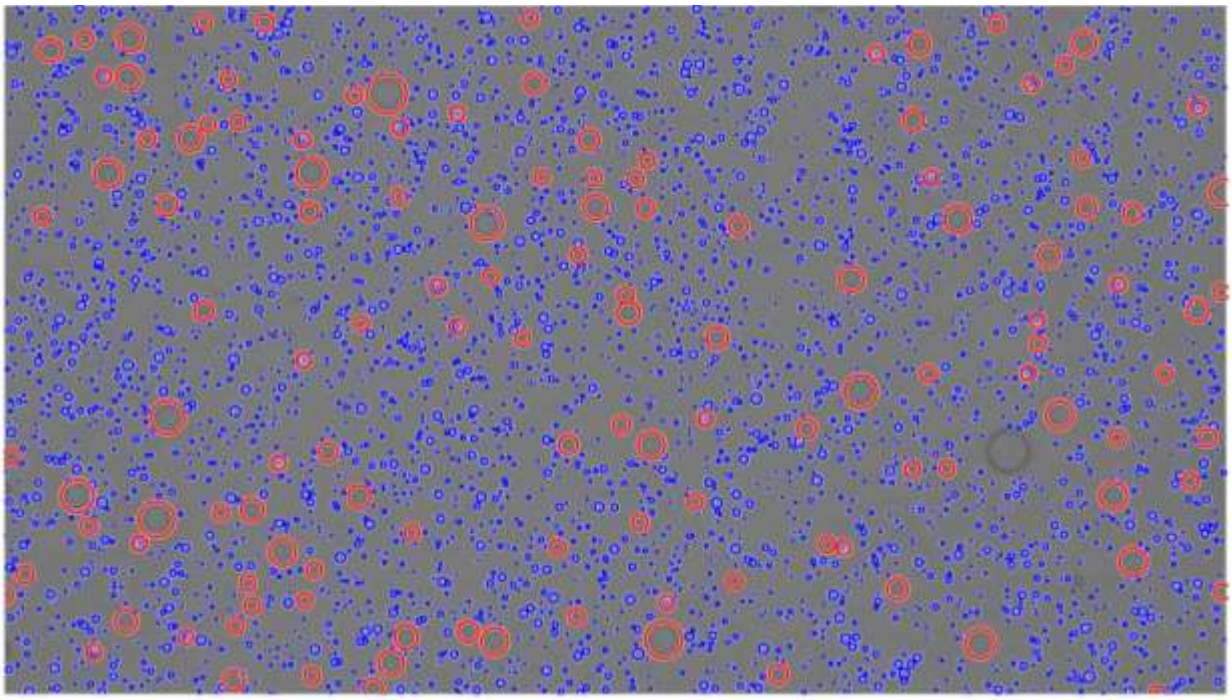

Figure 4.5: Processed photomicrograph of 10 wt.% water-in-Meropa oil emulsion using MATLAB software.

The droplet size distribution of the samples taken immediately and after four hours is shown in Figure 4.6. The result obtained from the analysis of all the samples is summarized in Table 4.1. The full droplet size distribution is provided in Appendix B. The number-length mean droplet diameter (d_{NL}) and the number based Sauter mean diameter (d_{32}) are calculated using

$$d_{N,L} = \frac{\sum n_i d_i}{N} \tag{4.3}$$

$$d_{32} = \frac{\sum n_i d_i^3}{\sum n_i d_i^2} \tag{4.4}$$

where n_i represents the frequency of the droplet of diameter d_i, and N is the total number of droplets.

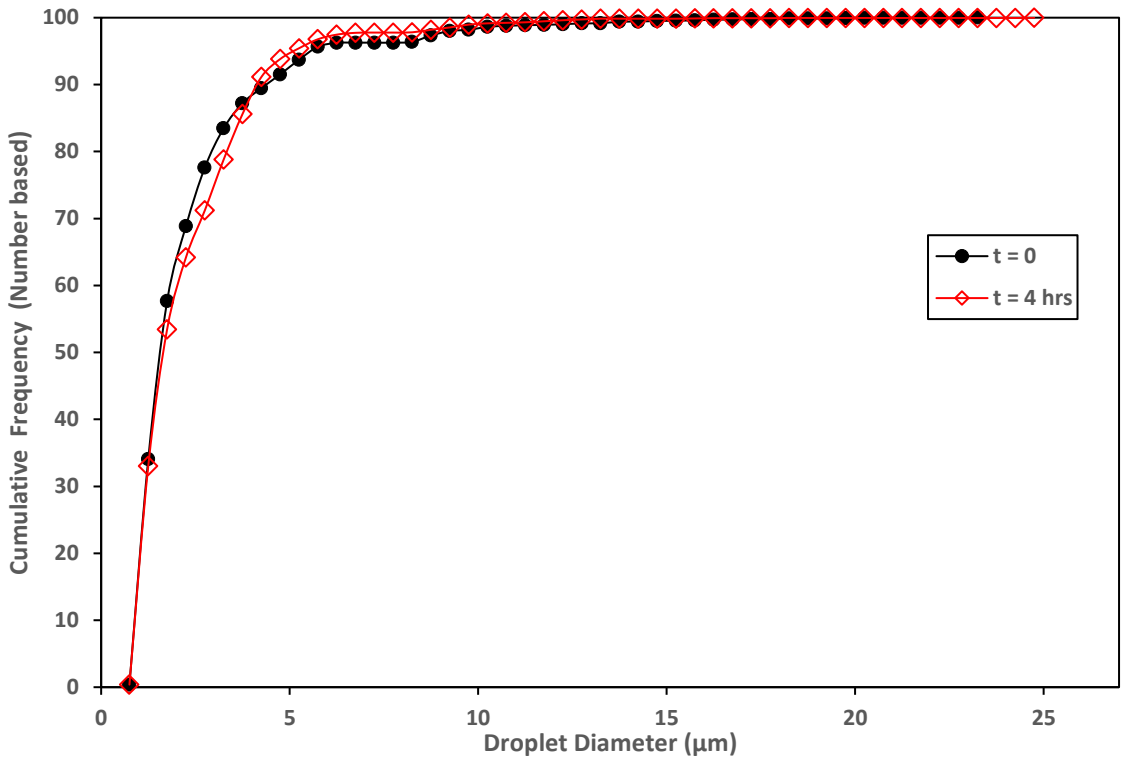

Figure 4.6: Droplet size distribution of the 10wt% water-in-Meropa oil Emulsion 1 sample B and C taken immediately and after 4 hours.

Table 4.1**:** Emulsion stability assessment result

Emulsion	**Sample**	**Point of sample collection**	**Time (hrs)**	**Number Length mean** d_{NL} **(µm)**	**Sauter mean diameter** d_{32} **(µm)**	**Group average droplet diameter based on** d_{NL} **(µm)**
Emulsion 1	Sample A	Top	0	2.7	5.4	2.6
	Sample B	Bottom	0	2.7	6.8	
	Sample C	Top	4	2.5	6.3	
	Sample D	Bottom	4	2.5	7.9	

The results presented in Table 4.1 show a great similarity between the samples collected under different conditions at t = 0 and t = 4 hours. This shows that the emulsion prepared remains stable within this period. The number-based droplet diameters obtained are significantly different from the Sauter mean diameters. This is because the Sauter mean diameter considers the contribution of larger droplets in the emulsion more than smaller droplets due to the cubic relationship of diameter in the formula. This means that the presence of a few larger droplets in the emulsion will have more influence on the Sauter mean diameter, resulting in a larger value. Figure 4.6 shows that there is no significant change in the droplet size range within the test period. The similarity in the size distribution of the droplets obtained at the different intervals further demonstrates the emulsion stability. The physical observation of the emulsion during the experiments also shows that the emulsion remained stable throughout without any phase separation.

4.2.2 Emulsion Reproducibility

In order to confirm the reproducibility of the result obtained in the stability test, two additional emulsions (Emulsion 2 and Emulsion 3) were prepared with similar constituents using the same experimental procedure. The number mean diameter of the droplets obtained from all the samples taken at different points is presented in Table 4.2. The full droplet size distribution is provided in Appendix B. The average droplet diameters of the two additional emulsions prepared are 2.6 μm and 2.7 μm, respectively. These values are consistent with the average droplet diameter obtained in the emulsion stability tests. Figure 4.7 presents the result of the three emulsions (Emulsion 1, Emulsion 2, and Emulsion 3) prepared separately with the same composition of oil and water. The figure shows a good similarity in the droplet size distribution of the three emulsions prepared separately using the same experimental procedure, with no significant change in the droplet size range. This demonstrates that the technique for the preparation of emulsions used in this work produced a stable and reproducible emulsion with consistent droplet size distribution.

Table 4.2**:** Emulsion Reproducibility Result

Emulsion	**Sample**	**Point of sample collection**	**Time (hrs)**	**Number Length mean d_{NL} (µm)**	**Sauter mean diameter d_{32} (µm)**	**Group average droplet diameter based on d_{10} (µm)**
Emulsion 2	Sample 2A	Top	0	2.8	6.5	2.6
	Sample 2B	Bottom	0	2.5	8.1	
	Sample 2C	Top	4	2.5	7.8	
	Sample 2D	Bottom	4	2.5	9.4	
Emulsion 3	Sample 3A	Top	0	3.0	5.9	2.7
	Sample 3B	Bottom	0	2.6	9.8	
	Sample 3C	Top	4	2.3	7.2	
	Sample 3D	Bottom	4	2.7	10.1	

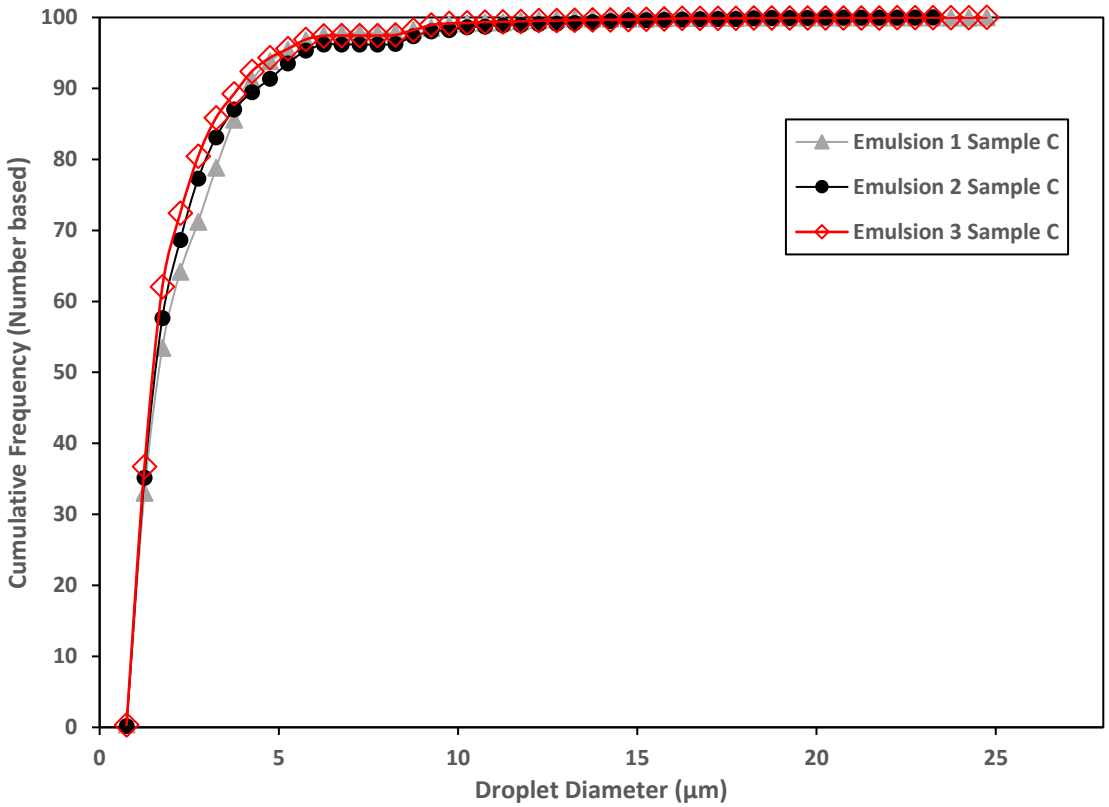

Figure 4.7: Reproducibility assessment of 10wt% water-in-Meropa oil emulsion

4.3 Preliminary Experiment Flow Pattern Classification

The Couette flow experiments were conducted using the VT550 concentric cylinder viscometer. All the preliminary experiments were performed using the water-in-Meropa oil emulsion prepared in Section 4.3. The emulsion samples were sheared at different spindle speeds in the annular gap between the cup and the spindle. The torque exerted by the emulsion on the rotating spindle was measured over time. The result obtained gives the details of the flow condition of the emulsion being sheared in the annulus of the viscometer. The two prominent flow conditions observed during the shearing experiment are as follows:

I. Non-lubricating flow (NLF): Under this flow condition, there is no reduction in the initially observed torque. The reason for this is that the dispersed water droplets do not migrate to the high-shear region to form the lubricating layer. This flow pattern is presented in Figure 4.8.

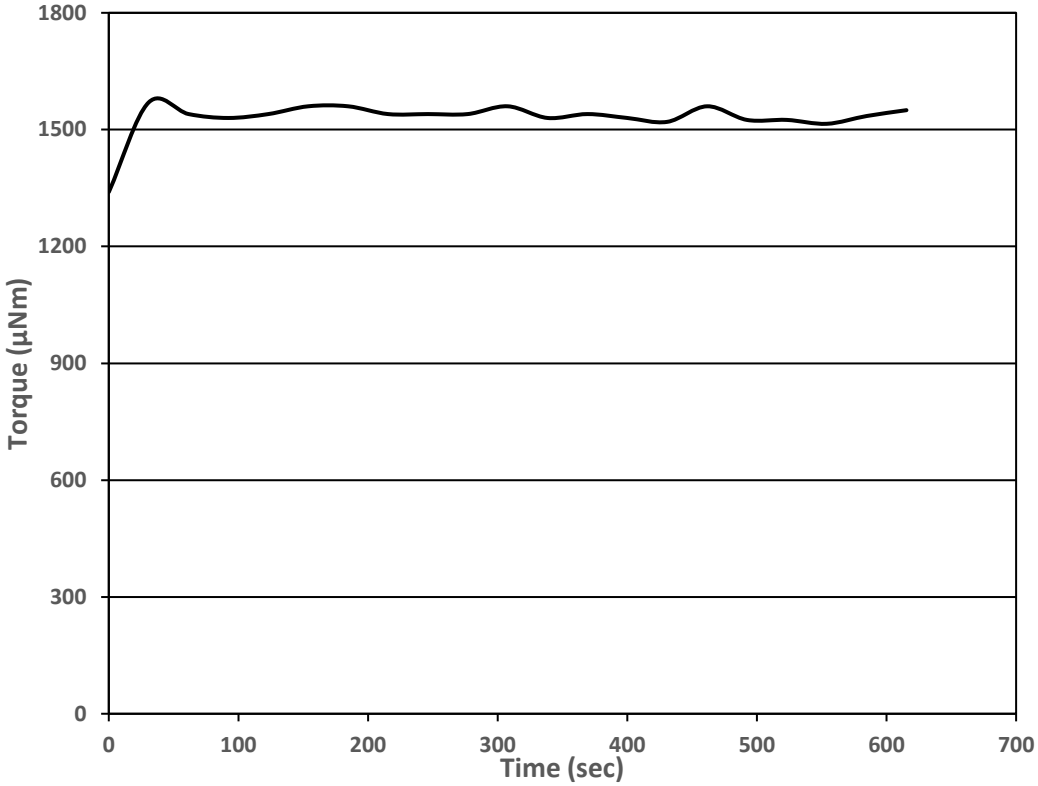

Figure 4.8: Non-lubricating flow of water-in-Meropa oil emulsion. n=16 rpm. T = 25 ℃. FST = 30,000 µNm

II. Self-Lubricating Flow (SLF): The onset of self-lubricated flow is characterized by a drastic reduction in the measured torque, as shown in Figure 4.9. The resulting low torque observed could be attributed to the lubricating water layer formed when the water droplets migrate towards the high shear region. This observation is consistent with the previous findings in the literature in both pipe flow and Couette flow experiments [15,17,22,23].

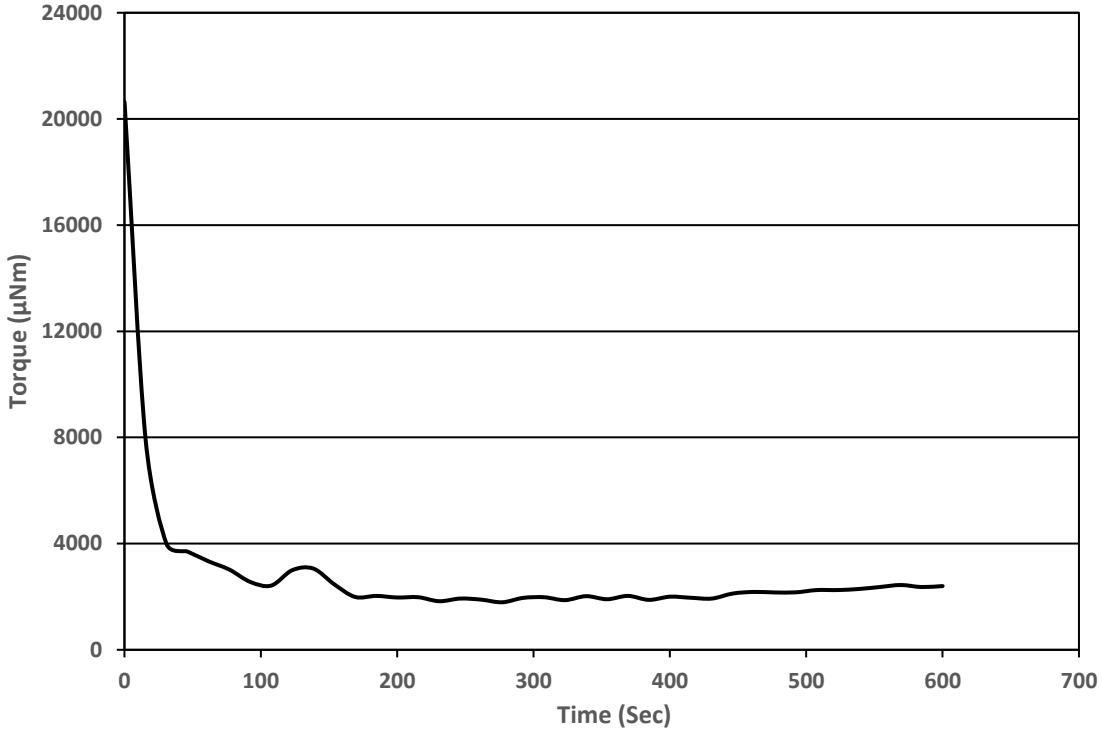

Figure 4.9: Self-Lubricating Flow water-in-Meropa oil emulsion. n = 500 rpm. T = 25 ℃. FST = 30,000 µNm

4.4 Effect of Water Concentration on Self-lubrication

The effect of water concentration on the mechanism of self-lubrication was examined in the Couette cell at 10 wt.%, 25 wt.%, and 30 wt.% water concentrations. The aim was to validate whether the experimental procedure employed in this study could yield results consistent with the previous findings of Bello [17] on the impact of water concentration on self-lubricated flows. Figure 4.10 presents the flow map for the experiment results. All the shearing experiments conducted with 10 wt.% and 25wt% water-in-Meropa oil resulted in a Non-Lubricating Flow. Under this condition, there was no reduction in the measured torque. However, for the 30wt% water-in-Meropa oil emulsion, the self-lubricated flow was obtained at 420 rpm. This result shows that the self-lubricating flow mechanism is strongly dependent on water concentration and spindle speed. Both factors are very important in facilitating the migration of the dispersed water droplets within the emulsion to form the crucial layer necessary to produce a lubricated flow. The increase

in water concentration increases the water droplets available in the dispersed phase, thus making it easier to produce a self-lubricated flow.

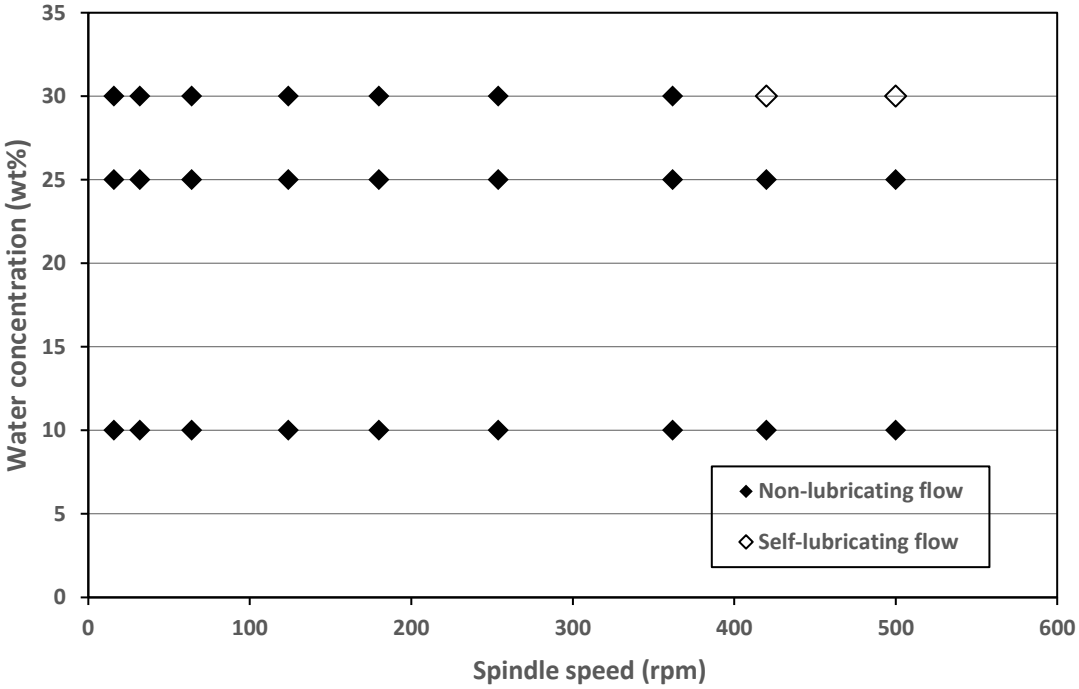

Figure 4.10: Flow map of the effect of water concentration on self-lubrication

The self-lubricating and non-lubricating flow patterns observed in this work are comparable to core-annular flow patterns reported by Charles et al [20] and Wang et al. [60]. Charles et al. [20] observed the existence of two boundaries that are critical to oil-water core annular flow; the lower critical and upper critical velocity. The lower critical velocity represents the first velocity at which the core-annular flow is achieved, similar to the critical spindle speed in the Couette flow experiment [15,18]. The upper critical velocity is the velocity at which oil slugs in water are formed due to the breakage of the oil continuous phase by the water turbulence in the annular region [18]. For the geometry used in this study, no upper critical velocity was observed. The results are consistent with the previous findings reported by Joseph et al. [18] and Bello [17]. Using the relationship between the Couette flow and pipe flow, where the critical spindle speed is comparable to critical flow velocity, a higher flow velocity will be required to produce a self-lubricated flow at lower water concentrations.

To confirm the reproducibility of the preliminary experimental results, the tests were repeated at different spindle speeds under the same experiment conditions. Similar results were obtained from the reproducibility runs. Figure 4.11 shows an example of the result obtained from the reproducibility run conducted for the same experimental condition. More results are shown in Appendix D.

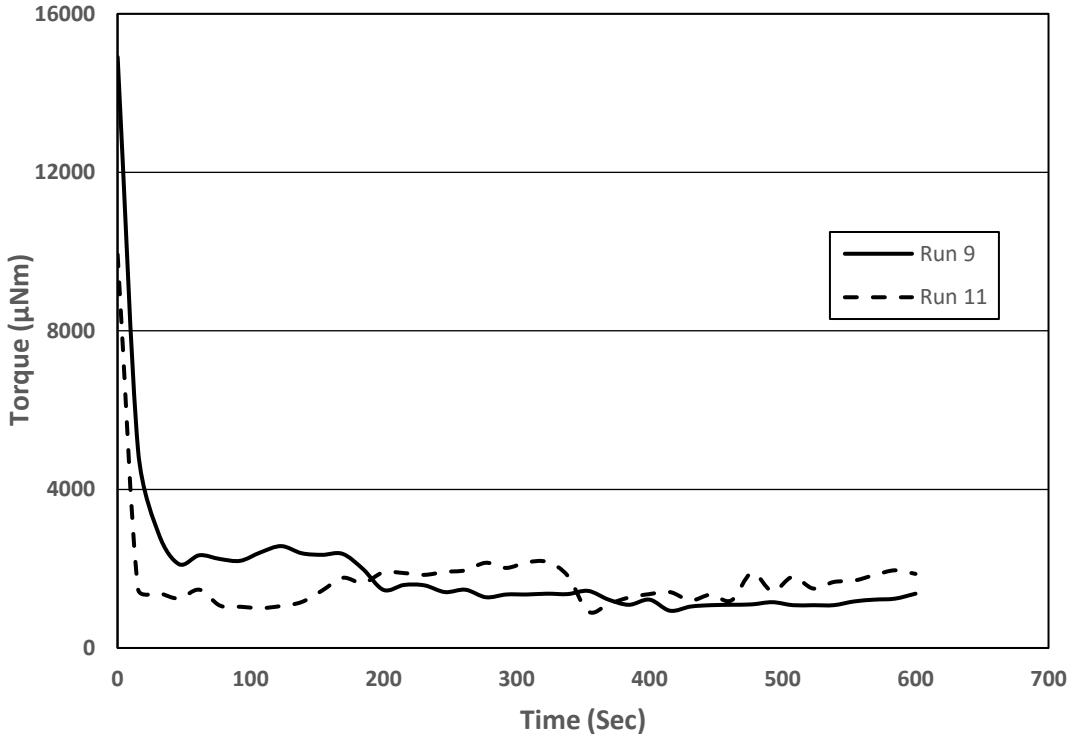

Figure 4.11: Self-lubricating flow reproducibility runs at n = 420 rpm. 30wt% water-in-Meropa Oil emulsion. FST = 30,000 µNm.

The preliminary experiments conducted in this study produced results that are consistent with the findings of Bello [17], who investigated the factors influencing the self-lubrication mechanism using the Couette cell device. The consistency of the result indicates that the parameters affecting self-lubricated froth flow can be studied using a concentric cylinder viscometer. Hence, the Couette flow device was used to conduct the main experiment to investigate the effect of carrier fluid properties on self-lubricated froth flow.

Chapter 5 Results and Discussion

5.1 Bitumen Viscosity Measurement

The viscosity of the bitumen froth sample used for the temperature test was measured before the shearing experiments. The froth was preheated and premixed using the procedures described in Chapter 3. The froth sample was allowed to attain thermal equilibrium with the water bath by shearing it at low spindle speed (2 rpm) for 45 minutes. Figure 5.1 shows an example of the torque measured as a function of time. It can be observed that there is a significant initial reduction in torque with time. This observation is because of variation in temperature within the sample in the viscometer annulus. The rotation of the spindle at low speed over time helps promote the even distribution of heat and facilitates the attainment of thermal equilibrium, where the measured torque does not significantly change with time [17].

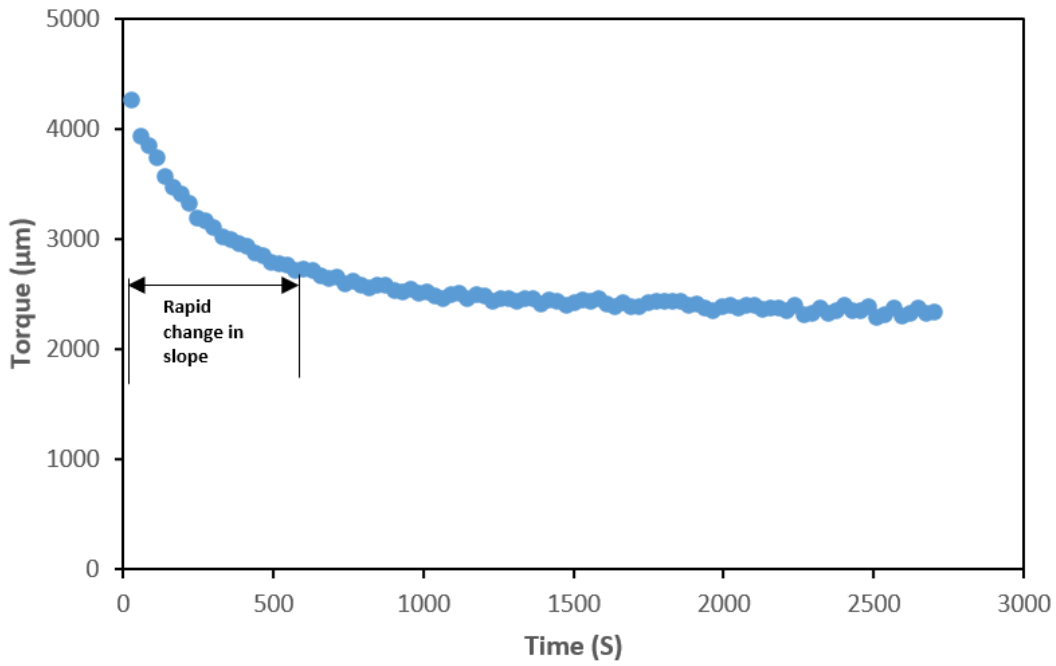

Figure 5.1: Transient behavior of torque measurement of bitumen froth. T = 50 ℃. n = 2 rpm. FST = 30,000 µNm. Bitumen froth A.

The viscosity test was conducted after the bitumen froth attained thermal equilibrium with the water bath. Figure 5.2 presents the torque measured at different angular velocities. The remaining

Figures are provided in Appendix G. The viscosity of the froth was determined by using the slope of the graph and the Bingham model equation [58].

$$T = \frac{4\pi L\mu_p}{\frac{1}{R_1^2} - \frac{1}{R_2^2}} .\omega + \frac{\frac{\tau_B}{\mu_p} \ln\left(\frac{R_2}{R_1}\right)}{\frac{1}{R_1^2} - \frac{1}{R_2^2}} .4\pi L\mu_p \quad (5.1)$$

$$\text{Slope} = \frac{4\pi L\mu_p}{\frac{1}{R_1^2} - \frac{1}{R_2^2}} \quad (5.2)$$

Where τ_y is the Bingham yield stress, μ_p is the plastic viscosity, T is the torque, L is the spindle length and ω is the angular velocity. R_2 and R_1 are the radii of the cup and the spindle, respectively.

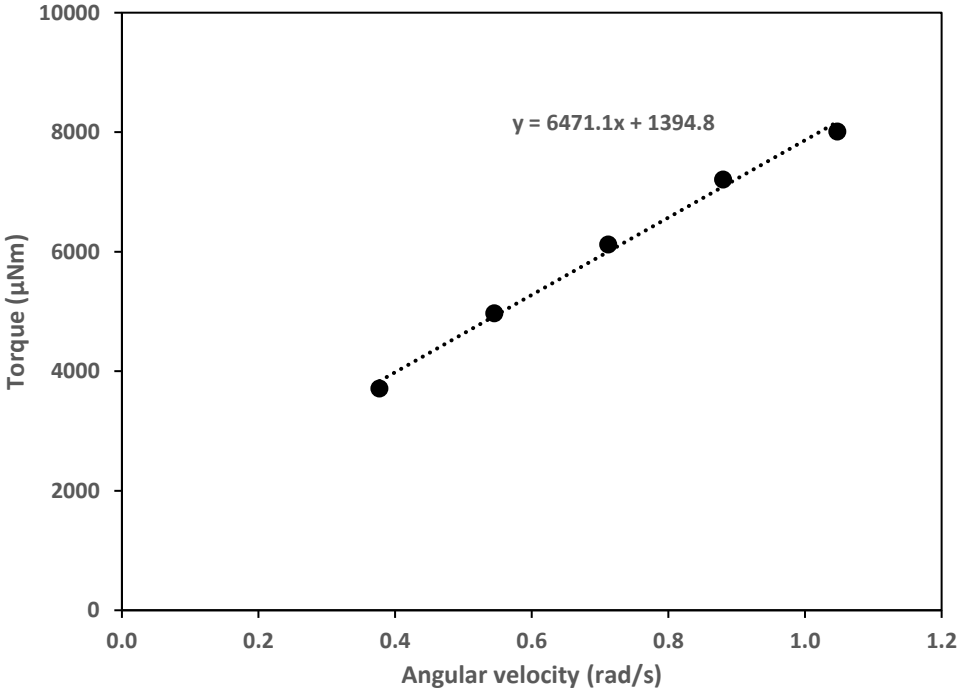

Figure 5.2: Bitumen froth rheology measurement at 50 ℃.

The viscosities of the bitumen froth at 50 ℃, 55 ℃, and 60 ℃ are 17.69 Pa.s, 10.22 Pa.s, and 7.99 Pa.s, respectively. The reduction in bitumen froth viscosity with the increase temperature can be attributed to the decrease in the intermolecular forces in the bitumen-continuous mixture. As a result of this, the resistance to flow will reduce. The measured froth viscosity in this study is within the range of bitumen viscosity reported in the literature. For example, the bitumen viscosities

reported by Nourozieh et al. [61] at 50 ℃, 55 ℃, and 60 ℃ are 15.8 Pa.s, 9.75 Pa.s, and 6.06 Pa.s, respectively. The yield stresses of the bitumen froth at 50 ℃ and 60 ℃ were found to be 11.79 Pa and 4.62 Pa, respectively. At 55 ℃, the froth behaved like a Newtonian fluid with no yield stress. A similar anomalous behavior was observed in the rheology tests conducted by Bello [17]. The author reported a non-linear relationship between the yield stresses of lubricating oil measured at different temperatures. The yield stress initially decreased from 0.02 Pa to 0.01 Pa at 15 ℃ and 30 ℃. However, the yield stress value of 0.39 Pa was obtained at 50 ℃. The yield stresses obtained in this part of the investigation should be treated with suspicion, as it is most likely related to experimental error. It is not expected that bitumen froth should have a yield stress. Further work is required to understand the reason for this type of fluid behaviour.

5.2 Bitumen Froth Flow Pattern Classification

The three different types of flow patterns observed during the experiments are as follows:

i. Non-lubricating flow (NFL): Under this flow condition, there was little or no reduction in the initial torque, as shown in Figure 5.3.

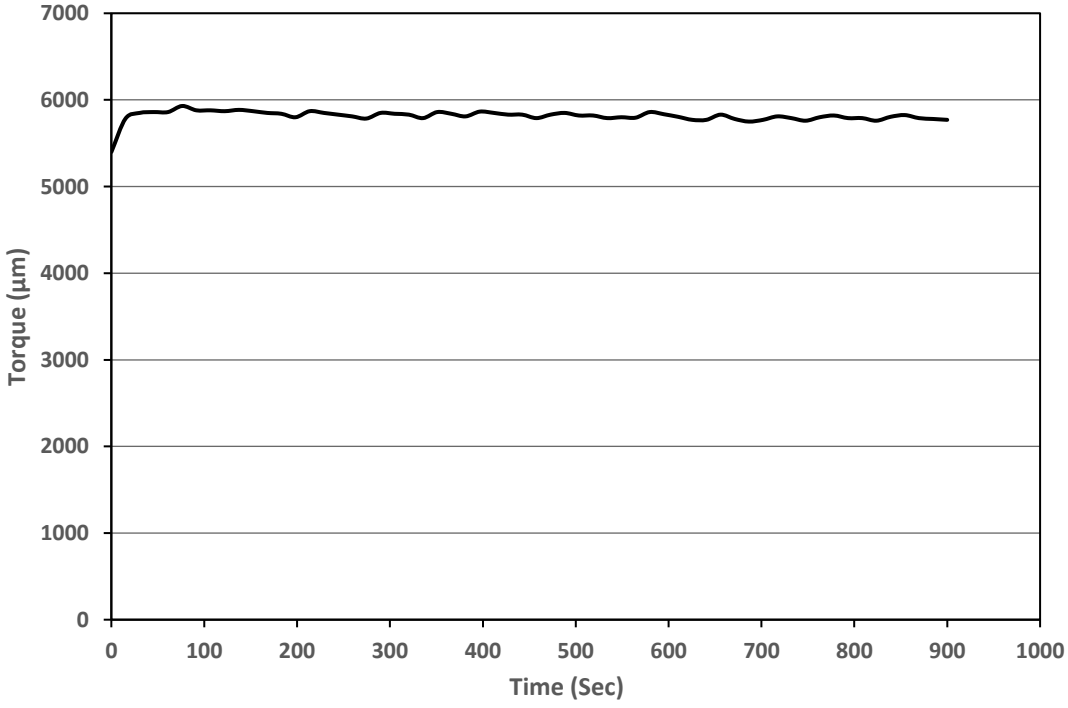

Figure 5.3: Non-Lubricating Flow of Bitumen Froth. n=8 rpm. T=50 ℃. FST = 30,000 µNm. Bitumen froth A.

ii. Imperfect Self-Lubricating Flow (ILF): This flow pattern is characterized by a significant reduction in the initial torque, followed by fluctuating torque values as shown in Figure 5.4. This observation is due to the instability of the water droplets in the lubricating layer region. The water droplets under this condition appear to move back and forth between the lubricating layer and the bitumen continuous phase.

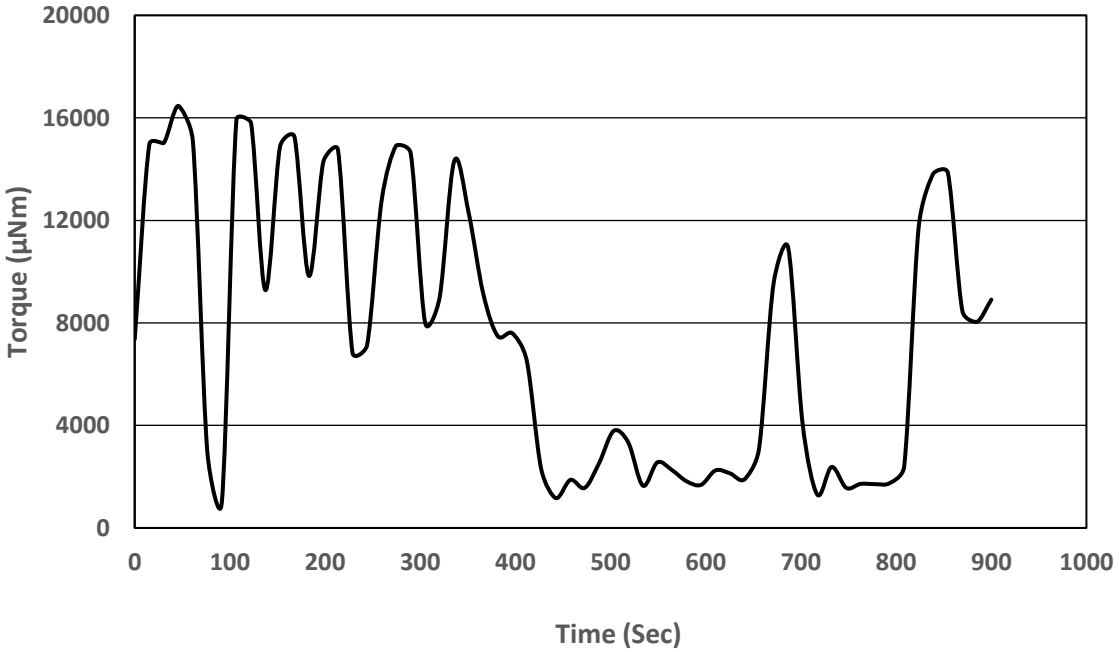

Figure 5.4: Imperfect Self-Lubricating Flow of Bitumen Froth. n=90 rpm T=55℃. FST = 30,000 µNm. Bitumen froth A.

iii. Self-Lubricating Flow (SLF): Under this flow condition, there is a drastic reduction in the initially high measured torque, as shown in Figure 5.5. After the initial torque reduction, the torque remains low with negligible fluctuations.

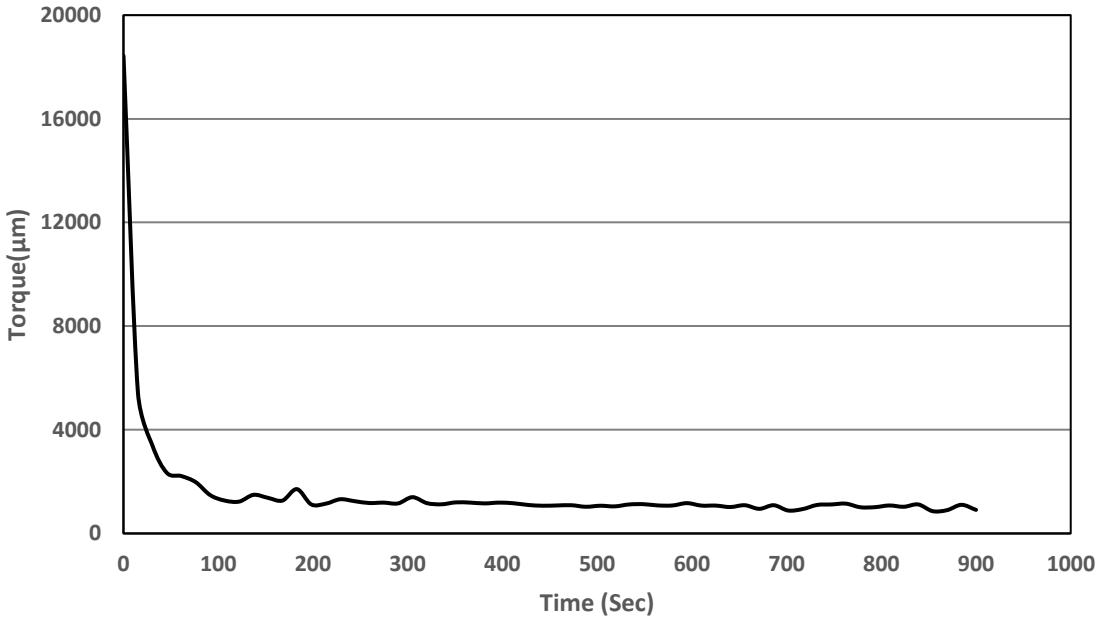

Figure 5.5: Self-Lubricating Flow of Bitumen Froth. n=164 rpm. T = 60 ℃. FST = 30,000 µNm. Bitumen froth A.

5.3 Effect of Temperature on Self-lubrication Flow of Bitumen Froth

The effect of temperature on self-lubricated froth flow was studied using the Couette cell by shearing the froth sample inside the annular gap between the cup and the spindle. The flow map for the effect of temperature on the self-lubrication of bitumen froth is presented in Figure 5.6. The result shows that the increase in temperature increases the speed required to achieve self-lubricated flow. The critical spindle speeds are 90, 128, and 164 rpm at 50, 55, and 60 ℃, respectively. This observation can be ascribed to the reduction in the viscosity of the bitumen in the froth, which is strongly affected by a change in temperature. Consequently, the viscosity ratio of the continuous bitumen phase to the dispersed water phase will reduce, thereby increasing the shear rate required to produce a self-lubricated flow. A similar trend was observed in the previous study conducted by Bello [17] to investigate the effect of temperature on self-lubricated flow using a water-in-oil emulsion as a bitumen froth analog.

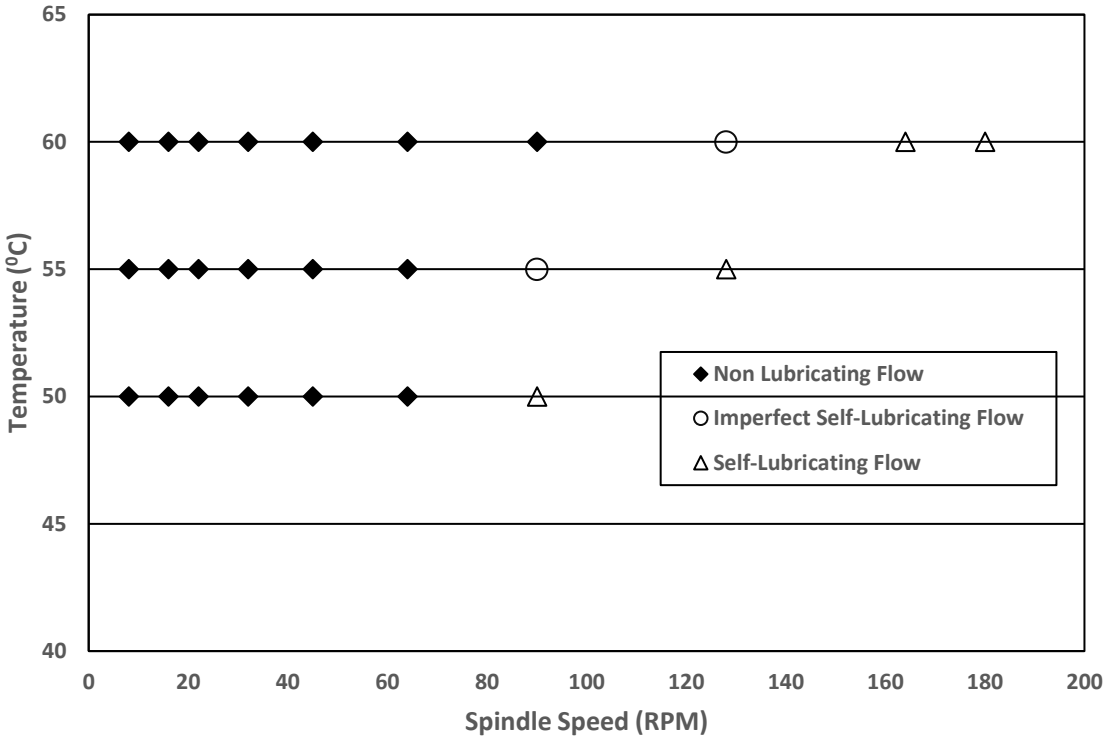

Figure 5.6: Flow map of the effect of temperature on self-lubricated flow. 23 wt.% water concentration. Bitumen froth A.

To demonstrate the impact of continuous phase viscosity on the shear rate required to produce a self-lubricated flow, the viscosity of bitumen was calculated from the bitumen froth viscosity measured in section 5.1 the equation [62]

$$\frac{\mu_m}{\mu_L} = 1 + 2.5C \qquad 5.3$$

Where μ_m and μ_L represent the viscosities of bitumen froth (mixture) and bitumen, respectively, while C_C represents the volume concentration of the dispersed water phase. It is assumed that the water droplets have the same contribution as the fine particles in the carrier fluid in terms of augmenting the froth viscosity. The volume concentration of the dispersed water is calculated using the equation

$$C = \frac{V_w}{V_w + V_B} \qquad 5.4$$

Where V_w and V_B represent the volume of water and the volume of bitumen, respectively. The volumes were calculated by dividing the mass of the bitumen and water by their densities. As

discussed in Chapter 3, the bitumen used for the temperature tests contains 77% bitumen and 23% water by mass. Using 800 g of bitumen froth as a basis, the volume fraction of the bitumen and water will be 0.77 and 0.23, respectively. The detail of the viscosity analysis is provided in Table 5.1. Einstein's equation was used to estimate the bitumen viscosity because other empirical correlations considered resulted in an underestimation of bitumen viscosity compared to values reported in the literature. Therefore, even though Einstein's equation is not ideal for this type of system, it was chosen due to its alignment with experimental bitumen viscosities obtained at similar temperatures [61].

Table 5.1: Bitumen viscosity calculation at different temperatures

Water concentration	Temperature (℃)	Froth Viscosity (Pa.s)	Calculated Bitumen Viscosity (Pa.s)
0.23	50	17.69	11.20
	55	10.25	6.49
	60	7.99	5.06

Figure 5.7 shows the effect of continuous phase viscosity on the critical speed required to produce a self-lubricated flow. The consistency of the results with the findings of Bello [17] on the effect of temperature on self-lubricated flow using analogous water-in-oil emulsions further demonstrates that the factors affecting the mechanism of self-lubrication of bitumen froth can be studied using a Couette cell device. Joseph [51] highlighted some of the criteria that are critical to the self-lubricated flow phenomenon, e.g. that the dispersed water droplets will migrate to the wall if the oil-continuous core viscosity is greater than 500 mPa.s. The Author also noted that drag reductions of the order of the viscosity ratio are possible when the oil-water viscosity ratio is equal to 10^5. The results obtained in this work are within the range of the conditions described by Joseph. The viscosity ratios are in the order of 10^3 to 10^5. The findings of this study further demonstrate that self-lubricated flow is highly beneficial for transporting bitumen froth and heavy crude oil with high viscosities in pipelines. Using the relationship between the Couette flow and pipe flow, the increase in temperature will increase the flow velocity required to produce a self-lubricated flow.

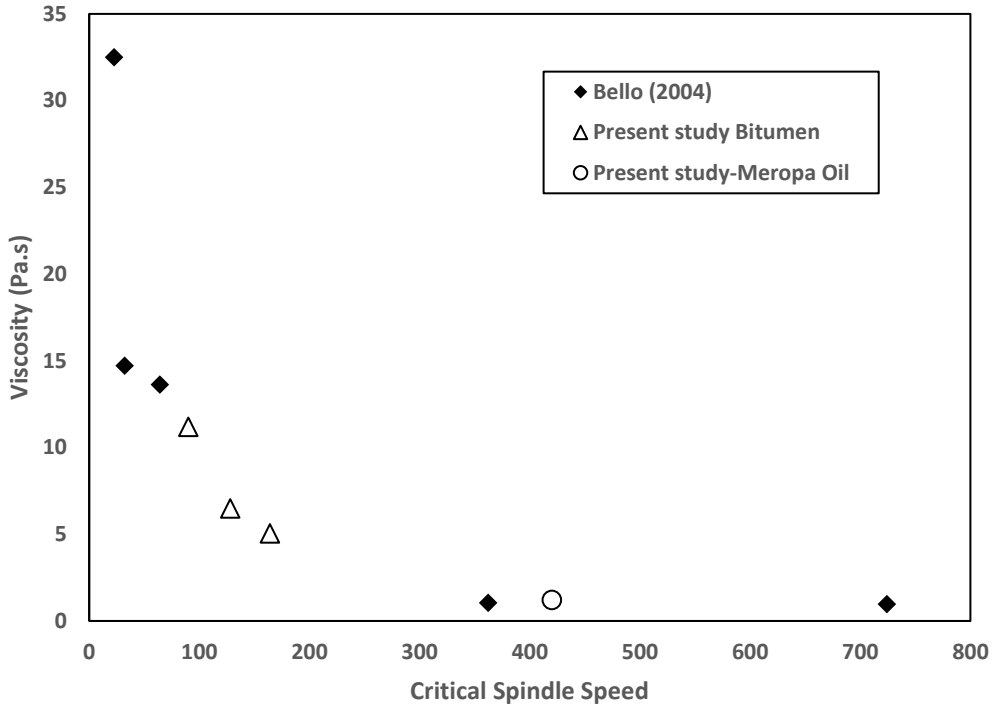

Figure 5.7: Effect of continuous phase viscosity on the critical spindle speed required to achieve self-lubrication.

5.4 Effect of Carrier fluid properties on self-lubricating flow

This section discusses the results of the experiments performed to investigate the effects of carrier fluid properties on the self-lubrication of bitumen froth. Carrier fluid, as discussed in Chapter 2, is the mixture of water, fines, and dissolved ions in the bitumen froth. The properties of the carrier fluid were adjusted by adding NaOH, NaCl, and kaolinite clay to the bitumen froth during the preheating stage of the experiment. The results obtained from the experiments will be discussed in the subsequent sections. As mentioned in Chapter 3, Bitumen froth B was used for all the experiments conducted in this section.

5.4.1 Effect of Carrier Fluid pH

The effect of carrier fluid pH on the self-lubrication of bitumen froth was investigated at different shear rates. The carrier fluid pH was varied from 8.5 to 10 by adding 0.1 N sodium hydroxide solution to the froth during the preheating process. Figure 5.8 shows the flow map of the froth for the Couette flow tests as a function of carrier fluid pH. The results show that the

increase in the pH increases the speed required to attain the self-lubricating flow. At a pH of 8.5 and 9, there was no noticeable change in the critical spindle speed. This observation could be because the reduction in bitumen-water interfacial tension at this pH range is insufficient to significantly impact the droplet deformation and influence the self-lubricated flow phenomenon. However, above pH 9, a higher shear rate was required to produce a self-lubricated flow. Figure 5.9 compares the result obtained at a shearing speed of 100 rpm at pH 8.5, 9.5, and 10. At the same speed, while self-lubricating flow was obtained at pH 8.5, imperfect and non-lubricating flow were obtained at pH 9.5 and pH 10, respectively.

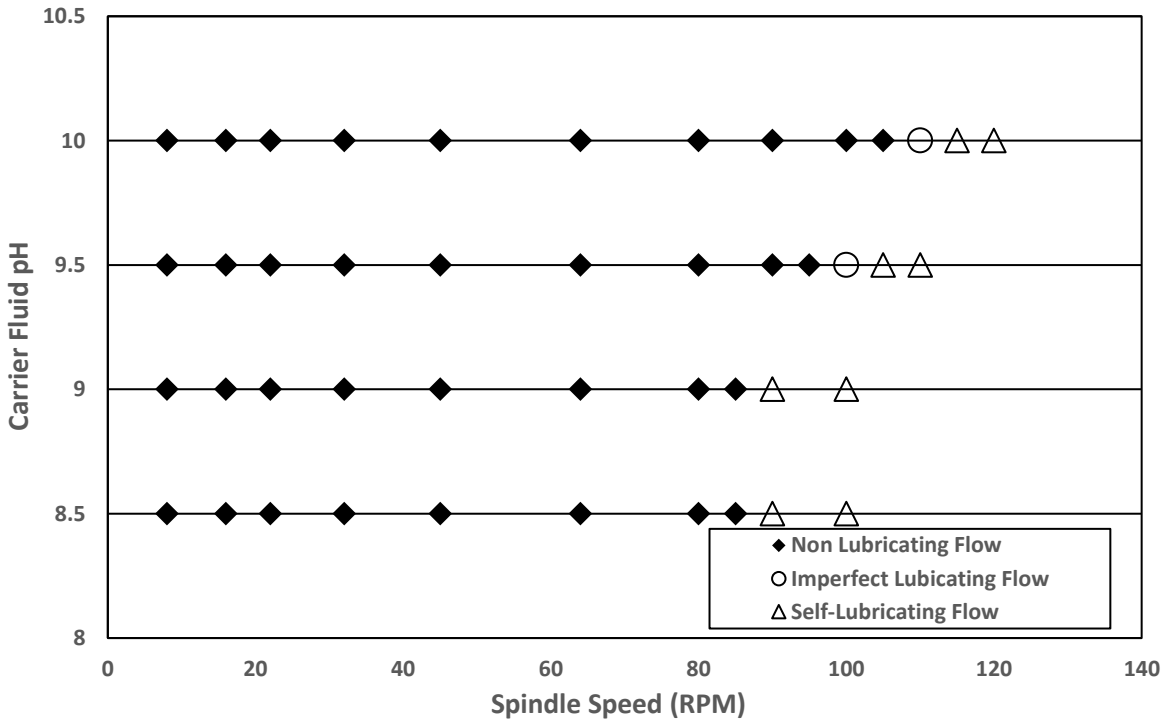

Figure 5.8: Effect of carrier fluid pH on froth lubrication. 30 wt.% water concentration. Bitumen froth B.

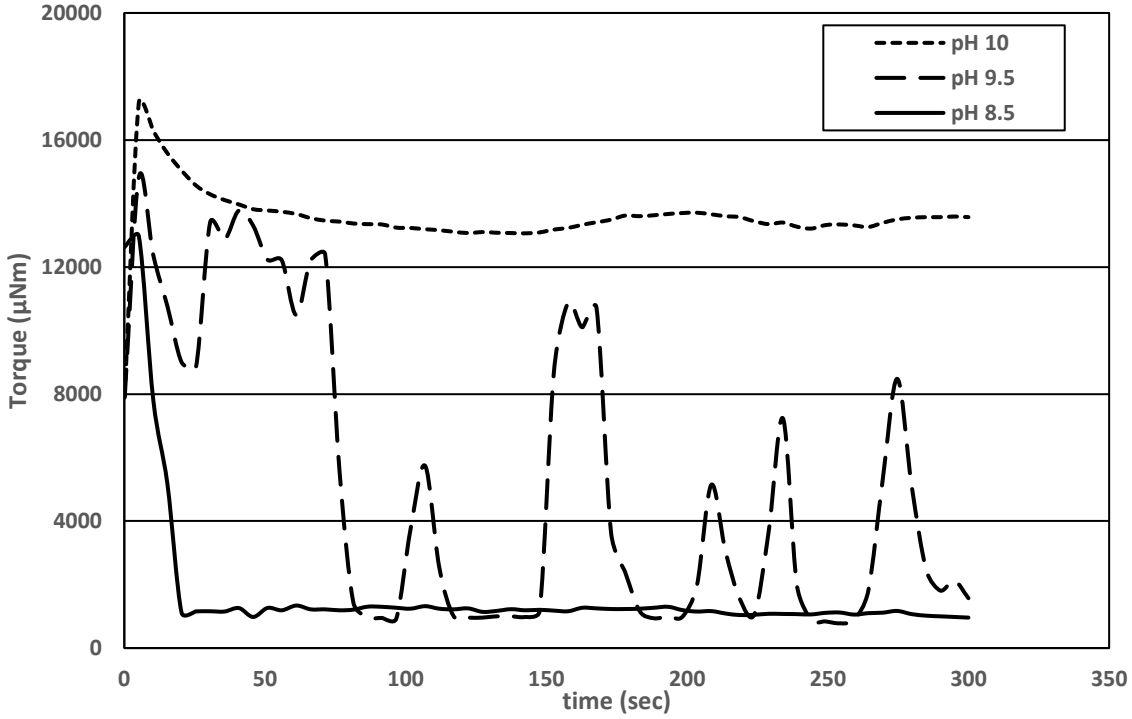

Figure 5.9: Effect of carrier fluid pH on froth lubrication at 100 rpm.

This observation can be attributed to the change in the interfacial properties of the bitumen froth associated with the increase in pH. Masliyah et al. [4] noted that when bitumen makes contact with the aqueous phase, the surface-active components migrate from the bulk bitumen phase to the bitumen-water interface. The migration is such that the hydrophilic head moves to the aqueous phase while the hydrophobic tail stays in the bitumen phase [4]. Thus, an increase in the pH of the aqueous phase facilitates the ionization of the carboxylic group (-COOH) of the surface-active molecules to carboxylate (-COO-), thereby decreasing the bitumen-water interfacial tension in the froth [55]. The reduction in the interfacial tension will reduce the thickness of the interfacial film and make the droplets less rigid. Consequently, the droplets will have less resistance to deformation by hydrodynamic forces and require a higher shear rate to facilitate their migration to form the lubricating water layer. In other words, the reduction in bitumen-water interfacial tension will decrease the amount of water released from the froth to produce the lubricating layer. An illustration demonstrating the influence of pH on bitumen-water interfacial tension, as presented by Wan et al. [45], can be found in Appendix F.

When the bitumen-water interfacial tension reduces due to the increase in pH, two likely conditions could result. The first is that the water droplets might migrate to the lubricating layer but find it difficult to remain in the layer due to the low bitumen-water interfacial tension. The droplets under this condition will move back and forth between the lubricating layer phase and the bulk bitumen froth phase, as in the case of imperfect self-lubricated flow. The second condition is that at a very low bitumen-water interfacial tension, the droplets will have no significant resistance to deformation, thus preventing any kind of migration to form a lubricating layer. In other words, the droplets will remain in the bitumen continuous phase, as in the case of non-lubricating flow. It is worth mentioning that the pH of the carrier fluid in bitumen production varies significantly, ranging between 8.5 and 9.5 [31]. The findings of this work show that the carrier fluid pH will significantly influence the self-lubricated froth flow mechanism within the pH range commonly encountered in industrial applications. Using the relationship between spindle speed and flow velocity in Couette flow and pipe flow, an increase in the pH of the carrier fluid from 8.5 to 9.5 will increase the flow velocity required to produce a self-lubricated flow by 16.7%.

5.4.2 Effect of Salt Concentration

The salt concentration in this work refers to the concentration of sodium chloride in the carrier fluid. The flow map of the results obtained for the experiments conducted on the effect of salt concentration on the self-lubrication of bitumen froth is presented in Figure 5.10. The result shows that the increase in salt concentration does not have any noticeable impact on the self-lubricating flow at 1205 ppm and 2000 ppm salt concentrations. The critical spindle speed at these salt concentrations is 90 rpm. This observation could be because the reduction in bitumen-water interfacial tension at this salt concentration is insufficient to significantly impact the droplets deformation and their resistance to hydrodynamic forces. However, at 3000 ppm salt concentration, the critical spindle speed for the self-lubricated flow increased to 110 rpm. This observation can be ascribed to the reduced resistance of the droplets to deformation due to the decrease in interfacial tension. Consequently, the shear conditions required to produce a self-lubricated flow will increase.

The reduction in interfacial tension can be attributed to the increase in surface activities of asphaltenes. This is because asphaltenes act like weak ionic surfactants. Thus, the increase in salt concentration will facilitate the ionization of the polar group in bitumen and decrease the bitumen-

water interfacial tension [41]. Rocha et al. [41] examined the effect of salt concentration on bitumen-water interfacial tension. In their study, they found a direct relationship between the increase in salt concentration and a reduction in the bitumen-water interfacial tension. An illustration demonstrating the influence of salt concentration on bitumen-water interfacial tension, as presented by Rocha et al. [41], can be found in Appendix F. As previously discussed, the resistance of the dispersed droplets to hydrodynamic forces is strongly dependent on the viscous and interfacial forces. While the hydrodynamic forces tend to deform the droplets and hinder their migration in the bitumen continuous phase, the viscous and interfacial forces prevent the droplet deformation. When the interfacial tension reduces due to the increase in salt concentration, the droplets will be less rigid and can be more easily deformed. A higher shear force will be required to facilitate the migration of the deformed droplets to produce the lubricating layer compared to rigid droplets. In other words, when the droplets are significantly deformed due to reduced interfacial tension, a higher spindle speed will be required to produce a self-lubricated flow. If the relationship between the Couette flow and pipe flow holds, an increase in the concentration of salt in the carrier fluid will increase the flow velocity required to produce a self-lubricated flow.

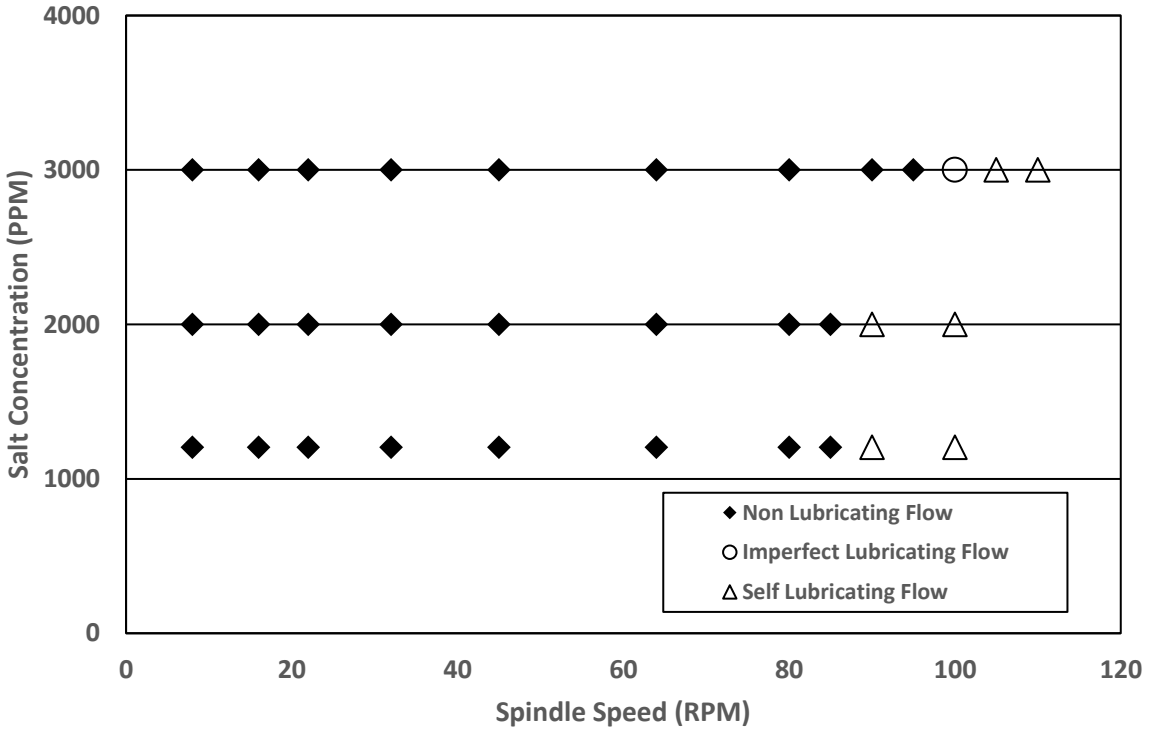

Figure 5.10: Effect of salt concentration on froth lubrication. 30 wt.% water concentration. Bitumen froth B.

5.4.3 Effect of Fines Concentration on Froth Lubrication

This section discusses the experiments conducted to investigate the effect of fines concentration on self-lubrication. Dry kaolinite clay was added to the bitumen froth during the preheating process. This was done to examine how the carrier fluid yield stress impact the self-lubricated flow. To determine the concentration of fines in the carrier fluid that will produce a non-Newtonian behaviour, some rheology tests were conducted by preparing kaolin suspensions at different fines concentrations. The aqueous phase of the suspension prepared has similar properties (pH and salt concentration) to the bitumen froth carrier fluid used for the experiments. The result of the kaolin suspension rheology test is shown in Figure 5.11.

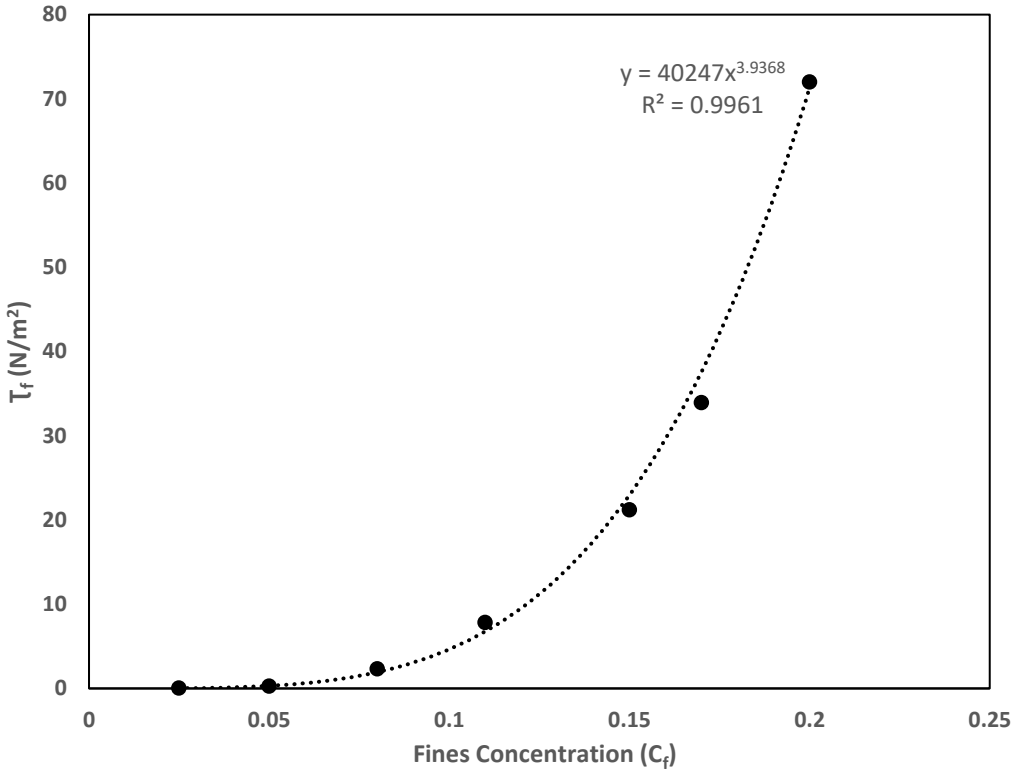

Figure 5.11: Kaolin suspension yield stress at different concentrations.

The rheology of the suspension changed from Newtonian to non-Newtonian around 5 vol% fines concentration. Thus, the experiment condition to test the impact of fines on froth lubrication was conducted around that range. The concentration of fines in the carrier fluid was adjusted to 4.1 vol% and 6.3 vol% by adding dry kaolin to the bitumen froth. Before the addition of fines, it

is assumed that the carrier fluid is Newtonian with negligible fine concentration. The experimental data presented in Figure 5.11 are fitted to obtain the following correlation to calculate the yield stress values for the system

$$\tau_f = 40247 C_f^{3.9} \qquad 5.5$$

The flow map for the effect of fines concentration on bitumen froth lubrication is presented in Figure 5.12 and Figure 5.13. Figure 5.12 represents the flow map when the initial concentration of fines in the carrier fluid was not considered, while Figure 5.13 represents the flow map when the initial concentration of fines in the carrier fluid is deemed to be 50% of the total solids in the bitumen froth. The vertical axis represents the yield stresses of the carrier fluid, while the horizontal axis represents the spindle speed at which experiments were conducted. Although the yield stress values in the two flow maps are slightly different, the trend of the result is consistent.

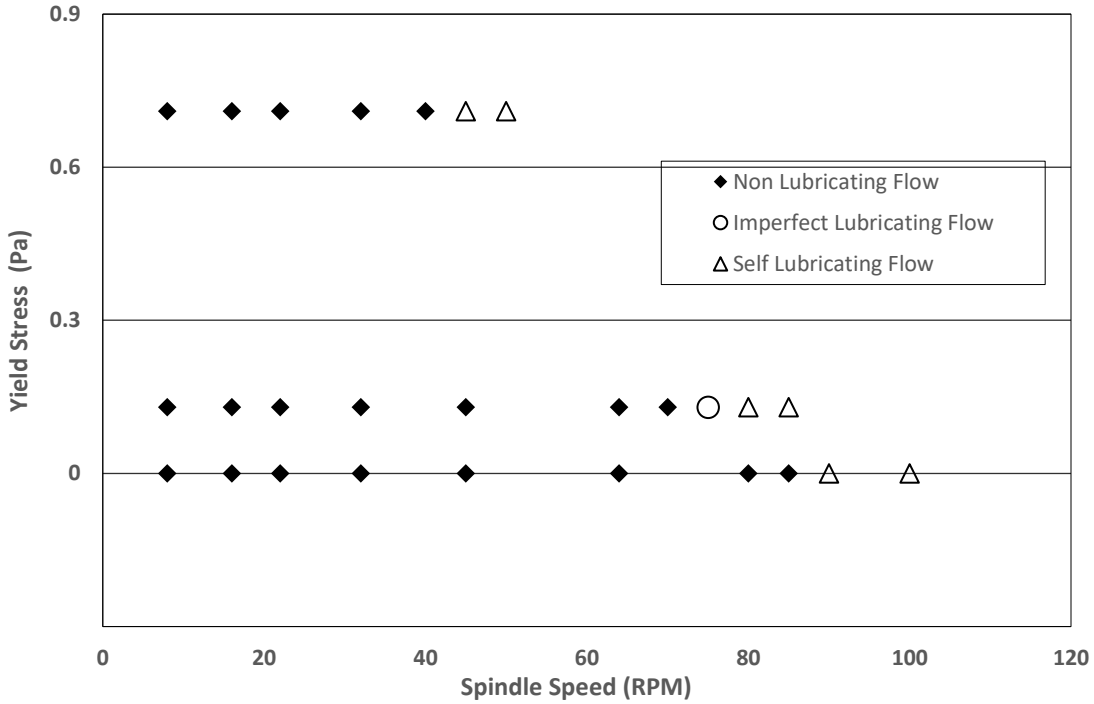

Figure 5.12: Flow map of the effect of bitumen froth carrier fluid fines concentration on self-lubrication without considering the initial concentration of fines in the bitumen froth carrier fluid. Bitumen froth B.

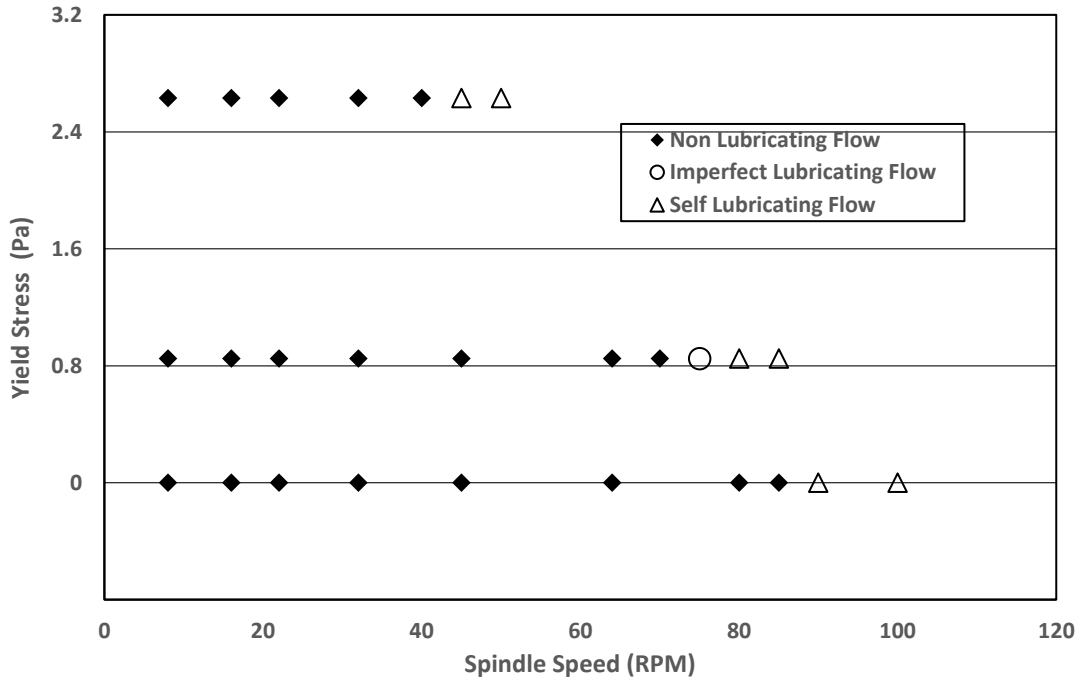

Figure 5.13: Flow map of the effect of bitumen froth carrier fluid fines concentration on self-lubrication considering the initial carrier fluid fines concentration in the bitumen froth. Bitumen froth B.

The result demonstrates that increasing the carrier fluid fines concentration reduces the shear rate required to produce a self-lubricated flow. This observation can be ascribed to the change in the rheological behavior of the carrier fluid from Newtonian to a non-Newtonian fluid with yield stress when the concentration of fines is increased. This is because the fines are hydrophilic and will end up in the aqueous phase. However, the uniformity of concentration of fines within each size range of droplets is uncertain. The increase in yield stress of the droplets will increase their resistance to deformation [38]. Allouche et al. [39] modelled the instability mechanism of the displacement of Bingham yield stress fluid by a low-viscosity Newtonian fluid using direct numerical simulations. They reported the yield stress fluid was more stable against deformation. Their observation demonstrates that the increase in yield stress will increase the resistance of the dispersed droplets to deformation, thereby making it easier for them to migrate to produce the lubricating layer when subjected to shear. In other words, the increase in the carrier fluid yield stress will reduce the spindle speed required to produce a self-lubricated flow. Additionally, at higher carrier fluid yield stress, the lubricating layer produced will also be more stable and will not break easily. This is due to the increased resistance to hydrodynamic forces. In other words,

the increase in carrier fluid yield increases the stability of the self-lubricated flow. A stable lubricating layer will help to reduce the bitumen wall fouling in pipelines, which can reduce the effective flow area and increase pressure losses [22]. This result demonstrates that an increase in fines concentration will reduce the flow velocity required to produce a stable self-lubricated flow in pipelines.

5.5 Self-Lubricated Flow Reversibility Test

The reversibility of the flow pattern observed in the self-lubricated flow experiment was examined at 55 ℃. This was done by gradually increasing the spindle speed (forward run) until the lubricating flow was attained and then decreasing the spindle speed (reverse run). It is evident from the result obtained that below the critical spindle speed, the droplets do not migrate to form the lubricating water layer. This is because the droplets require sufficient shear to overcome the hydrodynamic forces to migrate to the high-shear region to form the lubricating layer. The reversibility graphs for the forward run and the reverse run at 64 rpm, 80 rpm, and 90 rpm are presented in Figure 5.14 and Figure 5.15, respectively. A third forward run was also conducted right after the reverse run. All the results from the third run that was conducted by increasing the speed again in a stepwise manner resulted in non-lubricating flow as shown in Figure 5.16. The reason for this observation is due to the viscous heating effect. As a result of repeated shearing, heat is generated due to viscous friction, leading to an increase in froth temperature. Consequently, the viscosity ratio of the continuous phase to the dispersed phase will decrease, thereby increasing the shear rate needed to produce a self-lubricated flow.

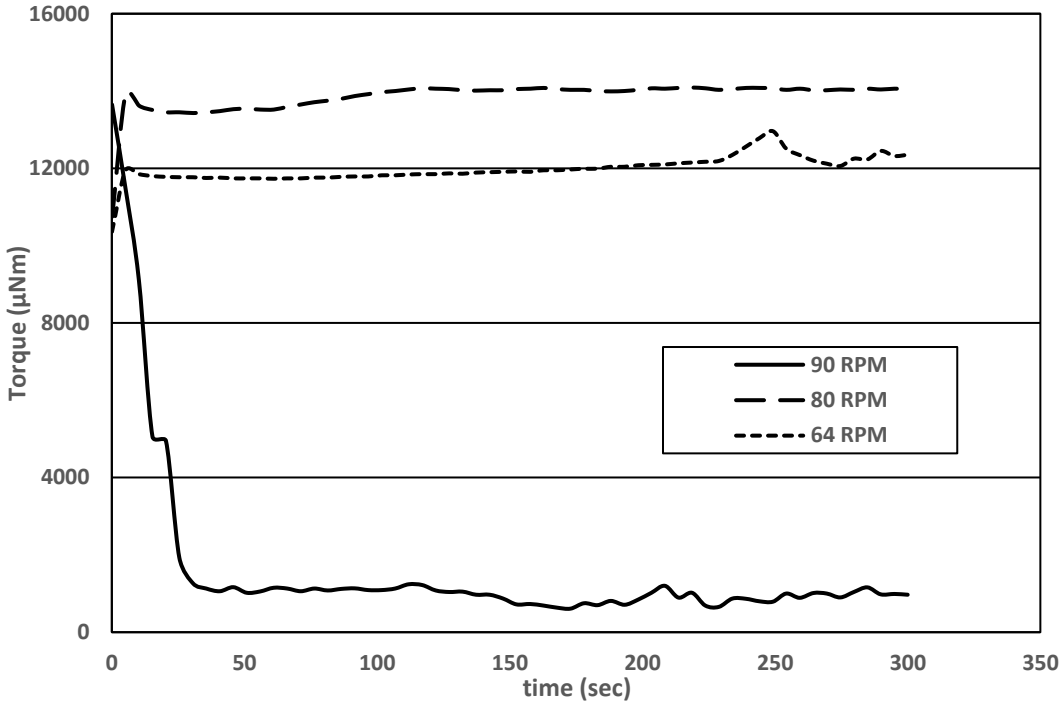

Figure 5.14: Bitumen froth reversibility test forward run (1). Increasing RPM (64 – 90). Bitumen froth B.

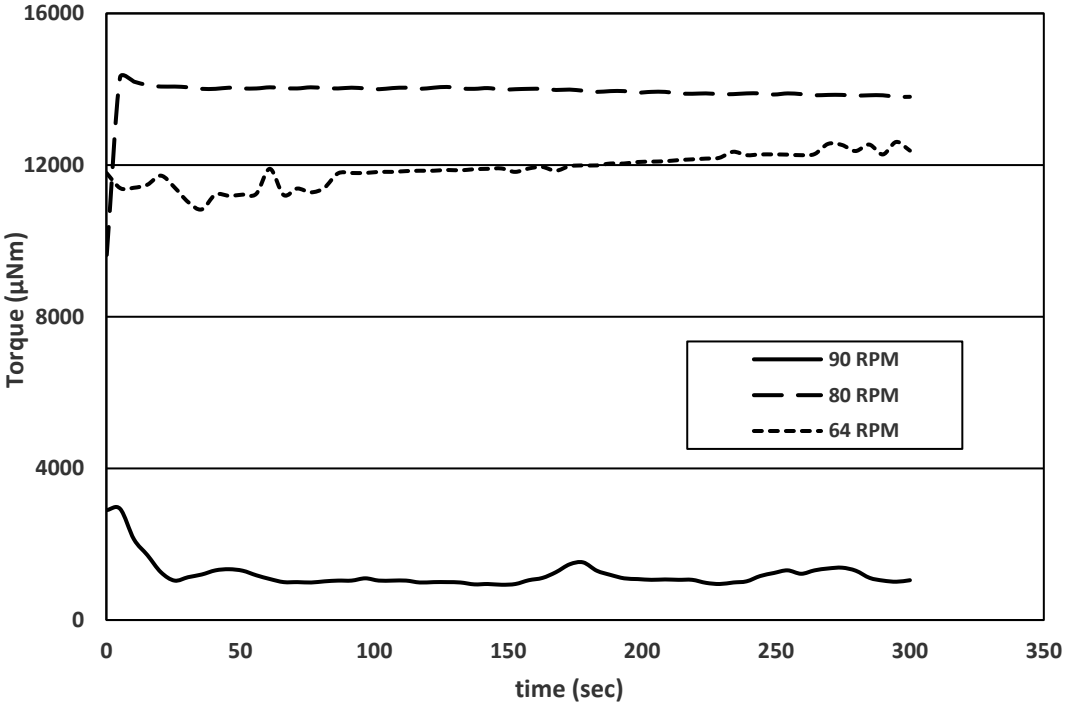

Figure 5.15: Bitumen froth reversibility test reverse run (2). Decreasing RPM (90 – 64). Bitumen froth B.

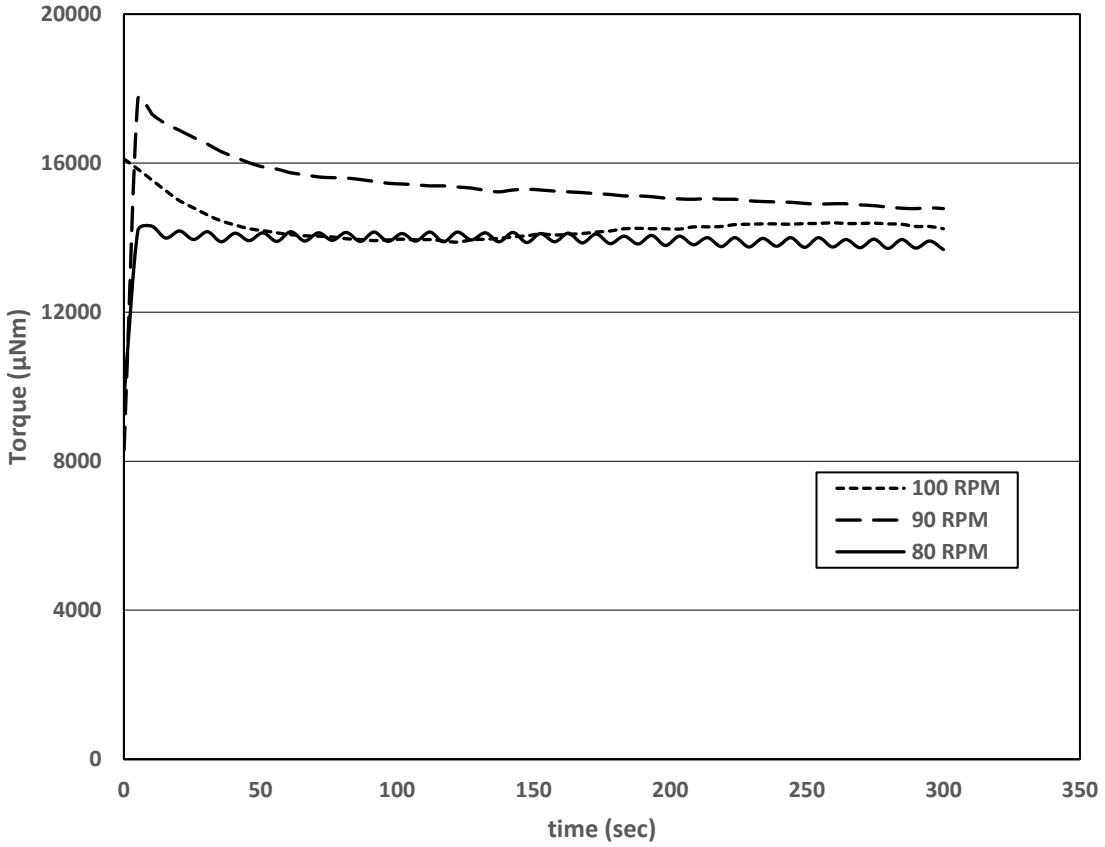

Figure 5.16: Bitumen froth reversibility test forward return run (3). Increasing RPM (80 – 100). Bitumen froth B.

It can be observed that at 90 rpm in Figure 5.15, the magnitude of torque reduction for the self-lubricating pattern obtained for the reverse run is less than that of the forward run. This is because the droplets are already in the lubricating layer region and do not have to start migrating from their initial positions in the froth.

The flow map for the reversibility tests is presented in Figure 5.17. The results show that the froth lubricating mechanism is reversible and indicates that the formation of the lubricating water layer is more driven by the migration of water droplets to the high shear region rather than coalescence. This observation is consistent with the findings of Bello [17]. The author noted that the critical spindle speed at which the self-lubricated flow is obtained is the same for both the forward and reverse runs in the reversibility tests conducted using water-in-oil emulsion as a bitumen froth analog.

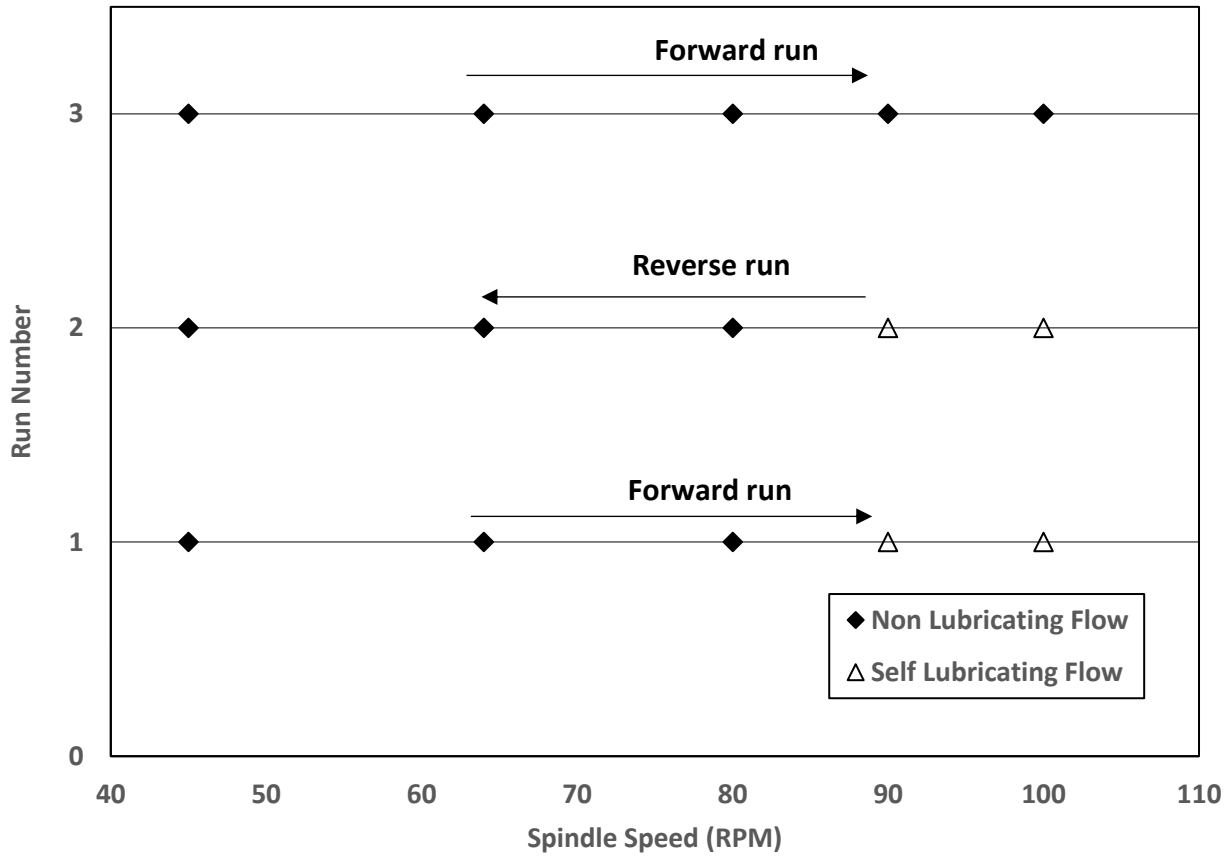

Figure 5.17: Bitumen froth reversibility test result. Bituen froth B.

5.6 Dimensionless Analysis

The Capillary number was used to characterize the different flow conditions observed in the experiments to deepen the understanding of the self-lubricated froth flow phenomenon. This dimensionless number quantifies the balance forces in a multiphase flow [63]

$$\mathrm{Ca} = \frac{\mu_o U}{\sigma} . \frac{\mu_o}{\mu_d}. \tag{5.6}$$

where μ_o and μ_d represent the viscosities of the continuous bitumen and dispersed water phases, respectively, σ represents the bitumen-water interfacial tension, and U is the velocity of the inner spindle calculated using

$$\mathrm{U} = \omega \mathrm{r} \tag{5.7}$$

$$\omega = \frac{2\pi n}{60} \tag{5.8}$$

The bitumen-water interfacial tensions at different pH, salt concentrations, and temperatures were obtained from the previous studies conducted in the literature [41,55,64]. For the fines concentration analysis, all the fines were assumed to be in the aqueous phase because they are hydrophilic. Table 5.2 presents the parameters that were used for the dimensionless analysis. The carrier fluid viscosity was obtained from Figure 5.17 using the correlation

$$\mu_d = 2\exp(11.622C_f) \tag{5.9}$$

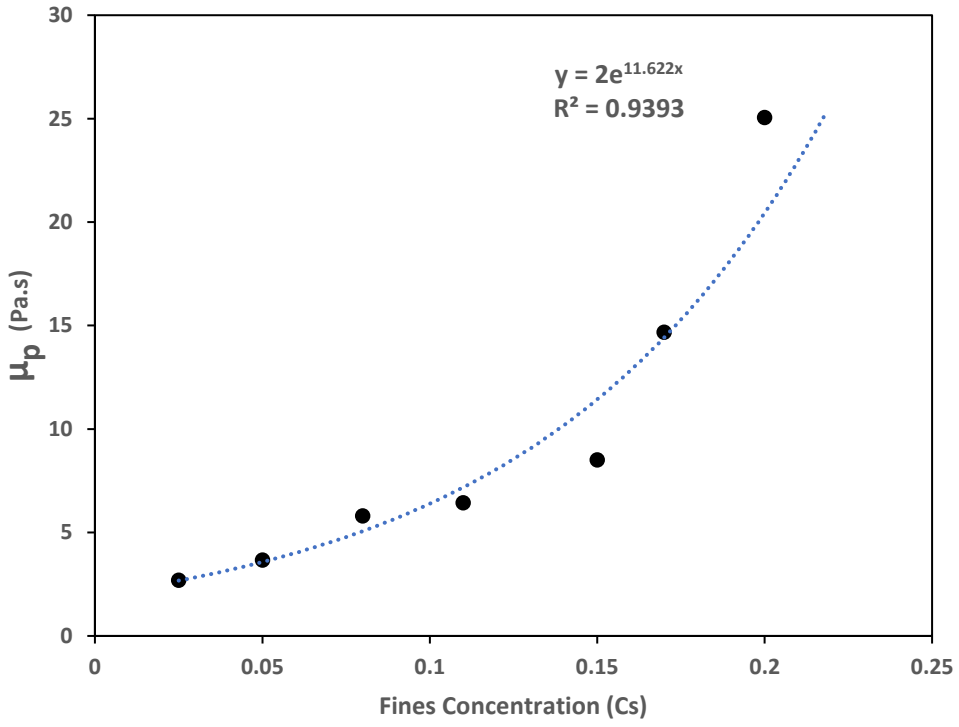

Figure 5.17: Kaolin suspension viscosity at different fine concentrations.

The result obtained from the dimensionless analysis is presented in Figure 5.18. The vertical axis represents the Capillary number, and the horizontal axis shows the critical spindle speed at which the self-lubricated flow was obtained under different experimental conditions. The result shows that the capillary number varies significantly under different conditions. The dominant forces are

the viscous force and the interfacial force. At a constant continuous phase viscosity, the interfacial tension plays the dominant role in determining the lubricated flow behavior. The significant variation in the capillary number at different pH and salt concentrations demonstrates how much the interfacial forces impact the balance of forces in the system and influence the self-lubricated flow phenomenon.

Table 5.2: Parameters used for the dimensionless analysis.

Parameter	Condition	Critical Spindle Speed	Interfacial tension (N/m)	μ_o (Pa.s)	μ_d (mPa.s)
Temperature (℃)	50	90	0.0151	11.20	0.5465
	55	128	0.0148	6.49	0.5036
	60	164	0.0144	5.06	0.466
Fines Conc (Vol%) In the carrier fluid.	0	90	0.0148	6.49	0.5036
	4.1	80			3.22
	6.3	45			4.16
Salt Concentration (ppm)	1205	90	0.0215	6.49	0.5036
	2000	90	0.0204		
	3000	105	0.0195		
pH	8.5	90	0.0091	6.49	0.5036
	9	90	0.0077		
	9.5	105	0.0065		
	10	115	0.0052		

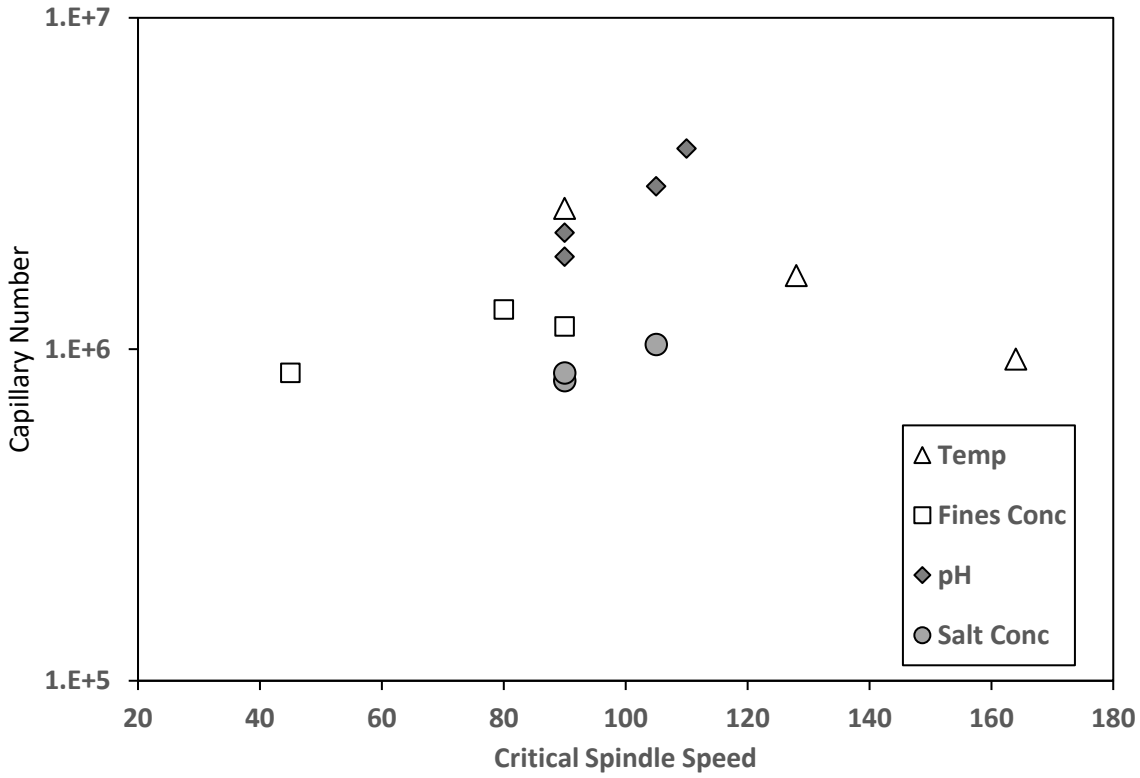

Figure 5.18: Capillary Number at different Critical Spindle Speeds.

The capillary number shows different trends for temperature and fines concentration effects even though the viscous force is dominant under these two conditions. This observation is likely due to the contribution of the yield stress of the carrier fluid. The increase in fine concentration increases the carrier fluid yield stress and makes the droplets more resistant to deformation. Consequently, the critical spindle speed required to produce a self-lubricated flow decreases. Hence, the inconsistency of the pattern of the capillary number for the viscous force dominant regime could be because the capillary number did not consider the viscous force contribution of the carrier fluid yield stress. This analysis demonstrates that viscous and interfacial forces play significant roles in the self-lubricated froth flow phenomenon. Future studies should include the yield stress contribution of the carrier fluid to increase the accuracy of the dimensionless analysis.

Chapter 6 Conclusions and Recommendations

6.1 Conclusions

This work investigated the factors affecting self-lubricated froth flow using a Couette flow device. The different flow patterns observed were classified, and flow maps were developed to categorize the flow conditions. The results obtained from this work broadened the understanding of the factors that are critical to the mechanism of self-lubrication.

The conclusions drawn from this study are summarized as follows:

- The critical spindle speed required to produce self-lubricating flow increases with the increase in the pH of the carrier fluid. The reason for this could be attributed to the reduction in the bitumen-water interfacial tension. This will decrease the resistance of the droplets to deformation by the hydrodynamic forces and increase the spindle speed required to produce the self-lubricated flow.
- The increase in carrier fluid salts concentration increases the spindle speed required to produce a self-lubricated flow. This observation can be ascribed to the reduced rigidity of the droplets due to the decrease in bitumen-water interfacial tension.
- The increase in fines concentration increases the stability of the self-lubricated flow. The reason for this is due to the increased resistance of the droplets to deformation because of the increase in yield stress. Consequently, a lower shear rate is required to produce the self-lubricated flow.
- The reversibility tests conducted at a constant temperature show that the self-lubricating flow is reversible. This observation indicates that the self-lubricating flow mechanism is more driven by the migration of water droplets to the high shear region rather than the coalescence of the dispersed water droplets to form a continuous water layer. It is not known if this observation applies only to Couette flows or if it also applies to pipeline flows.

6.2 Novel Contributions

This study addresses a significant research gap that has been largely overlooked in the literature. While numerous studies have explored factors affecting the self-lubrication mechanism

of bitumen froth, the influence of carrier fluid properties has not been investigated. Specifically, the impact of carrier fluid pH, salt concentration, and fines concentration on self-lubricated flow remains unexplored in the literature. A procedure was developed to study the effect of carrier fluid properties on self-lubricated froth flow using a concentric cylinder viscometer. The current study shows a connection between the interfacial properties of the bitumen froth and the self-lubricated froth flow phenomenon. Additionally, this study demonstrated how the yield stress of the carrier fluid impacts the stability of the self-lubricated flow. The findings of this work provide more information on the optimum condition required to operate a stable self-lubricated flow.

6.3 Limitations and Uncertainties

The limitations and uncertainties associated with this research are as follows:

- Important properties of the carrier fluid such as interfacial tension and rheology are assumed and not measured.
- It is not known if the distribution of the added fines and ions among the different droplet sizes in the froth is uniform or non-uniform.
- The change in dispersed phase viscosity and interfacial tension was not measured after the experiments.
- Important bitumen properties such as viscosity and asphaltene content were not measured.
- Possible differences between the concentric cylinder viscometer and pipelines may exist, in terms of self-lubricated flow regime. While the self-lubricated flow mechanism in pipe flows involves turbulent flow and droplet coalescence to produce a continuous lubricating water layer, it is likely that chains of droplets produce the self-lubricated laminar flow in the concentric cylinder viscometer.

6.4 Industrial Implications

Most existing studies have emphasized that friction losses and wall fouling in self-lubricated pipeline transport of bitumen froth are primarily determined by parameters such as velocity, water concentration, and oil-water viscosity ratio. However, the findings of this work have shown how the bitumen froth carrier fluid properties, specifically pH, salts concentration, and carrier fluid yield stress, significantly impact self-lubricated froth flow. The results of this study are directly applicable to oil sands companies operating a bitumen froth pipeline. It provides more information

on the conditions necessary to maintain a stable self-lubricated flow when transporting bitumen froth from the extraction site to the froth treatment and upgrading facilities. To put this in perspective, if the connection between the Couette cell and the pipe flow holds, an increase in the pH of the carrier fluid from 8.5 to 9.5 will increase the flow velocity required to produce a self-lubricated flow by 16.7%. Similarly, an increase in carrier fluid yield stress from 0.13 Pa to 0.71 Pa will reduce the flow velocity required to maintain a stable self-lubricated flow by 43.8 %. This work provides crucial information on how to reduce friction loss and wall fouling associated with self-lubricated pipeline transport of bitumen froth.

6.5 Recommendations for Future Work

The following recommendations are suggested for future work on this subject:

- **Study of Carrier Fluid Properties in Pipelines:** Further investigations should be conducted on the effects of carrier fluid properties on self-lubricated froth flow in an actual pipeline. This will provide more information on how to scale up the laboratory experiments to the conditions encountered in industrial applications. Additionally, properties of the carrier fluid such as interfacial tension and rheology should be measured before and after the experiments.
- **Critical bitumen-water interfacial Tension**: Further studies should be conducted to accurately measure the bitumen-water interfacial tension at different pH, salt concentration, and temperature. This will provide information on the critical bitumen-water interfacial tension required to maintain a stable self-lubricated flow.
- **Free water fraction**: More studies should be conducted to examine the effect of carrier fluid properties on the fraction of water released from the froth to form the lubricating layer (free water fraction). This can be achieved by using the holdup measurement test procedure described by Joseph et al. [18]. This will make it possible to quantitively determine how the change in carrier fluid properties impacts the free water fraction.
- **Improved characterization of self-lubricated flow using Dimensionless Capillary Number:** Further research should be conducted to characterize the self-lubricated flow behavior in pipe flow and Couette flow using the dimensionless capillary number. The analysis should include the viscous force contribution by the carrier fluid yield stress.

Additionally, the analysis should be done using the actual bitumen froth's interfacial properties instead of using the data obtained from different experimental conditions in the literature. This analysis will help to provide a direct relationship between the pipe flow and Couette flow since the capillary number is dimensionless, it is geometry independent.

- **Improved characterization of bitumen properties:** Future studies on self-lubricated froth flow should consider the characterization of important properties of bitumen such as asphaltenes. This is very important because asphaltenes significantly impact bitumen-water interfacial tension. This can be achieved by using the procedure reported by Rocha et al. [41].

References

[1] J.D. Miller, M. Misra, Hot water process development for Utah tar sands, Fuel Process. Technol. 6 (1982) 27–59. https://doi.org/10.1016/0378-3820(82)90038-8.

[2] F. Rao, Q. Liu, Froth treatment in athabasca oil sands bitumen recovery process: A review, Energy and Fuels. 27 (2013) 7199–7207. https://doi.org/10.1021/ef4016697.

[3] S. Ren, H. Zhao, J. Long, Z. Xu, J. Masliyah, Understanding weathering of oil sands ores by atomic force microscopy, AIChE J. (2009). https://doi.org/10.1002/aic.12000.

[4] J.Z. Masliyah, Jacob H.; Czarnecki, Handbook on Theory and Practice of Bitumen Recovery from Athabasca Oil Sands, Kingsley Knowledge Publishing, 2011.

[5] R.. Santos, W. Loh, A.. Bannwart, O.. Trevisan, An overview of heavy oil properties and its recovery and transportation methods, Brazilian J. Chem. Eng. 31 (2014) 571–590. https://doi.org/dx.doi.org/10.1590/0104-6632.20140313s00001853.

[6] S.M. Jordaan, Land and Water Impacts of Oil Sands Production in Alberta, (2012). https://doi.org/10.1021/es203682m.

[7] M.G. Dubé, J.M. Dunlop, C. Davidson, D.L. Beausoleil, R.R.O. Hazewinkel, F. Wyatt, History, overview, and governance of environmental monitoring in the oil sands region of Alberta, Canada, Integr. Environ. Assess. Manag. 18 (2022) 319–332. https://doi.org/10.1002/IEAM.4490.

[8] C. Wu, A. De Visscher, I.D. Gates, On naphthenic acids removal from crude oil and oil sands process-affected water, Fuel. 253 (2019) 1229–1246. https://doi.org/10.1016/J.FUEL.2019.05.091.

[9] A.D. Charpentier, J.A. Bergerson, H.L. MacLean, Understanding the Canadian oil sands industry's greenhouse gas emissions, Environ. Res. Lett. 4 (2009). https://doi.org/10.1088/1748-9326/4/1/014005.

[10] A. Betancourt-Torcat, A. Elkamel, L. Ricardez-Sandoval, Optimal integration of nuclear energy and water management into the oil sands operations, AIChE J. (2012). https://doi.org/10.1002/aic.13736.

[11] D. Kosior, E. Ngo, Y. Xu, Aggregates in Paraffinic Froth Treatment: Settling Properties and Structure, Energy and Fuels. 32 (2018) 8268–8276. https://doi.org/10.1021/acs.energyfuels.8b01656.

[12] R. Xing, D. V. Chiappori, E.J. Arbuckle, M.T. Binsted, E.G.R. Davies, Canadian oil sands

extraction and upgrading: A synthesis of the data on energy consumption, co2 emissions, and supply costs, Energies. 14 (2021). https://doi.org/10.3390/en14196374.

[13] B. Bayestehparvin, J. Abedi, S.M. Farouq Ali, Dissolution and mobilization of bitumen at pore scale, Soc. Pet. Eng. - SPE Canada Heavy Oil Tech. Conf. 2015, CHOC 2015. (2015) 157–179. https://doi.org/https://doi.org/10.2118/174482-MS.

[14] Y. Wang, S. Ren, Synergistic effect of water layer and divalent metal ions in a model oil sand on bitumen liberation from solids surface, J. Dispers. Sci. Technol. 40 (2019) 1300–1307. https://doi.org/10.1080/01932691.2018.1510784.

[15] R.S.S. Sanders, T. Ko, R. Bai, D.D.D. Joseph, Factors Governing Friction Losses in Self-lubricated Transport of Bitumen Froth: 1. Water Release, 82 (2004) 735–742. https://doi.org/https://doi.org/10.1002/cjce.5450820412.

[16] H. Li, J. Long, Z. Xu, J.H. Masliyah, Novel polymer aids for low-grade oil sand ore processing, Can. J. Chem. Eng. 86 (2008) 168–176. https://doi.org/10.1002/cjce.20030.

[17] R. Bello, Water-Lubricated Oil Flows In A Couette Apparatus, University of Saskatchewan, 2004.

[18] D.D. Joseph, R. Bai, C. Mata, K. Sury, C. Grant, Self lubricated transport of bitumen froth, J. Fluid Mech. 386 (1999) 1–38. https://doi.org/DOI: https://doi.org/10.1017/S0022112099004413.

[19] S. Rushd, M. McKibben, R.S. Sanders, A new approach to model friction losses in the water-assisted pipeline transportation of heavy oil and bitumen, Can. J. Chem. Eng. 97 (2019) 2347–2358. https://doi.org/DOI 10.1002/cjce.23492.

[20] M.E. Charles, G.W. Govier, G.W. Hodgson, The Horizontal Pipeline Flow of Equal Density Oil Water Mixtures, Can. J. Chem. Eng. 39 (1961) 27–36. https://doi.org/https://doi.org/10.1002/cjce.5450390106.

[21] R. Bai, K. Chen, D.D. Joseph, Lubricated pipelining: Stability of core—annular flow. Part 5. Experiments and comparison with theory, J. Fluid Mech. 240 (1992) 97–132. https://doi.org/10.1017/S0022112092000041.

[22] R. Sayeed, A New Approach To Model Friction Losses In The Water-Assisted Pipeline Transportation Of Heavy Oil and Bitumen, University of Alberta, 2016.

[23] K. Chen, R. Bai, D.D. Joseph, Lubricated pipelining. Part 3 Stability of core-annular flow in vertical pipes, J. Fluid Mech. 214 (1990) 251.

https://doi.org/10.1017/S0022112090000131.

[24] H. Al-Awadi, Multiphase Characteristics of High Viscosity Oil, Cranfield University, 2011.

[25] J. Jing, X. Yin, B.N. Mastobaev, A.R. Valeev, J. Sun, S. Wang, H. Liu, L. Zhuang, Experimental study on highly viscous oil-water annular flow in a horizontal pipe with 90° elbow, Int. J. Multiph. Flow. 135 (2021) 103499. https://doi.org/10.1016/j.ijmultiphaseflow.2020.103499.

[26] R. Sayeed, S. Rasel, M. Shahriar, Modeling Friction Losses in the Water-Assisted Pipeline Transportation of Heavy Oil, IntechOpen. (2019) 1–21. https://doi.org/http://dx.doi.org/10.5772/intechopen.82356.

[27] D.D. Joseph, R. Bai, K.P. Chen, Core-Annular Flows, Ann.Rev. Fluid Mech. 29 (1997) 65–90. https://doi.org/https://doi.org/10.1146/annurev.fluid.29.1.65.

[28] M.S. Arney, G.S. Ribeiro, E. Guevara, R. Bai, D.D. Joseph, Cement Lined Pipes For Water Lubricated, Int. J. Multiph. Flow. 22 (1996) 207–221. https://doi.org/https://doi.org/10.1016/0301-9322(95)00064-X.

[29] M. McKibben, R. Gillies, S. Sanders, A new method for predicting friction losses and solids deposition during the water-assisted pipeline transport of heavy oils and co-produced sand, Soc. Pet. Eng. - SPE Heavy Oil Conf. Canada 2013. 2 (2013) 1218–1228. https://doi.org/10.2118/165480-ms.

[30] P.C.H. Chan, L.G. Leal, An experimental study of drop migration in shear flow between concentric cylinders, Int. J. Multiph. Flow. 7 (1981) 83–99. https://doi.org/10.1016/0301-9322(81)90016-1.

[31] J. Smith, Measurement of Carrier Fluid Viscosities for Oil Sand Extraction and Tailings Slurries, University of Alberta, 2013.

[32] G.I. Khan, Measurement of Carrier Fluid Viscosities of Oil Sand Slurries, University of Alberta, 2019.

[33] F. Bjornseth, Heavy Oil Production Technology Challenges and the Effect of Nano Sized Metals on the Viscosity of Heavy Oil: A literature review and an experimental study, Norwegian University of Science and Technology, 2013.

[34] P.B. Dehkordi, Experimental and numerical analysis of multiphase flow within horizontal pipeline with variable cross-sectional area, Politecnico Di Milano A, 2017.

[35] A. Hart, A review of technologies for transporting heavy crude oil and bitumen via

pipelines, J. Pet. Explor. Prod. Technol. 4 (2014) 327–336. https://doi.org/10.1007/s13202-013-0086-6.

[36] I. Dubdub, S. Rushd, M. Al-Yaari, E. Ahmed, Application of ANN to the water-lubricated flow of non-conventional crude, Chem. Eng. Commun. 209 (2022) 47–61. https://doi.org/10.1080/00986445.2020.1823842.

[37] O. Kaminsky, Heather; Thomas, Etsell;Douglas, Ivey;Oladipo, Characterization of clay minerals in froth , middlings and tailings streams produced by hot water extraction of Athabasca oil sands, in: Conf. PDMIW 07, 2014: pp. 1–29.

[38] M. Zare, A. Roustaei, I.A. Frigaard, Buoyancy effects on micro-annulus formation: Density stable displacement of Newtonian–Bingham fluids, J. Nonnewton. Fluid Mech. 247 (2017) 22–40. https://doi.org/10.1016/J.JNNFM.2017.06.002.

[39] M. ALLOUCHE, I.A. FRIGAARD, G. SONA, Static wall layers in the displacement of two visco-plastic fluids in a plane channel, J. Fluid Mech. 424 (2000) 243–277. https://doi.org/10.1017/S0022112000001956.

[40] A. Cabrera, Sandra; Winnubst, Louis;Richter, Hannes;Voist, Ingolf;Nijmeijer, Industrial application of ceramic nanofiltration membranes for water treatment in oil sands mines, Sep. Purif. Technol. 256 (2021) 1–13.

[41] J.A. Rocha, E.N. Baydak, H.W. Yarranton, D.M. Sztukowski, V. Ali-Marcano, L. Gong, C. Shi, H. Zeng, R. Arrieta, Role of Aqueous Phase Chemistry, Interfacial Film Properties, and Surface Coverage in Stabilizing Water-in-Bitumen Emulsions, Energy and Fuels. 30 (2016) 5240–5252. https://doi.org/10.1021/acs.energyfuels.6b00114.

[42] T. Jiang, G.J. Hirasaki, C.A. Miller, S. Ng, Effects of Clay Wettability and Process Variables on Separation of Diluted Bitumen Emulsion, Energy & Fuels. 25 (2011) 545–554. https://doi.org/10.1021/ef101085j.

[43] S.K. Kiran, S. Ng, E.J. Acosta, Impact of Asphaltenes and Naphthenic Amphiphiles on the Phase Behavior of Solvent−Bitumen−Water Systems, Energy & Fuels. 25 (2011) 2223–2231. https://doi.org/10.1021/ef1016285.

[44] J. Shi, H. Al-Awadi, H. Yeung, An experimental investigation of high-viscosity oil-water flow in a horizontal pipe, Can. J. Chem. Eng. 95 (2017) 2423–2434. https://doi.org/10.1002/cjce.22903.

[45] L. Wang, T. Dang-Vu, Z. Xu, J.H. Masliyah, Use of short-chain amine in processing of

weathered/oxidized oil sands ores, Energy and Fuels. 24 (2010) 3581–3588. https://doi.org/10.1021/ef100243n.

[46] S. Poteau, J.-F.F. Argillier, D. Langevin, F. Pincet, E. Perez, Influence of pH on stability and dynamic properties of asphaltenes and other amphiphilic molecules at the oil-water interface, Energy and Fuels. 19 (2005) 1337–1341. https://doi.org/10.1021/ef0497560.

[47] S. Keleşoğlu, P. Meakin, J. Sjöblom, Effect of Aqueous Phase pH on the Dynamic Interfacial Tension of Acidic Crude Oils and Myristic Acid in Dodecane, J. Dispers. Sci. Technol. 32 (2011) 1682–1691. https://doi.org/10.1080/01932691.2010.516416.

[48] R.J. Phillips, R.C. Armstrong, R.A. Brown, A.L. Graham, J.R. Abbott, A constitutive equation for concentrated suspensions that accounts for shear-induced particle migration, Phys. Fluids A. 4 (1992) 30–40. https://doi.org/10.1063/1.858498.

[49] Z.M. Aman, A. Haber, N.N.A. Ling, A. Thornton, M.L. Johns, E.F. May, Effect of brine salinity on the stability of hydrate-in-oil dispersions and water-in-oil emulsions, Energy and Fuels. 29 (2015) 7948–7955. https://doi.org/10.1021/acs.energyfuels.5b02277.

[50] C. Gabard, J.-P. Hulin, Miscible displacement of non-Newtonian fluids in a vertical tube, Eur. Phys. J. E. 11 (2003) 231–241. https://doi.org/10.1140/epje/i2003-10016-8.

[51] D. Joseph, IUTAM Symposium on Lubricated Transport of Viscous Materials, Springer Netherlands, Dordrecht, 1998. https://doi.org/10.1007/978-94-011-5248-8.

[52] A.C. Bannwart, Modeling aspects of oil-water core-annular flows, J. Pet. Sci. Eng. 32 (2001) 127–143.

[53] R. Rhoheth, The effects of viscosity on core-annular flow, Delft University of Technology, 2016.

[54] G. Ooms, A. Segal, A.J. van der Wees, R. Meerhoff, R.V.A. Oliemans, A theoretical model for core-annular flow of a very viscous oil core and a water annulus through a horizontal pipe, Int. J. Multiph. Flow. 10 (1983) 41–60. https://doi.org/https://doi.org/10.1016/0301-9322(83)90059-9.

[55] K. Moran, A. Yeung, J. Czarnecki, J. Masliyah, Micron-scale tensiometry for studying density-matched and highly viscous fluids - With application to bitumen-in-water emulsions, Colloids Surfaces A Physicochem. Eng. Asp. 174 (2000) 147–157. https://doi.org/10.1016/S0927-7757(00)00507-0.

[56] H. Rahman, Yield Stresses of Mixtures with Bimodal Size Distributions, University of

Alberta, 2011.

[57] G.P. Laplante, On Mixing and Demulsifier Performance in Oil Sands Froth Treatment, University of Alberta, 2011.

[58] R.S. Shook, C.A., Gillies, R.G., Sanders, Pipeline Hydrotransport with Applications in the Oil Sand Industry, Saskatoon: Saskatchewan Research Council, 2002.

[59] Y. Pan, Y. Xu, L. Zhu, X. Liu, G. Zhao, S. Wang, L. Yang, T. Ma, H. Liu, Stability and rheological properties of water-in-oil (W/O) emulsions prepared with a soyasaponin-PGPR system, Futur. Foods. 4 (2021) 100096. https://doi.org/10.1016/J.FUFO.2021.100096.

[60] W. Wang, J. Gong, P. Angeli, Investigation on heavy crude-water two phase flow and related flow characteristics, Int. J. Multiph. Flow. 37 (2011) 1156–1164. https://doi.org/10.1016/j.ijmultiphaseflow.2011.05.011.

[61] H. Nourozieh, M. Kariznovi, J. Abedi, Density and Viscosity of Athabasca Bitumen Samples at Temperatures Up to 200°C and Pressures Up to 10 MPa, SPE Reserv. Eval. Eng. 18 (2015) 375–386. https://doi.org/10.2118/176026-PA.

[62] D.G. Thomas, Transport characteristics of suspension: VIII. A note on the viscosity of Newtonian suspensions of uniform spherical particles, J. Colloid Sci. 20 (1965) 267–277. https://doi.org/10.1016/0095-8522(65)90016-4.

[63] J. Gunther, Axel; Klavs, Multiphase microfluidics : from flow characteristics to chemical and materials synthesis, 6 (2006) 1487–1503. https://doi.org/https://doi.org/10.1039/b609851g.

[64] E.E. Isaacs, K.F. Smolek, Interfacial Tension Behavior of Athabasca Bitumen/Aqueous Surfactant Systems, Can. J. Chem. Eng. 61 (1983) 233–240. https://doi.org/10.1002/cjce.5450610215.

Appendix A – Safe work procedures

Safe work procedure (SWP) Pipeline Transport Processes Research Group

Laboratories: LAB2-151, LAB 2-156, LAB 3-121 CME building

Job title: Emulsion shear measurement	**Date:** July 16, 2021
Written by: Mubarak Gbadamosi	**Conducted by**: Mubarak Gbadamosi

Required Personal Protective Equipment (PPE): Facemask, safety glasses, hand gloves, closed-toe shoes, Lab coat
First Aid Measures: First aid kit, large spill kit and fire extinguisher.

Materials:

- Microscope slide & Cover slip
- PYREX beaker
- Funnel
- Graduated cylinder
- Plastic gloves

Equipment:

- Electronic scale balance
- Homogenizer
- Water bath
- Concentric cylinder viscometer.

Procedure

SN	Sequence of SWP steps	Potential hazards
1	**Viscosity measurement (VT 550 Viscometer)** • Measure the oil sample with a graduated cylinder and pour the sample inside the cup (outer cylinder).	Oil spill and splash due to rotation between cup and spindle and inappropriate tightening.

	• Pour the oil sample into the viscometer cup to a designated level. • Check the oil level in the cylinder to ensure that the volume of the oil poured touches the datum line for the selected spindle. • Attach the rotating spindle firmly to the cup by tightening the bolt, and check the connections to ensure the spindle is well tightened to the viscometer rotor. • Turn on the water bath and set it to the desired temperature using the control system. • Turn on the computer to control the operation mode of the viscometer using RheoWin Job Manager. • Shear the oil sample with the spindle and monitor the torque at different spindle speed. • Obtain the data for each test using the RheoWin Data Manager.	Spill Kit, paper towel, clean-up bucket, first aid kit and mops should be available nearby. Use full PPE
2	**Emulsion Preparation (Homogenizer VWR 250)** • Draw up some oil sample in to a secondary container for easier use. • Measure 90, 75 and 70 wt.% oil sample in different beakers. • Measure 10, 25, and 30 wt.% water in a separate beaker. • Label each beaker to indicate the oil and water quantity. • Check the homogenizer to ensure that it is in adequate working condition. Inspect the cables to ascertain that there is no defect. • Add the water slowly into the oil under the action of the homogenizer. Shear the oil/water mixture for at least 10	Emulsion splash and spill due to high homogenizing speed. Use appropriate PPE.

	minutes and remove the beaker containing the emulsion sample. • After preparing the emulsion, turn off the homogenizer and unplug it.	
3	**Homogenizer Cleaning** • Place an empty beaker under the homogenizer • Put the toluene jar and empty wash bottle under the fume hood. Pour the toluene inside the empty wash both. • Carefully clean the outer wall of the homogenizer probe with DI water and toluene under the fume hood. • Empty the beaker that contains the mixture of water, toluene and dissolved materials into a big bottle, and label it as organic waste. • Leave the homogenizer inside the fume hood to dry off. • Wash all the beakers used with tap water and soap.	Breakage of glassware in the process of washing. Water splash to the eyes, and possibility of cuts due to broken glassware. Spill Kit, paper towel, clean-up bucket, first aid kit and mops should be available nearby. Use full PPE
4	**Droplet size analysis** (**Axioskop-40**) • Dip the pipette into the emulsion in the beaker to withdraw small emulsion sample. • Using the pipette, put a small droplet of the emulsion on the microscope slide. Afterwards, carefully put another slide on it and allow the droplet to expand between the slides. • Turn in the light of the microscope and place the slide under the objective lens of the microscope. • Select the appropriate lens for the image observation. • Manipulate the lens to ensure that it is well focused on the image to have a high contrast picture.	Cuts due to the sharp edges of the microscope slides. Use appropriate PPE.

5	**Shear measurement** 8. Add the emulsion sample inside the outer cylinder of the couette cell. 9. Check the emulsion level inside the cup to ensure it reaches the datum line of the selected spindle (MV3 in this case). 10. Carefully attach the spindle to the to the cup, and ensure that the bolt is properly tightened. 11. Turn on the water bath and set it to the desired temperature using the temperature control system. 12. Launch the RheoWin job manager which is a software for controlling the operating condition of the viscometer. 13. Shear the emulsion at different spindle speed using stepwise and constant speed procedure. 14. Obtain the data for each test using the RheoWin Data Manager.	Oil spill and splash due to rotation between cup and spindle and inappropriate tightening. Use full PPE
6	**Shutting Down** • Clean the electronic balance to ensure it free of any oil or water spill. • Stop the viscometer and clean the cup and spindle. • Shutdown the computer. • Clean the microscope slide and cover the microscope. • Clean the pycnometer and all the beakers used.	
	Upon the completion of all the experiments, disinfect all the apparatus used with wipes and tidy up the Lab area. Wash all the apparatus used and properly dispose all the waste into the appropriate waste disposal area. Contact Terry Runyon on 780-248-1554 or trunyon@ualberta.ca to inform her about the waste that needs to be disposed.	

Safe Work Procedure (SWP) Pipeline Transport Processes Research Group

Laboratories: LAB2-151, LAB 6-120 CME building

Job title: Bitumen froth self-Lubricating flow Experiment	**Date:** December 16, 2021
Written by: Mubarak Gbadamosi	**Conducted by**: Mubarak Gbadamosi

Equipment Required: Viscometer (VT 550), computer, water bath, Ethylene glycol bath, thermometer, mixer (electric motor), Cart.

Materials: Bitumen froth, Deionized water, Toluene, Wash bottles, Funnel, Paper towel, Glass jar, Plastic container, Organic waste bottle.

Safety equipment: Respirator, Latex gloves, Safety glasses, Flame resistance Lab coat, Large rubber gloves (for cleaning), Kneel Pad, Fire extinguisher, Spill kit.

PPE required throughout all the following steps: Flame resistance Lab coat, Latex gloves, respirator, safety goggles, kneel pad, rubber gloves for cleaning.

Procedure

1	**Bitumen froth prewarming *Lab 6-120* (day before)** • Wear latex gloves and open the fume hood, clear the workspace and create space for the bitumen froth can. • Take the can containing the bitumen froth out of the refrigerator and carefully place it inside the fume hood A. • Label the bitumen froth can with a marker to indicate the material inside the can and the user. • Carefully close the fume hood. • Remove the latex gloves and put them inside the Ziplock and place it inside the bitumen contaminated waste bucket in the fume hood B. • Ensure that the cart is in Lab 6-120.	**Potential hazards**: Direct contact with bitumen which might cause skin irritation, eye irritation and throat irritation. **Additional PPE**: N/A **Supplies needed**: Paper towel.
2	**Preheating the bitumen froth (Lab 6-120)**	**Potential hazards**: Direct contact with bitumen which

	• Visually inspect the Ethylene glycol bath to ensure that the bath is free of any form of contaminant. • Open the froth can and carefully immerse it inside the bath. • Adjust the can holder to ensure that the can is well positioned and firm. • Connect the power cable to the power source and turn on the Ethylene glycol bath. • Insert the thermometer inside the froth can to monitor the froth temperature. • Set the bath to the desired temperature (70^0C), and heat the froth for about 1.5 hours. • During the heating process stir the froth gently to promote the heat transfer. • Once the froth reaches at temperature of 70^0C, remove the thermometer and prepare for the premixing process.	might cause Skin burn, skin irritation, eyes irritation, throat irritation. **Additional PPE**: Kneel pad. **Supplies needed**: Paper towel.
3	**Bitumen froth premixing (Lab 6-120)** • Wear the kneel pad and put two layers of paper towel on the floor where bitumen contaminated materials will be placed underneath the fume hood. • Adjust the height of the mixer so that the pitch blade impeller can be conveniently attached to the mixer. • Fit the can with a lid and the baffle and attach the pitched-blade impeller to the mixer. Ensure to maintain an off-bottom clearance of 1/3 the height of the container. • Doublecheck to ensure that the baffle does not have contact with the impeller. • Attach the protective cover shield to the shelve inside the fume hood.	**Potential hazards**: Direct contact with bitumen which might cause Skin burn, skin irritation, eyes irritation, throat irritation. **Additional PPE**: Kneel pad. **Supplies needed**: Paper towel.

	• At a temperature of 70^0C, gradually increase the rotating speed of the impeller from 100rpm to 1000 rpm (indicated by the black mark on the adjustment knob). A duration of about 3 min will be allowed at each mixing speed before moving to the next. • Shear the bitumen froth at 1000rpm for 15min with the mixer to homogenize the sample in the can. • Stop the mixer and disconnect it from the power source. • Adjust the electric motor to a height sufficient to easily remove the impeller. • Carefully remove the impeller and the baffle and put them on the paper towel placed on floor. • With paper towel wrapped around the hand, carefully lift the froth can from the top and put the can on the paper towel placed on the floor beside the fume hood. • With paper towel wrapped around the hand, pour about 400ml froth inside a 600ml beaker. Afterwards, transfer 100 ml bitumen froth from the beaker to the glass jars and carefully close the jars. • Put the glass jars inside a container, place them on the cart and prepare to transfer them to Lab 2-151 where the shearing experiments will be conducted. • Turn off the bath and unplug it from the power source.	
4	**Transferring the froth from 6-120 to 2-151** • Put paper towels on the cart to ensure that it doesn't get stained with bitumen. • Put the glass jars in a container and place it on the cart. • Cover the bitumen froth can with the lid.	**Potential hazards**: Direct contact with bitumen which might cause skin irritation, eye irritation and throat irritation. **Additional PPE**: N/A

	• Hold the froth can with paper towel and put it on the cart for waste collection of used froth after the shearing experiment in Lab 2-151. • Remove one of the latex gloves before leaving the Lab (6-120) to open the doors and touch the elevator buttons. • Take proper precautions when taking the cart out of the lab, use one hand to support the door when going out of the Lab. • Hold the cart firmly on the walkway to ensure none of the materials on it falls.	**Supplies needed**: Paper towel.
5	**Maintaining froth temperature (Lab 2-151)** • With the aid of the cart, transfer the glass jars to the fume hood (c), and place all the jars inside the bath. • Take the cart to a clear work area to stay organized and ensure the fume hood workspace is free. • Take one jar at a time for each shearing experiment to be conducted.	**Potential hazards**: Direct contact with bitumen which might cause skin irritation, eye irritation and throat irritation. **Additional PPE**: Respirator **Supplies needed**: Paper towel.
6	**Shear measurement** 15. Turn on the water bath of the viscometer and set it to the desired temperature. 16. Turn on the viscometer and the computer. 17. Pour 75ml of the bitumen froth sample from the glass jar inside the cup of the concentric cylinder viscometer inside the fume hood. 18. Check the emulsion level inside the cup to ensure it reaches the datum line of the selected spindle (MV3). 19. With gloves worn and paper towel wrapped around the hand, transfer the cup to the viscometer workspace. 20. Carry the spindle with two hands from the fume hood to the viscometer workspace.	**Potential hazards**: Direct contact with bitumen which might cause skin irritation, eye irritation and throat irritation. **Additional PPE**: Respirator **Supplies needed**: Paper towel.

	21. Carefully attach the spindle to the rotor, and ensure that the connection is tight. 22. Launch the RheoWin job manager and set the operating condition of the viscometer. 23. Shear the bitumen froth at a low speed (2 rpm) to allow the froth attain thermal equilibrium with the water bath. 24. Estimate the froth viscosity by shearing it at low spindle speed(2-10rpm). This will be used to determine the maximum shearing speed to prevent over torquing the viscometer. 25. Shear the emulsion by gradually increasing the spindle speed (stepwise spindle speed procedure). A period of about 5 min will be allowed at each speed. 26. Conduct subsequent experiments by shearing the froth at the same speed for about 15 min (constant spindle speed procedure). 27. Observe the measured torque as function of time and obtain the data for each test using the RheoWin Data Manager. 28. Once the experiment is completed, put paper towels under the viscometer. 29. Carefully remove the cup of the viscometer with two hands and dispose the froth inside the froth can. 30. Place the viscometer cup on a paper towel inside the fume hood. 31. Carefully remove the spindle of the viscometer with two hands, wrap paper towel around it and take it to the fume hood for cleaning. 32. Repeat this procedure for all the experiment runs.	
7	**Cleaning the Viscometer/ waste disposal**	**Potential hazards**: Direct contact with bitumen which

	• Dispose the bitumen froth in the viscometer cup inside the froth can. • Wipe the spindle and the cup with paper towel sprayed with toluene until both are very clean. • Clean the cup and spindle of the viscometer with soap and deionized water. • Put all the paper towels inside the Ziplock and put them on the cart. • Put the froth can and the used glass jars on the cart and transfer them to Lab 6-120. • Label the froth can to indicate it contains waste and properly dispose it inside the organic waste bucket. • Clean the impeller, beaker, thermometer and stirrer used in the premixing procedure with toluene and deionized water. • Pour toluene and DI water used for washing inside the organic waste bottle in the fume hood B. • Put all the used paper towel inside the Ziplock and place them in the fume hood B to dry up.	might cause skin irritation, eye irritation and throat irritation. **Additional PPE**: Respirator **Supplies needed**: Paper towel.
	Contact Terry Runyon on 780-248-1554 or trunyon@ualberta.ca to inform her about the waste that needs to be disposed.	

Appendix B: Emulsion Images

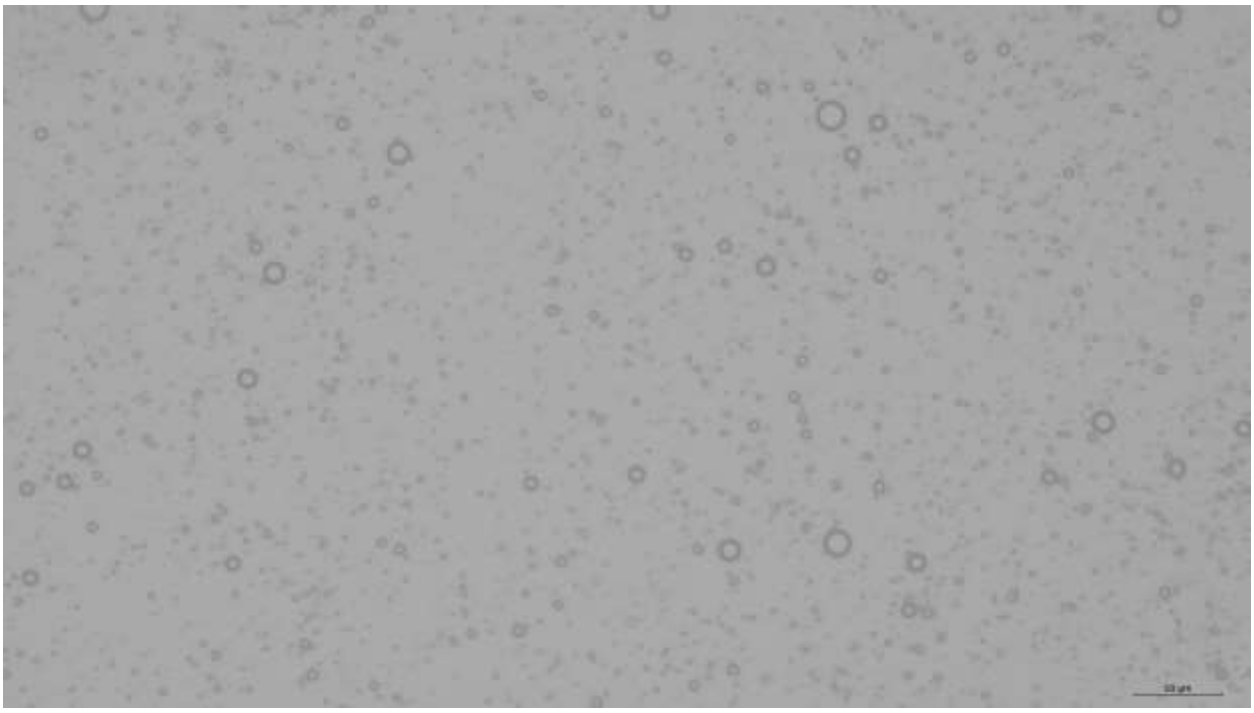

Figure B.1: Photomicrograph of Emulsion 1 sample A, t = 0

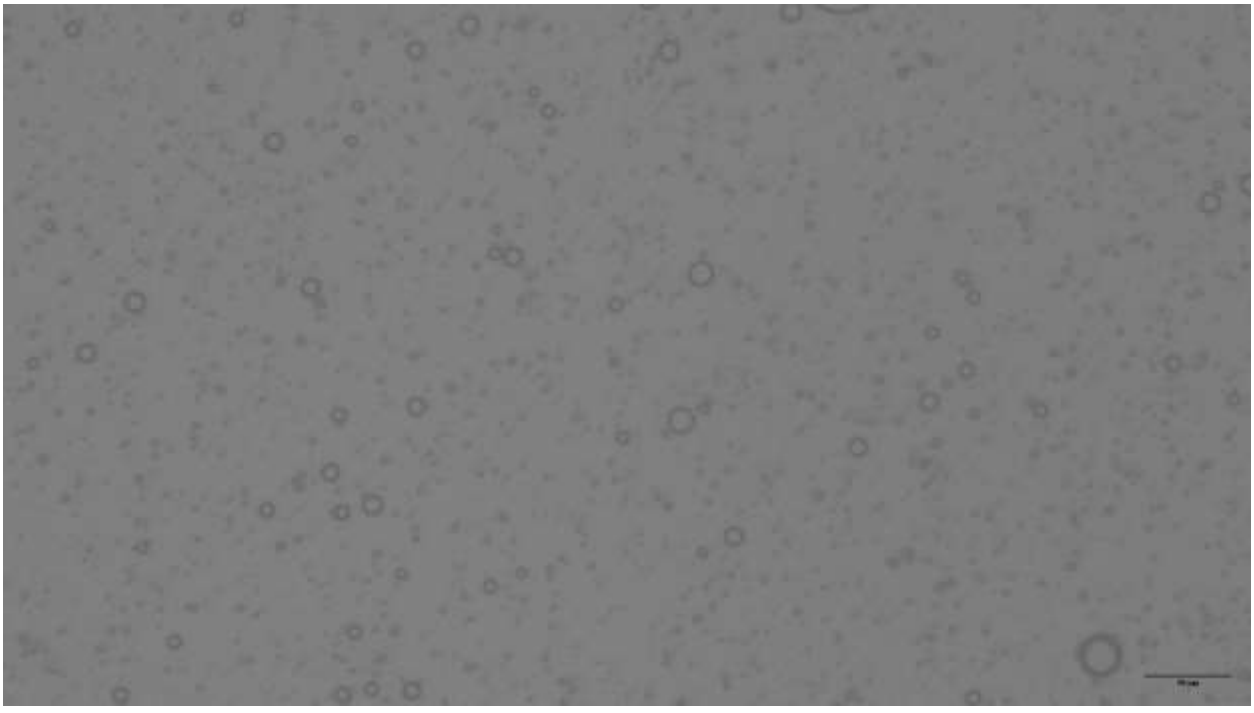

Figure B.2: Photomicrograph of Emulsion 1 sample C, t = 4hrs

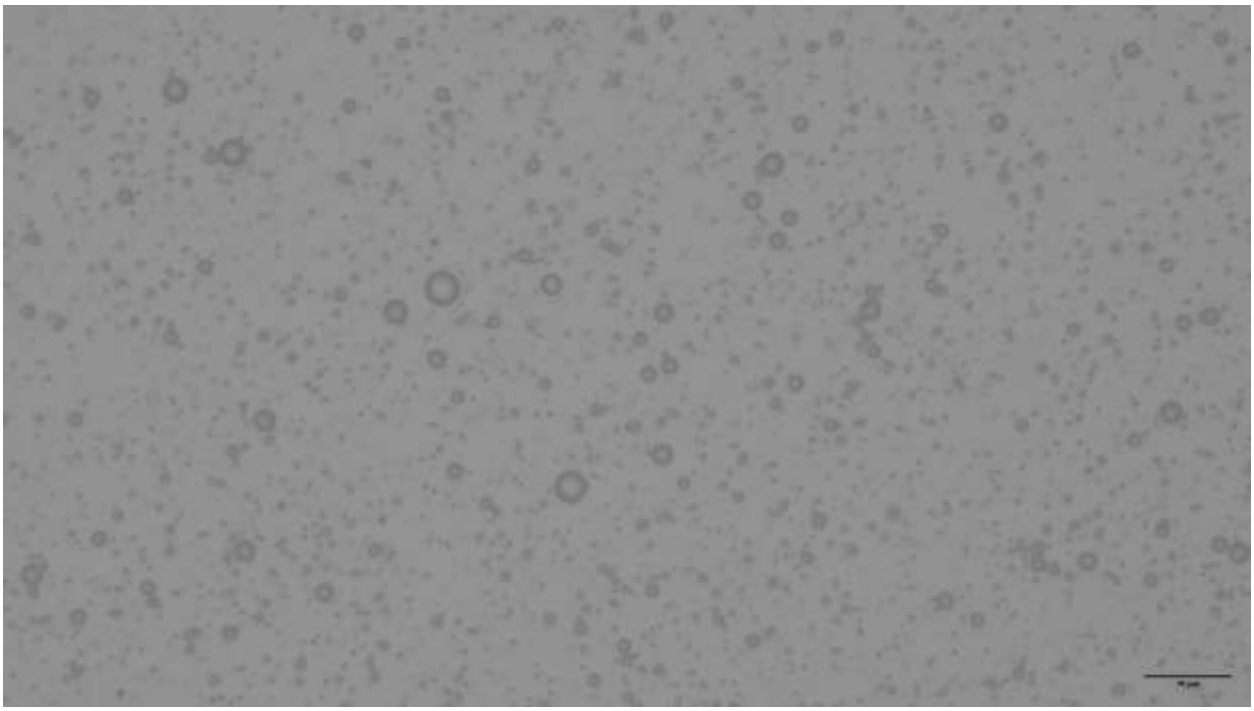

Figure B.3: Photomicrograph of Emulsion 2 sample A, t = 0

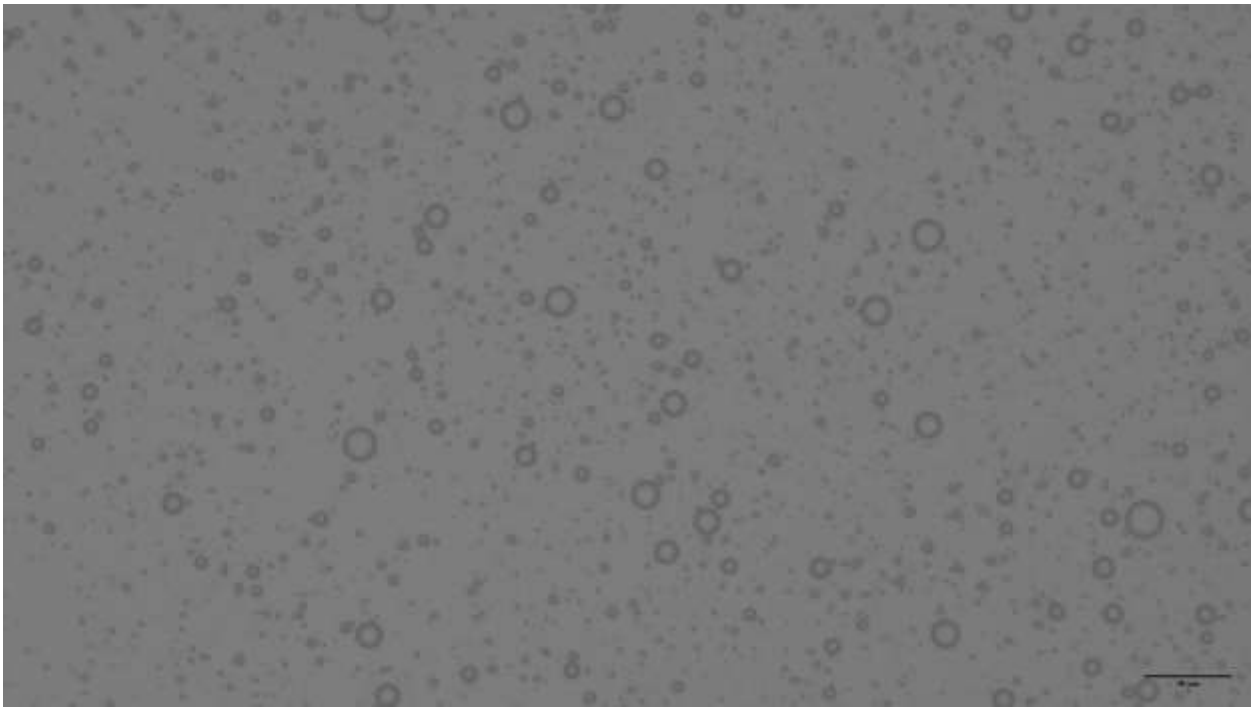

Figure B.4: Photomicrograph of Emulsion 2, sample C, t = 4hrs

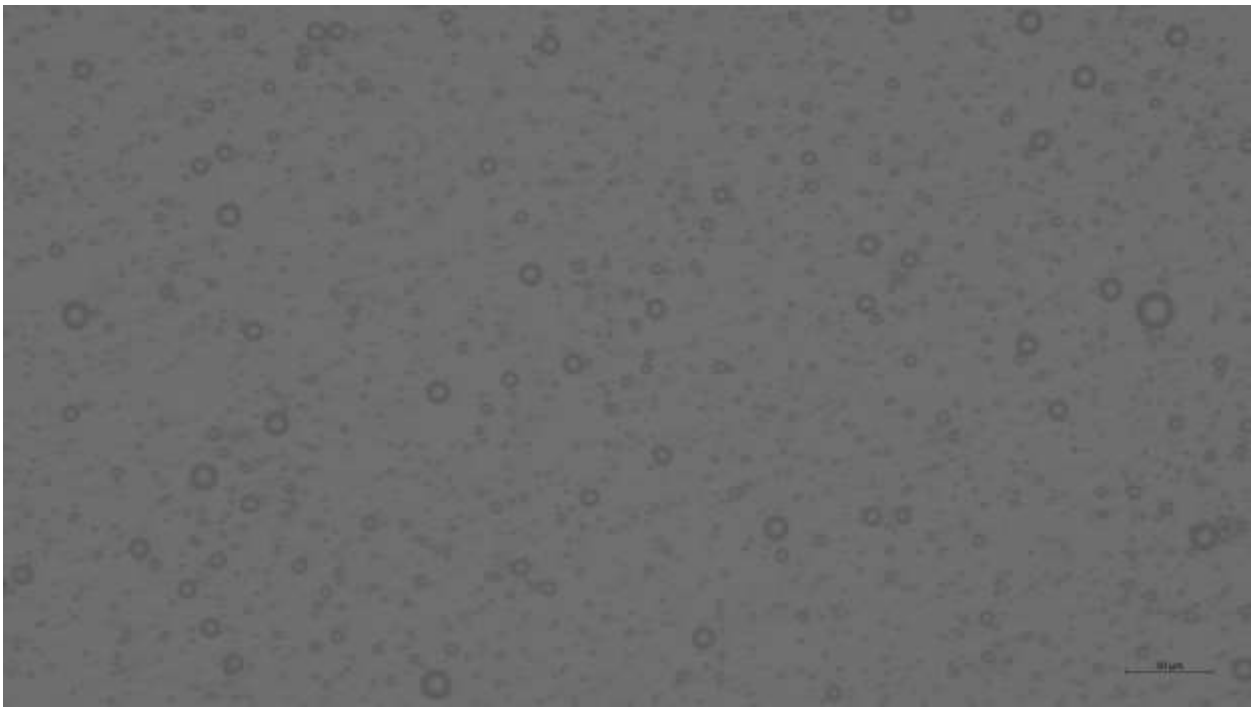

Figure B.5: Photomicrograph of Emulsion 3, sample A, t = 0

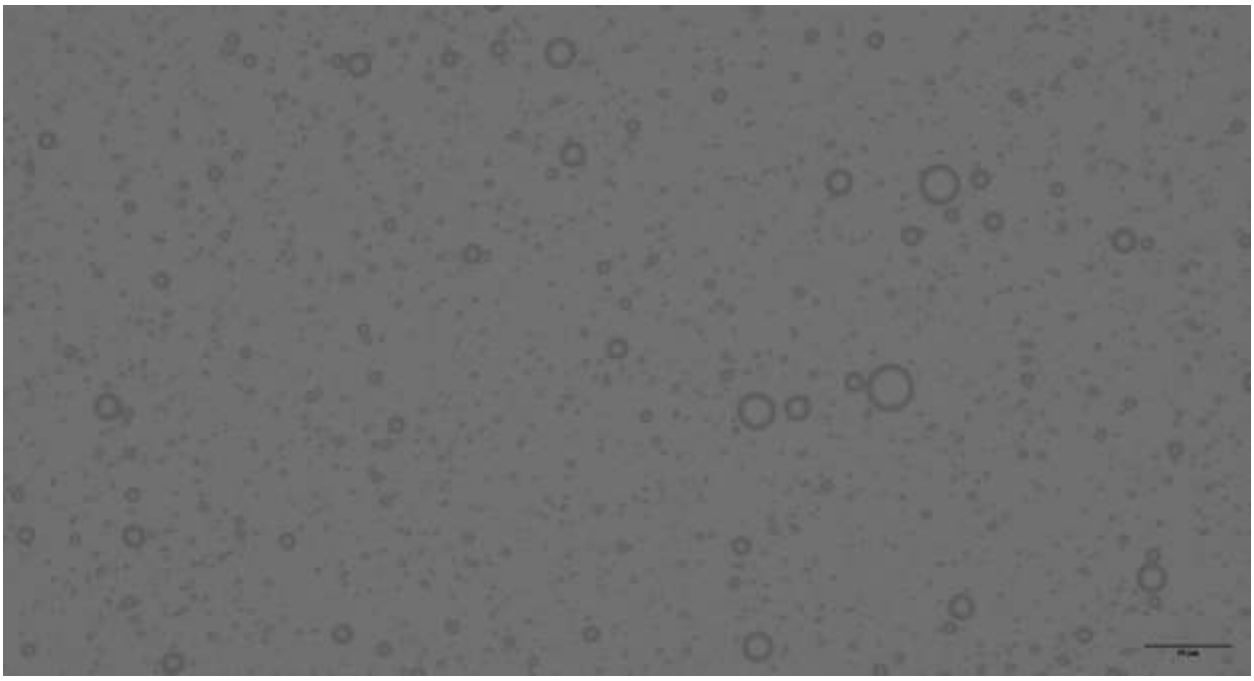

Figure B.6: Photomicrograph of Emulsion 3 sample C, t = 4 hrs

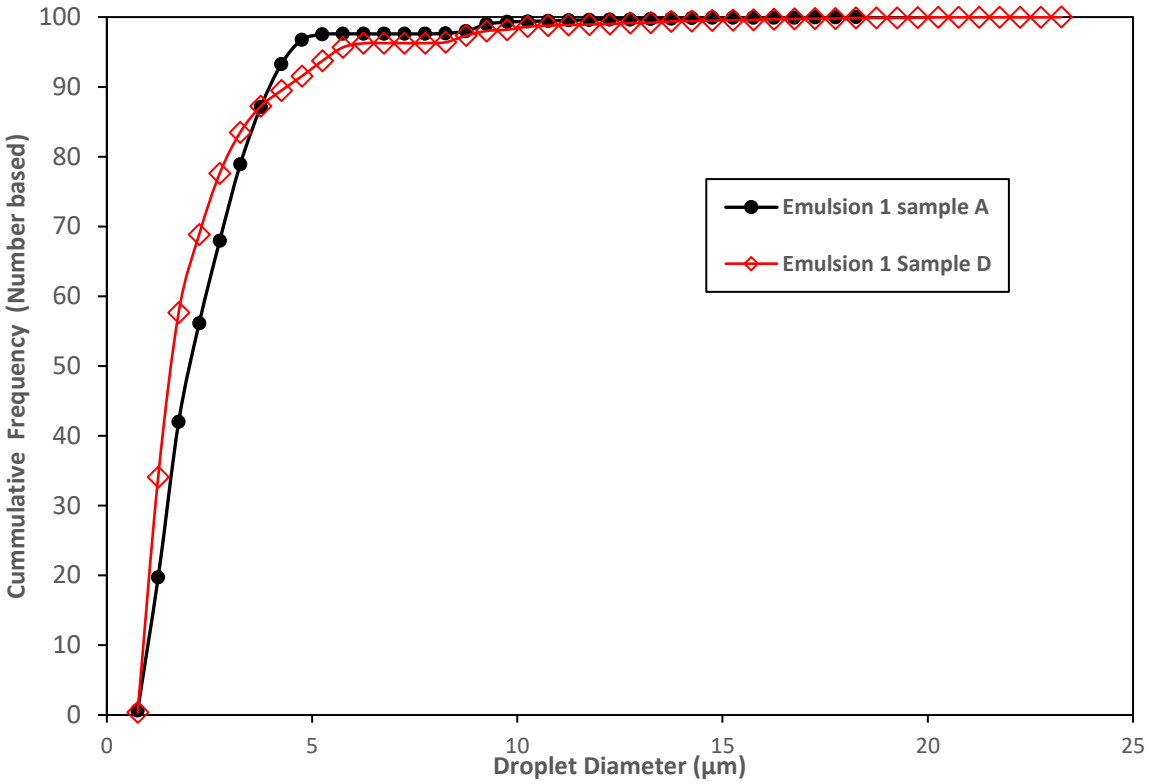

Figure B.7: Size distribution of Emulsion 1 sample A and sample D

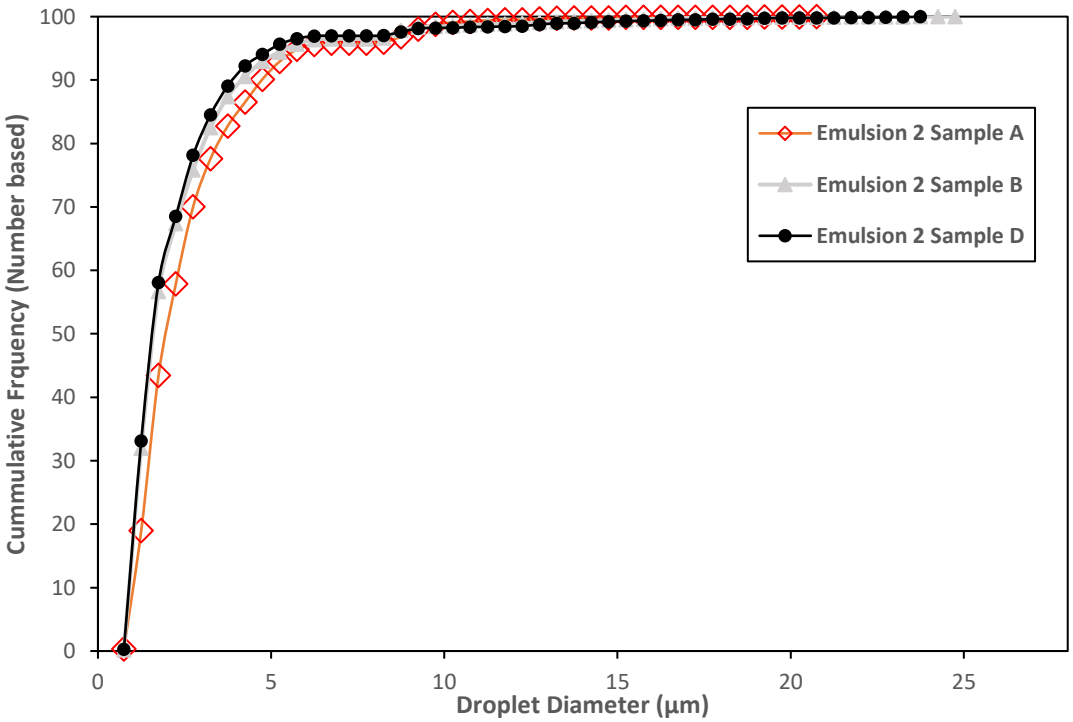

Figure B.8: Size distribution of Emulsion 2 A, B and D.

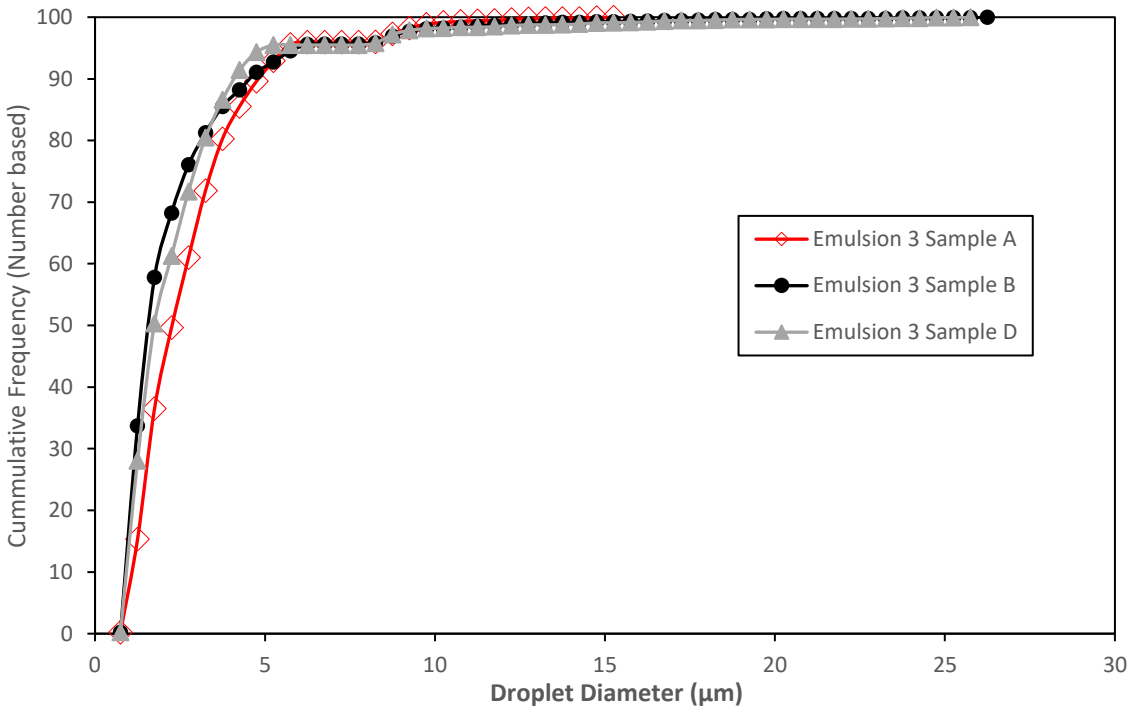

Figure B9 : Emulsion 3 Sample A,B, D droplet size distribution.

Appendix C: MATLAB script used to obtain the emulsion droplets size distribution

```
% Load original image
x = imread('Sample A top t=0.tif');
figure
imshow(x)
title(' W/O Emulsion Microscope Image Captured with Droplets Detected and Measured')

% Image is pre-processed by ImageJ to improve contrast, quality and
% transform to black and white

% Hough Transform to find circular droplets
% The droplet is darker than background, so it is appropriate to use 'dark'
% for object polarity

% Decrease sensivitiy for less droplets and vice versa
% Decrease Edge Threshold for more droplets

% Break up the droplets into 2 radius range to avoid overlap and imrpove
% detection quality

% Pick out small particles first
[centersDarksmall, radiiDarksmall, metricDarksmall] = imfindcircles(x,[2 20], ...
    'ObjectPolarity','dark','Sensitivity',0.72,'EdgeThreshold',0.05);
hDarksmall = viscircles(centersDarksmall, radiiDarksmall,'Color','b');

[centersDarkbig, radiiDarkbig, metricDarkbig] = imfindcircles(x,[21 70], ...
    'ObjectPolarity','dark','Sensitivity',0.85,'EdgeThreshold',0.05);
hDarkbig = viscircles(centersDarkbig, radiiDarkbig,'Color','r');
% Range for 20x: [3 18] and  [18 40]
% Range for 50x: [12 40] and [40 75]

n = numel(radiiDarksmall)+ numel(radiiDarkbig); % Number of droplet detected
combinedradius_pixels = [radiiDarkbig;radiiDarksmall];
combinedradius_microns = combinedradius_pixels ./ 5.3;
% Pixel/microns ratio determined by ImageJ with scalebar on image
% 2.95 px/um for 20x and 7.33 px/um for 50x

diameter = combinedradius_microns .*2;

% Distribution
figure
histogram(diameter);
title('Droplet Size Distribution of O/W Emulsion from Microscope Image')
```

Appendix D: Self-lubricating Flow Reproducibility Tests

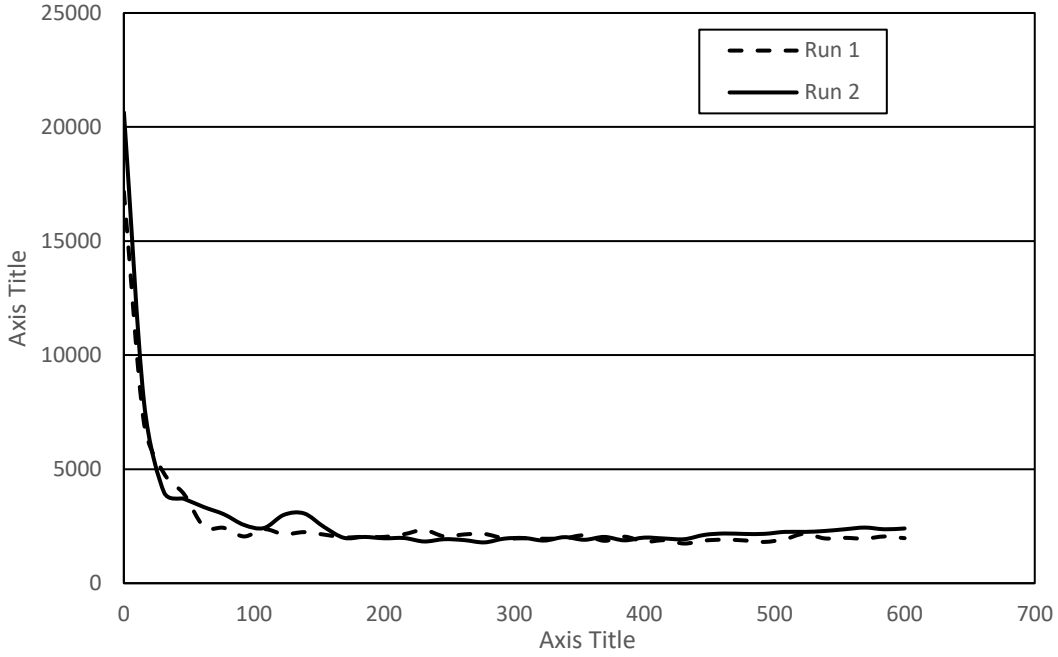

Figure D1: Preliminary test reproducibility run. 30 wt.% water -in- Meropa oil emulsion. n = 500 rpm

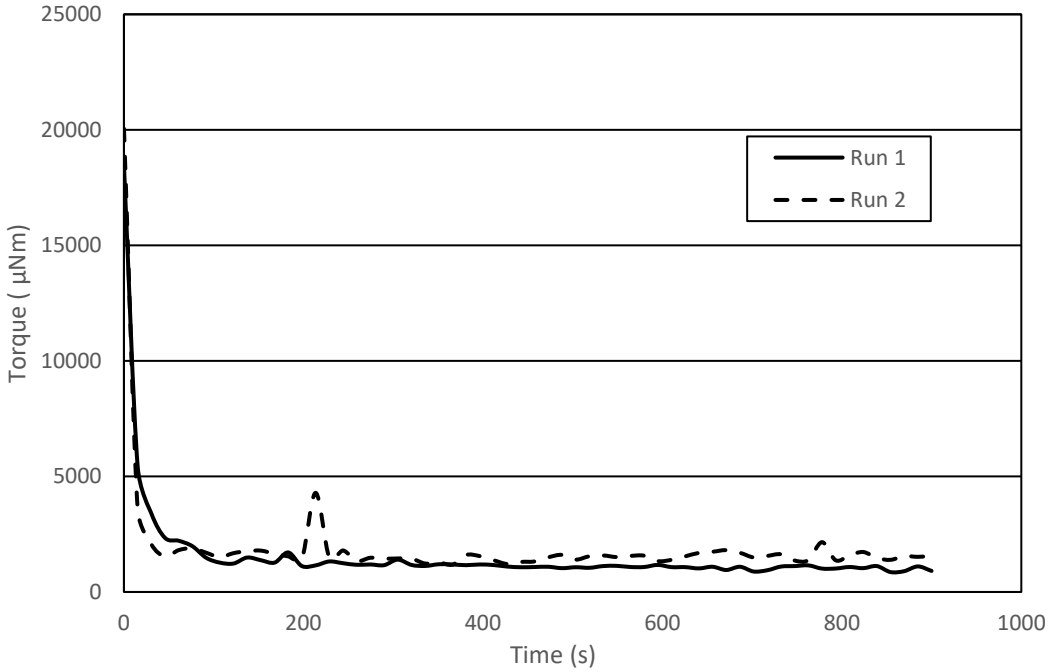

Figure D2: Reproducibility run of bitumen froth Self-Lubricating flow. T=60^0C, n = 180 rpm.

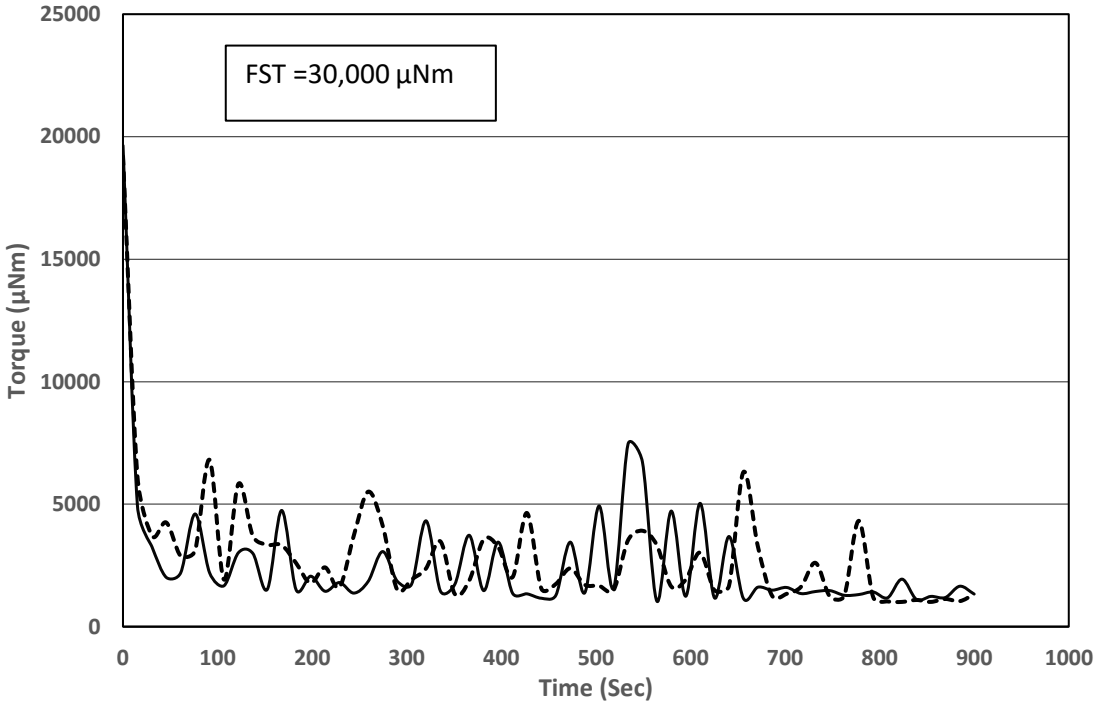

Figure D3: Reproducibility runs of bitumen froth Self-Lubricating flow. T=55^{0}C, n = 128 rpm.

Appendix E: Bitumen froth water concentration adjustment procedure

Consider a 800g bitumen Froth

Froth composition Bitumen: 69wt%, Water: 25wt%, Fines: 6wt%.

Water content in the froth = 0.25 * 800
Initial water content = 200 g

To increase the water content to 30wt.%

$$30\ wt\% = \frac{200 + X}{800 + X}$$

X = 57.14 g

Initial aqueous phase volume= $\frac{mass}{density}$

Initial aqueous phase volume = $\frac{200}{0.998}$

= 200.4 mL

Additional aqueous phase = $\frac{57.14}{0.998}$

= 57.3 mL

Total aqueous phase volume = 257.7 mL

To adjust the fines concentration to 3 vol% for example:

Assumption : Carrier fluid is Newtonian.

$$M_f = \frac{C_f V_L \rho_f}{(1 - C_f)}$$

V_L → Total aqueous phase volume

$$M_f = \frac{0.03 \times 257.7 \times 2.696}{(1 - 0.03)}$$

$$M_f = 21.49$$

Appendix F: Effect of pH and Salts Concentration on Bitumen-Water Interfacial Tension

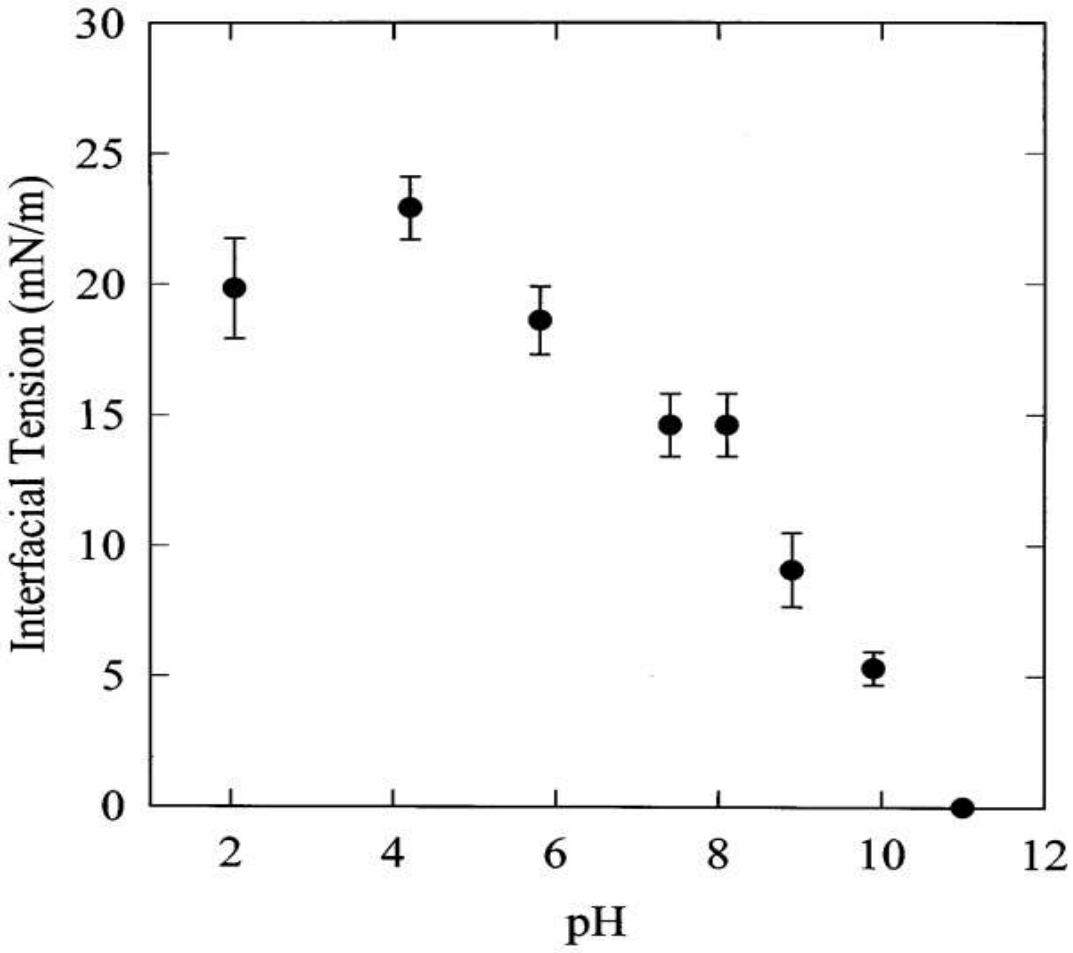

Appendix F1: Effect of pH on bitumen water interfacial tension [45].

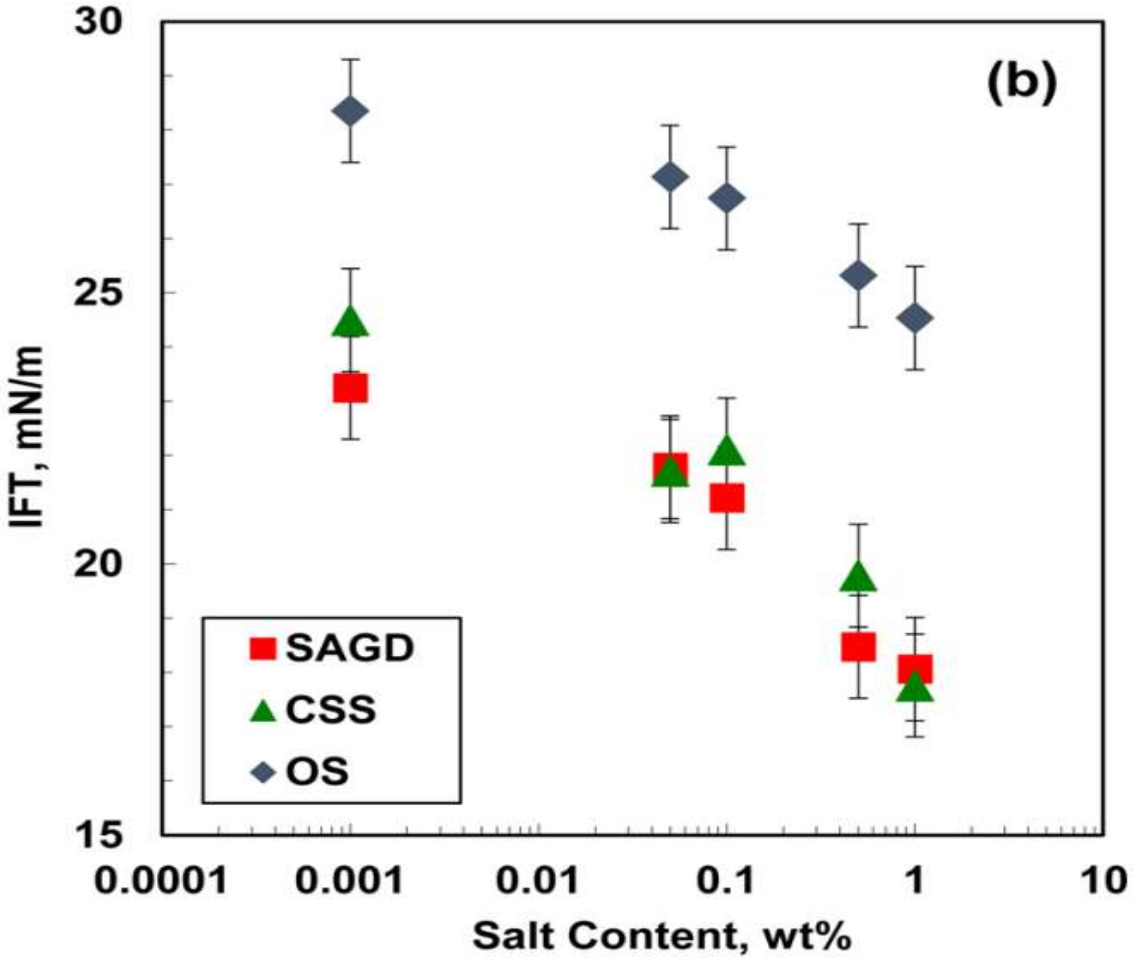

Appendix F2: Effect of salt concentration on bitumen-water interfacial tension [41].

Appendix G: Bitumen Froth Viscosity Test

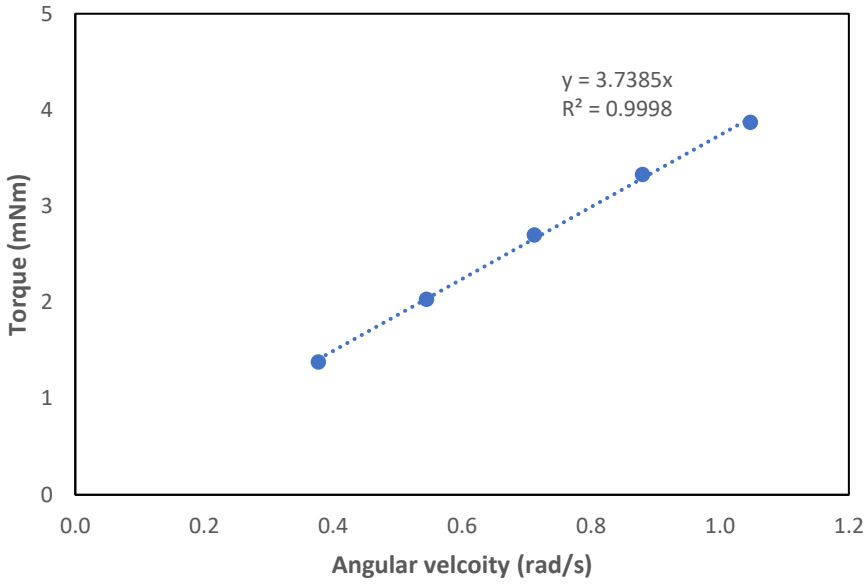

Appendix G1: Bitumen Froth Viscosity Test at 55 ^{0}C

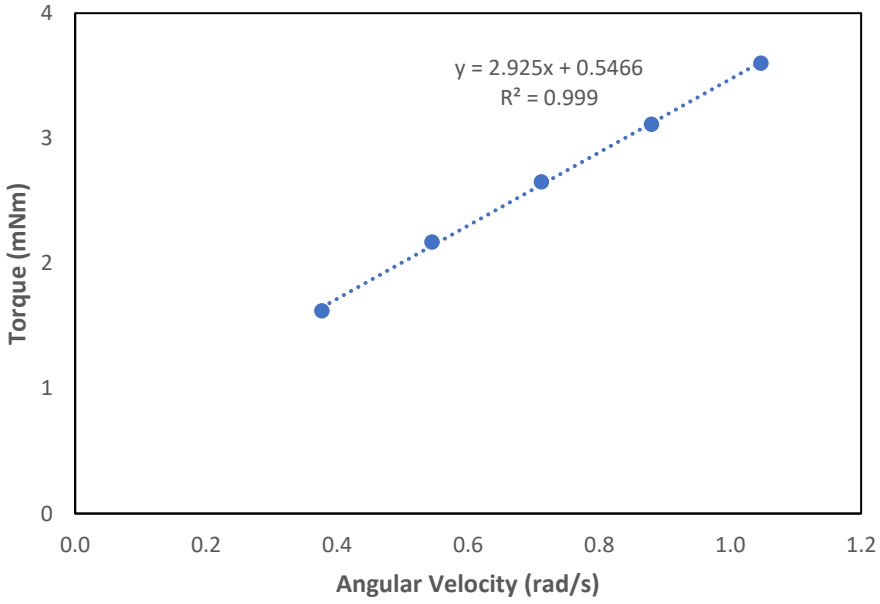

Appendix G2 : Bitumen Froth Viscosity Test at 60 ^{0}C

Appendix H: Experiment Results

Nomenclature: Run numbers e.g., 1a, 1b, 1c represent tests that are conducted using the same sample. Run number e.g., 5, represents a standalone experiment.

Effect of Water Concentration

Run no	Water Concentration (wt%)	Spindle speed (rpm)	Flow type
1a	30	16	NLF
1b	30	32	NLF
1c	30	64	NLF
1d	30	124	NLF
1e	30	180	NLF
1f	30	254	NLF
1g	30	362	SLF
1h	30	420	SLF
1i	30	500	SLF
2	30	254	NLF
3	30	254	NLF
4	30	16	NLF
5	30	362	NLF
6	30	362	NLF
7	30	420	SLF
8	30	420	SLF
9	30	420	SLF
10	30	420	SLF
11	30	420	SLF
12	30	500	SLF
13	30	500	SLF
14	30	500	SLF
15	30	500	SLF
16	30	64	NLF
17	30	420	SLF

Effect of Water Concentration

Run no	Water Concentration (wt%)	Spindle speed (rpm)	Flow type
18A	25	16	NLF
18B	25	32	NLF
18C	25	64	NLF
18D	25	124	NLF
18E	25	180	NLF
18F	25	254	NLF
18G	25	362	NLF
18H	25	420	NLF
18I	25	500	NLF
19	25	362	NLF
20	25	180	NLF
21	25	420	NLF
22	25	500	NLF

Run no	Water Concentration (wt%)	Spindle speed (rpm)	Flow type
23A	10	16	NLF
23B	10	32	NLF
23C	10	64	NLF
23D	10	124	NLF
23E	10	180	NLF
23F	10	254	NLF
23G	10	362	NLF
23H	10	420	NLF
23I	10	500	NLF
24	10	362	NLF
25	10	420	NLF
26	10	500	NLF

Effect of Temperature

Run no	Temperature	Spindle speed (rpm)	Flow type
33A	50	8	NLF
33B	50	16	NLF
33C	50	22	NLF
33D	50	32	NLF
33E	50	45	NLF
33F	50	64	NLF
33G	50	90	SLF
34	50	90	SLF
39	50	64	NLF
40	50	90	SLF
54	50	64	NLF
59	50	8	NLF
60	50	64	NLF
61	50	64	NLF

Run no	Temperature	Spindle speed (rpm)	Flow type
35A	60	8	NLF
35B	60	16	NLF
35C	60	22	NLF
35D	60	32	NLF
35E	60	45	NLF
35F	60	64	NLF
35G	60	90	NLF
35H	60	128	ILF
35I	60	164	SLF
35J	60	180	SLF
36	60	128	ILF
37	60	164	SLF
38	60	164	SLF
41	60	180	SLF
42	60	180	SLF

Run no	Temperature	Spindle speed (rpm)	Flow type
43A	55	8	NLF
43B	55	16	NLF
43C	55	22	NLF
43D	55	32	NLF
43E	55	45	NLF
43F	55	64	NLF
43G	55	90	ILF
43H	55	128	SLF
56	55	128	SLF
57	55	128	SLF
58	55	90	ILF

Reversibility Test

Run no	Temperature	Spindle speed (rpm)	Flow type
62A	Forward	8	NLF
62B	Forward	16	NLF
62C	Forward	22	NLF
62D	Forward	32	NLF
62E	Forward	45	NLF
62F	Forward	64	NLF
62G	Forward	80	NLF
62H	Forward	90	SLF
62I	Forward	100	SLF
62H1	Reverse	90	SLF
62G1	Reverse	80	NLF
62F1	Reverse	64	NLF
62E1	Reverse	45	NLF
62F2	Forward	64	NLF
62G2	Forward	80	NLF
62H2	Forward	90	NLF
62I2	Forward	100	NLF

Reversibility Test

Run no	Run type	Spindle speed (rpm)	Flow type
63A	Forward	8	NLF
63B	Forward	16	NLF
63C	Forward	22	NLF
63D	Forward	32	NLF
63E	Forward	45	NLF
63F	Forward	64	NLF
63G	Forward	80	NLF
63H	Forward	90	SLF
63I	Forward	100	SLF
63H1	Reverse	90	SLF
63G1	Reverse	80	NLF
63F1	Reverse	64	NLF
63E1	Reverse	45	NLF
63F2	Forward	64	NLF
63G2	Forward	80	NLF
63H2	Forward	90	NLF
63I2	Forward	100	NLF

Effect of Carrier fluid pH

Run no	pH	Spindle speed (rpm)	Flow type
64A	8.5	8	NLF
64B	8.5	16	NLF
64C	8.5	22	NLF
64D	8.5	32	NLF
64E	8.5	45	NLF
64F	8.5	64	NLF
64G	8.5	80	NLF
64H	8.5	85	NLF
64I	8.5	90	SLF
65	8.5	85	NLF
66	8.5	90	SLF
67	8.5	80	NLF

Run no	pH	Spindle speed (rpm)	Flow type
68A	9	8	NLF
68B	9	16	NLF
68C	9	22	NLF
68D	9	32	NLF
68E	9	45	NLF
68F	9	64	NLF
68G	9	80	NLF
68H	9	85	NLF
68I	9	90	SLF
68J	9	100	SLF
69	9	90	SLF
70	9	80	NLF

Run no	pH	Spindle speed (rpm)	Flow type
71A	9.5	8RPM	NLF
71B	9.5	16RPM	NLF
71C	9.5	22RPM	NLF
71D	9.5	32RPM	NLF
71E	9.5	45RPM	NLF
71F	9.5	64RPM	NLF
71G	9.5	80RPM	NLF
71H	9.5	90RPM	NLF
71I	9.5	95RPM	SLF
71J	9.5	100RPM	ILF
71K	9.5	110RPM	SLF
72A	9.5	100RPM	ILF
72B	9.5	105RPM	SLF

Run no	pH	Spindle speed (rpm)	Flow type
73A	10	8	NLF
73B	10	16	NLF
73C	10	22	NLF
73D	10	32	NLF
73E	10	45	NLF
73F	10	64	NLF
73G	10	80	NLF
73H	10	90	NLF
73I	10	100	NLF
73J	10	110	ILK
73K	10	120	SLF
74A	10	105	NLF
74B	10	110	ILF
74C	10	115	SLF
75	10	110	ILF
76	10	110	ILF

Effect of salt-concentration

Run no	Salt Conc (ppm)	Spindle speed (rpm)	Flow type
77A	1205	8	NLF
77B	1205	16	NLF
77C	1205	22	NLF
77D	1205	32	NLF
77E	1205	45	NLF
77F	1205	64	NLF
77G	1205	80	NLF
77H	1205	90	SLF
77I	1205	100	SLF
78	1205	85	NLF
79	1205	90	SLF

Run no	Salt Conc (ppm)	Spindle speed (rpm)	Flow type
80A	2000	8	NLF
80B	2000	16	NLF
80C	2000	22	NLF
80D	2000	32	NLF
80E	2000	45	NLF
80F	2000	64	NLF
80G	2000	80	NLF
80H	2000	85	NLF
80I	2000	90	SLF
80J	2000	100	SLF
81A	2000	64	NLF
81B	2000	80	NLF
81C	2000	85	NLF
81D	2000	90	SLF
81E	2000	100	SLF
82	2000	90	SLF

Run no	Salt Conc (ppm)	Spindle speed (rpm)	Flow type
83A	3000	8	NLF
83B	3000	16	NLF
83C	3000	22	NLF
83D	3000	32	NLF
83E	3000	45	NLF
83F	3000	64	NLF
83G	3000	80	NLF
83H	3000	85	NLF
83I	3000	90	NLF
83J	3000	100	NLF
83K	3000	110	NLF
84A	3000	90	NLF
84B	3000	95	NLF
84C	3000	100	ILF
84D	3000	110	SLF
85	3000	100	ILF
86	3000	105	SLF

Effect of Fines Concentration

Run no	Fines Conc (Vol%)	Spindle speed	Flow type
87A	4.1	8	NLF
87B	4.1	16	NLF
87C	4.1	22	NLF
87D	4.1	32	NLF
87E	4.1	45	NLF
87F	4.1	64	NLF
87G	4.1	80	NLF
87H	4.1	90	NLF
88A	4.1	70	NLF
88B	4.1	75	ILF
88C	4.1	85	SLF
89	4.1	85	SLF
90	4.1	90	SLF

Run no	Fines Conc (Vol%)	Spindle speed	Flow type
91A	6.3	8	NLF
91B	6.3	16	NLF
91C	6.3	22	NLF
91D	6.3	32	NLF
91E	6.3	45	SLF
91F	6.3	50	SLF
92A	6.3	40	NLF
92B	6.3	45	SLF
92C	6.3	50	SLF

Coutte flow experimental data

Run no	1a	1b	1c	1d	1e	1f	1g	1h	1I
t (secs)	M(μNm)	M(μNm)	M(μNm)	M(μNm)	M(μNm)	M(μNm)	M(μNm)	M(μNm)	M(μNm)
0.047	1200	2250	4110	7350	6590	14580	18970	21020	23860
6.375	1315	2510	4640	8455	11820	12830	12820	9650	14730
12.67	1310	2500	4660	8500	11700	14190	13880	8760	14250
18.95	1330	2500	4670	8560	10930	13050	12480	9710	14340
25.3	1315	2510	4670	8535	11900	13150	11990	10560	12880
31.62	1320	2515	4680	8580	10730	13340	10160	9370	13780
37.95	1340	2510	4685	8610	10750	12970	11000	9070	12510
44.25	1330	2510	4690	8575	11540	13490	10560	8475	13990
50.56	1315	2510	4700	8620	12140	12400	12350	9100	5230
56.84	1310	2520	4710	8640	11950	13250	11660	10080	14670
63.17	1335	2515	4720	8430	10780	11670	12660	10500	14000
69.5	1325	2510	4720	8550	10760	10350	11150	10110	13520
75.83	1320	2515	4720	8600	11270	10520	10570	5350	3745
82.12	1320	2510	4720	8640	9190	10970	10680	5430	4025
88.42	1335	2510	4730	8715	8825	10730	10650	4850	4230
94.78	1310	2515	4730	8735	8880	10820	11690	4120	4815
101.1	1320	2510	4740	8710	10740	10830	11950	4230	3990
107.4	1340	2515	4740	8580	11750	10880	11850	5430	3260
113.7	1310	2520	4750	8515	11800	10890	11560	4210	3165
120	1320	2510	4750	8590	11160	10930	12650	4290	3920

Run no	2	3	4	5	6	7	8
t (secs)	M(μNm)	M(μNm)	M(μNm)	M(μNm)	M(μNm)	M(μNm)	M(μNm)
0.047	13470	10170	1340	13550	15750	18670	14580
30.8	11750	11750	1570	8110	11160	8640	1730
61.61	10360	7240	1540	8090	10190	7255	2010
92.34	10350	8030	1530	9060	11700	8330	2985
123.1	9380	8970	1540	7400	8130	5040	2100
153.9	10490	6900	1560	7095	7850	3870	2710
184.7	9180	9180	1560	7420	8280	3220	2410
215.4	9650	6790	1540	11020	8210	3155	2210
246.2	9840	6080	1540	7170	6410	3760	2575
277	9490	6550	1540	7200	6640	3460	2410
307.7	9560	6065	1560	7675	7410	3310	2760
338.5	8970	5420	1530	8345	7820	3440	2120
369.3	8185	8185	1540	7245	7310	3955	2140
400	9850	5580	1530	7605	9075	3165	2430
430.8	9840	6410	1520	7580	8035	3640	2320
461.5	10290	6660	1560	8770	7255	3740	2600
492.3	10340	7510	1525	6570	8630	3055	2400
523.1	10450	4240	1525	6640	8805	3510	2600
553.9	10540	6550	1515	8065	8360	4210	2450
584.6	10650	6150	1535	6735	8280	3660	2350
615.4	10260	5100	1550	6500	8680	3210	2640

Run no	9	10	11	12	13	14	15
t (secs)	M(μNm)	M(μNm)	M(μNm)	M(μNm)	M(μNm)	M(μNm)	M(μNm)
0.078	14910	14640	9930	20640	17170	18720	19300
15.39	5005	5330	1490	7960	7045	6870	8470
30.81	2890	3040	1390	3990	4820	4460	4480
46.2	2115	3000	1250	3700	3910	3240	2930
61.56	2340	2235	1470	3335	2480	2610	2975
76.94	2245	1930	1070	3020	2425	2420	3270
92.34	2200	1840	1040	2555	2050	2205	2995
107.7	2415	2050	1005	2420	2370	2590	2990
123.1	2570	1920	1060	3000	2150	2225	2360
138.5	2390	2060	1160	3060	2240	2290	2190
153.9	2350	1930	1450	2465	2130	2340	2375
169.2	2375	2180	1770	1990	2010	2110	2380
184.6	1990	2300	1640	2030	2035	1985	2125
200	1465	2170	1910	1970	2030	2020	2050
215.4	1590	2130	1890	1980	2150	1945	2020
230.8	1580	2120	1845	1830	2330	2300	1650
246.2	1410	2270	1920	1930	2055	2055	1570
261.6	1470	2140	1960	1890	2140	1810	1610
277	1280	2150	2150	1790	2160	2010	1660
292.3	1350	2480	2020	1955	1970	1930	1470
307.7	1350	2130	2160	1980	1970	2030	1560
323.1	1370	2360	2170	1870	1950	1940	1420
338.5	1360	2400	1820	2020	1970	1970	1530
353.9	1440	2360	920	1905	2100	1840	1680
369.2	1220	2670	1110	2030	1860	1780	1610
384.6	1090	2530	1275	1880	2040	1920	1540
400	1220	2405	1360	2000	1820	1900	1570
415.4	940	2900	1410	1960	1885	2080	1575
430.8	1045	2435	1200	1930	1740	1890	1400
446.2	1080	2290	1345	2120	1870	1875	1500
461.6	1090	2290	1200	2180	1910	2040	1630
476.9	1100	2440	1895	2160	1875	1955	1540
492.4	1155	2540	1430	2165	1810	2000	1500
507.8	1080	2510	1795	2250	1930	2055	1590
523.1	1080	2660	1500	2250	2170	1980	1605
538.5	1080	2445	1665	2290	1965	2085	1630
553.9	1175	2450	1700	2365	1990	2080	1655
569.2	1220	2570	1840	2440	1955	2255	1560
584.6	1245	2390	1960	2365	2050	2150	1635
600	1370	2480	1870	2400	1975	2030	

Run no	16	17	19	20	21	22
t (secs)	M(μNm)	M(μNm)	M(μNm)	M(μNm)	M(μNm)	M(μNm)
0.047	6490	18670	16500	11130	12470	18940
30.83	6185	8640	9250	13820	18140	14390
61.55	6520	7255	11180	14120	18530	12420
92.33	6430	8330	10200	14300	18800	11650
123.1	5240	5040	7305	14300	17810	8970
153.9	5815	3870	7345	13810	17700	9845
184.7	5840	3220	7510	14370	17320	11940
215.5	5780	3155	6990	13550	17200	12510
246.2	5090	3760	7890	14770	18730	12820
277	5080	3460	8400	14790	15820	11060
307.7	6570	3310	7155	13950	16650	10450
338.5	5970	3440	7105	15010	18220	10830
369.2	4695	3955	8580	14960	15090	9120
400	4905	3165	6630	15120	13750	11780
430.8	7095	3640	7350	14310	13830	9020
461.5	6560	3740	10610	15230	14090	10490
492.3	7320	3055	6170	15180	12900	9100
523.1	7800	3510	7000	15330	13460	10410
553.9	6980	4210	6620	15390	17080	10680
584.7	6870	3660	7725	14020	19160	10210
615.4	6580	4290	8270	15480	20300	9500

Run no	18a	18b	18c	18d	18e	18f	18g	18h	18I
t (secs)	M(μNm)	M(μNm)	M(μNm)	M(μNm)	M(μNm)	M(μNm)	M(μNm)	M(μNm)	M(μNm)
0.046	1160	2300	3270	6100	10570	9550	18900	20940	23750
3.109	1275	2500	4660	8450	12130	16830	22320	21470	22350
6.218	1280	2490	4670	8510	12160	16890	22030	21330	18810
9.25	1300	2500	4660	8535	12190	16900	22860	21540	21360
12.34	1290	2490	4660	8520	12190	16930	23290	21620	22090
15.42	1290	2485	4670	8560	12230	16950	23470	20340	21820
18.5	1300	2490	4670	8575	12230	16920	23330	20230	21750
21.56	1270	2490	4670	8560	12260	16980	21600	16980	20310
24.64	1300	2490	4670	8590	12270	16990	20370	17850	21310
27.7	1290	2490	4680	8600	12270	17020	21530	19730	21010
30.83	1280	2490	4680	8580	12270	17000	23010	20440	20930
33.89	1305	2490	4680	8620	12280	17000	23010	17020	21510
36.98	1290	2480	4680	8620	12290	17050	22240	15570	20770
40.05	1310	2490	4680	8600	12310	17070	22790	15780	19020
43.08	1290	2490	4690	8640	12320	17040	21980	16950	19530
46.16	1300	2480	4680	8630	12330	17090	21170	18210	20030
49.26	1280	2500	4690	8620	12330	17080	23240	18710	18730
52.33	1305	2490	4690	8650	12330	17090	23340	19590	18080
55.39	1300	2480	4690	8640	12350	17080	23620	18680	17660
58.48	1290	2490	4690	8630	12350	17130	23580	15740	17200
61.55	1285	2490	4700	8665	12360	16690	23540	17900	17680
64.64	1305	2480	4690	8650	12360	16120	23000	18430	17710
67.73	1300	2490	4690	8650	12370	15810	21520	19240	17570
70.78	1280	2500	4700	8675	12380	16570	20600	19710	16590
73.89	1300	2490	4700	8660	12380	17110	20360	19920	15320
76.97	1300	2490	4700	8670	12370	17010	19630	20050	16200
80.05	1280	2490	4700	8690	12400	17010	19230	19990	16810
83.08	1305	2480	4700	8660	12410	17110	19430	20220	16630
86.16	1310	2490	4700	8690	12400	17200	17570	19910	15210
89.23	1270	2490	4700	8700	12410	17230	16560	19190	15480
92.34	1280	2490	4700	8670	12410	17250	17860	20250	15990
95.42	1290	2480	4710	8700	12420	17230	19070	20190	15500
98.47	1310	2490	4700	8700	12420	17270	18560	18540	14480
101.6	1280	2490	4710	8680	12440	16930	16050	18140	14200
104.6	1275	2480	4700	8710	12440	16160	17330	20400	14410
107.7	1290	2480	4710	8710	12450	15830	18010	20390	14830
110.8	1300	2485	4700	8685	12450	15820	18700	19920	12830
113.9	1285	2480	4710	8720	12370	16740	18590	20490	12350
116.9	1280	2490	4710	8710	12450	17260	19740	21400	12010
120	1290	2490	4710	8690	12460	17280	19710	20050	13640

Run no	23a	23b	23c	23d	23e	23f	23g	23h	23I
t (secs)	M(μNm)	M(μNm)	M(μNm)	M(μNm)	M(μNm)	M(μNm)	M(μNm)	M(μNm)	M(μNm)
0.047	910	1800	3590	6400	9630	11120	16670	12610	14270
6.375	990	2010	3980	7380	10540	14690	20570	23610	27660
12.66	1010	2010	3970	7405	10560	14720	20560	23610	27590
18.97	1020	2000	3970	7420	10580	14710	20560	23560	27530
25.3	970	2000	3980	7390	10560	14720	20540	23530	27480
31.61	1010	2010	3980	7415	10570	14720	20520	23530	27410
37.91	1010	2010	3980	7430	10580	14730	20510	23470	27360
44.25	1000	2010	3975	7400	10580	14740	20520	23470	27330
50.53	1000	2010	3980	7430	10580	14730	20510	23450	27290
56.87	1000	2010	3980	7430	10580	14730	20490	23410	27250
63.19	1010	2010	3970	7400	10590	14720	20490	23410	27210
69.49	1005	2010	3970	7430	10590	14730	20500	23380	27180
75.81	990	2010	3975	7435	10590	14710	20480	23360	27150
82.14	1000	2010	3970	7400	10590	14720	20480	23370	27140
88.47	1000	2010	3970	7430	10600	14710	20480	23350	27110
94.75	1000	2010	3970	7425	10600	14740	20460	23340	27090
101.1	1010	2010	3970	7410	10600	14720	20460	23330	27050
107.4	985	2010	3970	7430	10600	14730	20450	23320	27050
113.7	1010	1995	3970	7430	10610	14720	20440	23300	27020
120	1020	2000	3970	7410	10590	14730	20450	23310	27020

Run no	24	25	26
t (secs)	M(μNm)	M(μNm)	M(μNm)
0.062	18310	11820	18160
30.84	21320	22570	27850
61.58	21320	22530	27790
92.31	21290	22520	27740
123.1	21280	22480	27710
153.9	21270	22450	27670
184.6	21260	22400	27660
215.4	21240	22370	27620
246.2	21210	22330	27600
276.9	21180	22320	27560
307.7	21170	22300	27560
338.5	21140	22260	27570
369.3	21110	22260	27530
400	21090	22260	27470
430.8	21080	22260	27410
461.6	21070	22250	27360
492.3	21070	22240	27320
523.1	21070	22230	27270
553.9	21060	22220	27230
584.7	21050	22220	27170
615.4	21040	22200	27130

Run no	33A	33B	33C	33D	33E	33F	33G
t (secs)	M(μNm)	M(μNm)	M(μNm)	M(μNm)	M(μNm)	M(μNm)	M(μNm)
0.047	5030	7950	11220	13190	16140	9450	13850
7.719	6800	9080	10840	11370	13100	9990	19440
15.42	6810	9160	10930	10900	12880	9785	11380
23.11	6820	9120	10640	12530	12000	9415	22790
30.78	6750	9010	10690	11420	13820	9345	25940
38.52	6770	8980	10690	11760	13860	9755	27240
46.17	6790	8950	10760	12160	14590	9620	15210
53.91	6740	8830	10680	12770	13740	9400	16640
61.55	6760	8760	10510	11530	13070	9385	16520
69.23	6700	8585	10550	10620	14370	9330	28190
76.94	6730	8560	10540	11010	13520	9670	26310
84.64	6680	8580	10680	12370	13680	10470	18550
92.33	6700	8430	10270	11090	13890	9250	6370
100	6710	8350	10230	10390	13810	9225	1860
107.7	6680	8210	10290	11870	13700	9230	4500
115.4	6670	8220	9965	12640	13930	9255	5520
123.1	6675	8080	9895	10940	13250	9240	1810
130.8	6675	8140	10050	11250	12850	9270	1520
138.5	6690	8020	9810	12360	13160	9300	4520
146.2	6610	7945	9720	11350	13260	9260	2180
153.9	6655	7900	9560	11430	10960	9220	5350
161.6	6630	7850	10150	12280	11280	9190	1860
169.3	6580	7750	9800	11830	11600	9180	1640
177	6615	7890	9980	10860	11490	9080	4050
184.6	6575	7785	10310	11450	11280	9020	2890
192.3	6590	7810	9980	11680	11130	9040	2100
200	6610	7695	10140	11920	10900	9095	1440
207.7	6605	7690	9940	11420	11000	9990	1660
215.4	6580	7635	10390	11080	12140	9560	2670
223.1	6570	7670	10170	11160	11800	9905	2590
230.9	6535	7560	10270	11120	11780	10120	1630
238.5	6560	7615	9990	11030	11600	9225	1470
246.2	6530	7480	10100	11070	11700	9130	1690
253.9	6530	7490	10170	11400	11450	9025	1650
261.6	6470	7340	10050	11080	10890	8935	2070
269.3	6510	7445	9940	11170	12380	8790	1450
277	6540	7390	9570	10980	12040	8805	1470
284.7	6450	7430	9400	11360	11740	8750	2890
292.3	6510	7415	9070	10970	11450	8400	1640
300	6410	7360	9415	10960	11620		2060

Run no	35A	35B	35C	35D	35E	35F	35G
t (secs)	M(μNm)	M(μNm)	M(μNm)	M(μNm)	M(μNm)	M(μNm)	M(μNm)
0.063	2350	4470	6000	7500	7720	9310	9750
7.766	3055	5050	6530	7960	8680	9900	12810
15.41	3010	5100	6550	7880	8550	9460	12490
23.11	3020	5160	6530	7775	8390	9360	12310
30.81	3020	5170	6545	7665	8310	9280	12190
38.48	3000	5190	6510	7610	8200	9320	12060
46.16	2990	5190	6510	7570	8200	9270	11910
53.86	2955	5170	6510	7530	8120	9340	11740
61.55	3000	5190	6465	7460	8040	9420	12310
69.27	2990	5180	6440	7400	8190	9490	12120
76.94	2950	5200	6410	7360	8210	9550	11920
84.66	2970	5190	6410	7320	8380	9590	11290
92.36	2950	5170	6400	7255	8210	9590	11370
100	2970	5190	6405	7230	8260	9625	11280
107.7	2945	5200	6350	7220	7930	9630	11330
115.4	2960	5190	6350	7140	8020	9620	11350
123.1	2910	5170	6310	7140	8040	9620	11340
130.8	2960	5180	6285	7100	8100	9640	11350
138.5	2950	5175	6275	7100	8070	9670	11400
146.2	2920	5170	6270	7030	8000	9670	11340
153.9	2940	5190	6250	7000	7990	9640	11360
161.6	2900	5170	6220	6990	7990	9650	11330
169.2	2930	5150	6195	6920	8040	9680	11340
177	2930	5170	6160	6930	7990	9690	11320
184.6	2935	5140	6170	6880	7980	9680	11260
192.3	2930	5150	6200	6885	7950	9690	11240
200	2880	5155	6155	6860	7900	9680	11210
207.7	2930	5130	6150	6840	7870	9670	11200
215.4	2870	5150	6130	6790	7810	9655	11200
223.1	2900	5120	6100	6770	7760	9660	11180
230.8	2865	5115	6130	6790	7680	9640	11210
238.5	2880	5130	6100	6860	7660	9620	11430
246.2	2900	5110	6080	6755	7650	9630	11300
253.9	2870	5105	6070	6710	7580	9670	11240
261.5	2905	5105	6060	6760	7630	9660	11240
269.3	2880	5110	6010	6750	7560	9660	13080
276.9	2890	5120	6030	6760	7590	9645	12000
284.6	2845	5110	6050	6755	7540	9700	11660
292.3	2880	5150	6030	6755	7550	9680	11370
			6010	6745	7530	9650	11300

Run no	35H	35I	35J
t (secs)	M(μNm)	M(μNm)	M(μNm)
0.078	11600	9860	16690
7.719	15850	19800	10540
15.39	14320	13510	9725
23.11	13000	11300	8300
30.81	12100	10290	6850
38.48	11550	8965	4560
46.17	11330	7855	2620
53.87	10990	7210	2440
61.56	10520	4620	1275
69.28	13470	1910	1310
76.94	16530	1360	1410
84.62	7310	1360	1460
92.34	10290	1450	1285
100	1510	1440	1435
107.7	2425	1800	1630
115.4	920	1625	1400
123.1	17750	2325	2440
130.8	6880	2380	1545
138.5	885	2120	1750
146.2	1010	1460	1790
153.9	6950	1425	1310
161.5	14170	1520	1550
169.3	1130	1540	1390
176.9	1160	1600	1980
184.6	2260	1710	2300
192.3	2140	1565	2890
200	5245	1790	3295
207.7	6800	1800	1645
215.4	1390	1880	1640
223.1	1710	1820	1520
230.8	1310	1880	1530
238.5	1060	1740	1485
246.2	920	1770	1530
253.9	12750	1620	1590
261.6	6880	1615	1560
269.2	885	1690	1440
277	1010	1550	1510
284.7	6950	1630	1590
292.3	14170	1675	1470

	300		3265	1610		1630
Run no	37	38	39	40	41	42
t (secs)	M(μNm)	M(μNm)	M(μNm)	M(μNm)	M(μNm)	M(μNm)
0.047	14730	17760	21750	16370	18430	20050
15.27	4395	11020	18960	20060	5430	3570
30.53	2765	4065	20610	18000	3400	2060
45.77	1485	1230	19010	18420	2340	1545
61.06	2390	1020	20250	2560	2215	1810
76.31	1220	1310	21200	2350	1980	1890
91.53	1980	1020	21430	2650	1480	1700
106.8	1540	1830	21870	2720	1270	1510
122.1	1355	1065	21440	1320	1230	1680
137.3	1240	950	21660	2100	1490	1765
152.5	1260	1040	22200	7610	1375	1790
167.8	2650	1090	21530	2000	1270	1650
183.1	1590	960	22150	1320	1710	1540
198.4	1175	1040	19830	1290	1120	1440
213.6	1010	990	21140	2280	1150	4290
228.9	1010	980	20710	2240	1320	1485
244.1	1050	950	20180	2220	1245	1795
259.3	3965	890	19860	2410	1175	1340
274.7	1380	1060	19400	1600	1190	1480
289.9	1390	1140	17290	2480	1160	1440
305.1	3480	990	18380	2450	1400	1450
320.4	1360	1020	15620	3390	1170	1445
335.6	1050	930	10960	3880	1125	1230
350.9	980	910	11200	1450	1200	1280
366.2	945	975	11090	2580	1190	1180
381.4	1130	1030	11130	2640	1160	1600
396.7	1040	1030	11160	2870	1190	1550
411.9	1130	1030	11100	1870	1165	1375
427.1	1100	1090	11010	2540	1100	1210
442.4	975	1110	11080	2550	1070	1300

Cont	37	38	39	40	41	42
t (secs)	M(μNm)	M(μNm)	M(μNm)	M(μNm)	M(μNm)	M(μNm)
457.7	970	3880	10990	2480	1080	1320
472.9	1090	1230	10900	1650	1090	1500
488.2	1250	2920	10900	2600	1030	1605
503.4	1220	1650	10890	2540	1070	1400
518.7	1205	990	10800	3540	1045	1545
533.9	1120	960	10800	2370	1120	1580
549.2	1020	1110	10680	4700	1130	1510
564.4	1040	1040	10830	2290	1080	1560
579.7	1110	1110	10410	1950	1080	1570
594.9	1215	1060	11490	2540	1170	1335
610.2	1225	965	11470	1840	1075	1390
625.5	1170	1170	10300	1590	1075	1540
640.7	1170	1040	12130	1870	1020	1690
656	1160	1290	12950	1495	1090	1740
671.2	1040	1315	13140	745	950	1810
686.5	995	1210	14810	810	1090	1695
701.7	945	1260	13240	700	885	1495
717	1190	1270	18290	870	940	1560
732.3	1240	1110	14620	780	1100	1630
747.5	1130	1165	12650	955	1120	1360
762.8	1180	1305	12900	2510	1150	1380
778	1075	1255	10920	1230	1010	2155
793.2	1070	1300	10450	1010	1015	1370
808.5	1140	1240	11550	2110	1080	1580
823.7	1200	1240	11680	1790	1030	1730
839	1140	1250	12950	1150	1120	1470
854.3	1195	1295	11310	1030	860	1390
869.5	1090	1320	10620	2925	900	1550
884.8	1030	1240	11890	2040	1105	1520
900.1	1080	1300	12310	2060	910	1560

Run no	43A	43B	43C	43D	43E	43F	43G	43H
t (secs)	M µNm	M µNm	M µNm	M µNm	M µNm	M µNm	M µNm	M µNm
0.047	3500	5790	7610	10440	12780	13160	12460	26880
5.14	3680	6315	8555	11490	14290	17940	23190	27930
10.23	3620	6400	8530	11470	14120	17560	22900	27060
15.3	3690	6460	8550	11440	14090	17790	22930	25930
20.37	3670	6505	8550	11410	14120	18070	23240	26620
25.47	3690	6510	8570	11390	14110	18040	23010	28550
30.55	3670	6550	8545	11340	14040	17960	23550	25750
35.59	3670	6570	8570	11300	13970	18150	23420	23950
40.73	3670	6540	8545	11280	13900	18250	23080	23120
45.8	3610	6565	8570	11260	13910	18320	22640	21070
50.87	3675	6570	8510	11210	13860	18230	22050	19880
55.95	3640	6535	8505	11170	13850	18430	21760	21580
61.08	3640	6570	8510	11160	13850	18470	21640	20820
66.16	3640	6580	8540	11110	13820	18520	21250	20430
71.19	3620	6550	8550	11080	13810	18330	21060	20000
76.28	3630	6570	8510	11070	13770	18440	20980	19540
81.39	3605	6555	8505	11040	13720	18420	20850	19120
86.45	3610	6550	8500	11010	13700	18330	20710	20770
91.53	3600	6565	8490	10980	13690	18320	20620	20620
96.62	3570	6570	8500	10990	13670	18260	20460	20770
101.7	3620	6545	8490	10940	13650	18440	20260	20070
106.8	3585	6550	8510	10920	13680	18480	20090	19140
111.9	3620	6540	8500	10900	13630	18470	19990	17840
117	3615	6545	8505	10890	13560	18380	19740	19430
122.1	3580	6570	8470	10840	13430	18300	19490	18400
127.1	3580	6550	8460	10840	13360	18430	21030	17400
132.3	3570	6570	8470	10840	13380	18230	21580	15830
137.3	3605	6550	8450	10820	13390	18240	22670	18670
142.4	3580	6555	8465	10790	13450	18140	22410	17400

Cont	43A	43B	43C	43D	43E	43F	43G	43H
t (secs)	M µNm	M µNm	M µNm	M µNm	M µNm	M µNm	M µNm	M µNm
147.5	3595	6570	8470	10800	13470	18020	22110	17660
152.6	3595	6550	8490	10790	13460	18000	21380	18520
157.6	3540	6550	8455	10790	13470	17920	21290	18530
162.8	3595	6565	8450	10770	13390	17850	21420	17460
167.8	3570	6550	8445	10790	13400	17500	21350	16370
172.9	3555	6550	8440	10750	13410	17760	21450	19090
178	3580	6565	8480	10740	13330	17650	21280	17160
183.1	3585	6540	8445	10750	13340	17690	20990	16650
188.2	3540	6545	8460	10750	13320	17700	20870	15270
193.3	3570	6570	8460	10710	13370	17680	21020	16860
198.3	3555	6540	8470	10750	13380	17560	21050	15570
203.4	3590	6555	8420	10740	13350	17530	21030	14450
208.5	3570	6560	8435	10700	13380	17590	21160	15840
213.6	3550	6525	8430	10690	13320	17530	21110	15100
218.7	3565	6570	8450	10720	13320	17490	21110	13970
223.7	3540	6550	8440	10700	13380	17580	20980	12720
228.8	3575	6540	8430	10660	13400	17550	21060	14550
234	3550	6570	8440	10680	13370	17580	20990	14340
239	3530	6545	8430	10700	13380	17630	20790	13160
244.1	3580	6550	8445	10670	13410	17570	20750	13850
249.2	3560	6570	8420	10650	13330	17580	20840	13540
254.3	3530	6560	8430	10650	13350	17520	20850	13470
259.4	3570	6555	8445	10660	13360	17470	20800	13000
264.5	3555	6540	8440	10610	13370	17510	20760	12420
269.5	3570	6540	8445	10610	13310	17500	20810	11160
274.6	3550	6550	8410	10620	13380	17520	20440	12440
279.7	3510	6570	8410	10610	13410	17590	20480	11140
284.8	3560	6540	8415	10600	13410	17570	20450	12450
289.9	3560	6560	8440	10600	13430	17580	20470	11370
294.9	3555	6540	8450	10620	13530	17560	21830	10070
300	3540	6540		10630		17510	20260	

Run no	49	50	51	52	53	54
t (secs)	M (μNm)	M (μNm)	M (μNm)	M (μNm)	M (μNm)	M (μNm)
0.14	8580	14750	17740	20240	18450	19600
15.28	11550	15810	5150	4810	15500	18110
30.53	11080	13060	2950	3130	1530	18410
45.81	10200	9660	2135	1455	1275	19580
61.08	9570	13330	1735	1400	1240	19300
76.37	9980	8650	1580	1400	1220	20190
91.53	11830	8505	1480	1320	1420	19580
106.8	12040	8130	1720	1230	1670	19430
122.1	11180	10210	1535	1480	1615	15740
137.4	11620	15190	4345	1500	1570	17380
152.7	12440	9260	3920	1250	1600	18940
167.9	10520	7640	1330	1165	1580	19920
183.1	11510	6990	1560	1450	1360	18880
198.3	12010	6135	1380	1380	1300	19190
213.6	12160	5770	1220	1070	1370	21460
228.8	11900	1030	1080	1390	1360	14560
244.1	11070	880	1120	1570	1350	19200
259.5	11640	840	1180	1340	1430	21280
274.7	11930	860	1240	1570	1475	15960
290	11610	860	1300	1450	1340	15880
305.1	11860	880	1435	1380	1460	15500
320.5	12160	1035	1170	1575	1450	12140
335.7	11760	1125	1270	1295	1490	15680
350.9	10240	1010	2520	1400	1585	11790
366.2	10320	12190	1550	1080	1520	12290
381.4	10930	2250	1595	1310	1450	8450
396.6	9100	3980	1250	1420	1350	5165
411.9	9710	2980	1190	1220	1410	15540
427.2	9750	2620	1140	1425	1320	5380
442.4	11410	1120	1355	1360	1010	15010

Cont	49	50	51	52	53	54
t (secs)	M (μNm)	M (μNm)	M (μNm)	M (μNm)	M (μNm)	M (μNm)
457.7	11190	1025	1500	1130	1100	9560
473	11270	1440	1270	1170	1440	19150
488.2	9730	1150	1220	1240	1410	15720
503.4	9980	1250	1230	1330	1355	6530
518.7	9550	1325	1350	1285	1335	6750
534	10670	1220	1450	1240	1480	10400
549.2	9750	1350	1210	1100	1260	18200
564.4	9670	1250	1290	1230	1310	18360
579.7	9490	1295	1080	1210	1390	9740
595	9810	1230	1000	970	1430	16170
610.3	9770	950	1205	1345	1430	14640
625.6	9820	990	1270	1330	1430	6420
640.7	9720	1045	1040	1100	1450	7050
656.1	10790	1020	1030	1120	7780	10600
671.3	9320	960	1140	1240	1415	12050
686.6	9870	990	1150	1310	1230	16650
701.8	9830	1170	1100	1105	1220	14020
717	10770	1065	960	1290	1240	12940
732.3	10190	1020	1020	1330	1230	17710
747.5	10440	950	1150	1340	1365	14480
762.8	10320	900	1140	1750	1200	12190
778.1	10470	885	1130	6720	1240	23130
793.3	10380	990	1150	1380	1600	22770
808.6	9240	1050	1290	1390	1640	20560
823.8	10540	1045	1330	1320	1440	20680
839.2	9660	9235	1210	1250	1280	22190
854.3	10090	8155	1570	1440	1110	23770
869.5	9100	5760	1250	1240	1170	17540
884.9	9700	5740	1170	1260	1140	18120
900.1	10050	5015	1120	1240	1190	20600

Run no	55	56	57	58	59	60	61
t (secs)	M (μNm)	M (μNm)	M (μNm)	M (μNm)	M (μNm)	M (μNm)	t (secs)
0.14	19190	19640	19640	9600	9600	5400	13460
15.28	6150	4925	4925	14830	14830	5785	19110
30.53	3710	3270	3270	16720	16720	5850	18310
45.81	4250	2010	2010	15910	15910	5860	17840
61.08	2880	2200	2200	16560	16560	5860	16930
76.37	3110	4600	4600	13240	13240	5930	16570
91.53	6810	2200	2200	15780	15780	5880	16990
106.8	1920	1670	1670	14590	14590	5880	17500
122.1	5830	3020	3020	12630	12630	5870	17790
137.4	3700	2990	2990	13960	13960	5885	17700
152.7	3340	1520	1520	5640	5640	5870	17760
167.9	3325	4745	4745	15640	15640	5850	17310
183.1	2590	1500	1500	16020	16020	5840	17220
198.3	1780	2060	2060	6020	6020	5800	16710
213.6	2420	1445	1445	8170	8170	5870	16700
228.8	1605	1800	1800	4390	4390	5850	16710
244.1	3720	1370	1370	7510	7510	5830	15280
259.5	5510	1850	1850	6470	6470	5810	14480
274.7	4120	3065	3065	7780	7780	5785	14800
290	1510	1860	1860	8330	8330	5850	15110
305.1	1930	1730	1730	12930	12930	5840	15120
320.5	2370	4320	4320	14420	14420	5830	15490
335.7	3480	1455	1455	14810	14810	5790	15380
350.9	1330	1730	1730	10270	10270	5860	15240
366.2	1880	3730	3730	5840	5840	5840	14610
381.4	3560	1470	1470	15900	15900	5810	14930
396.6	3250	3450	3450	15000	15000	5865	15210
411.9	2025	1365	1365	8130	8130	5850	15220
427.2	4640	1340	1340	8140	8140	5830	15060
442.4	1550	1160	1160	10140	10140	5830	15000
457.7	1740	1280	1280	9650	9650	5790	15040

Cont	55	56	57	58	59	60	61
t (secs)	M in µNm	M in µNm	M in µNm	M in µNm	M in µNm	M in µNm	M in µNm
473	2380	3450	3450	9650	9650	5830	15570
488.2	1715	1380	1380	8880	8880	5850	15080
503.4	1670	4930	4930	7080	7080	5820	15430
518.7	1490	1570	1570	8860	8860	5820	15600
534	3520	1650	1650	9360	9360	5790	15630
549.2	3915	1850	1850	8510	8510	5800	15600
564.4	3330	1040	1040	8860	8860	5795	15780
579.7	1640	4720	4720	7770	7770	5860	16060
595	1920	1240	1240	7050	7050	5835	16130
610.3	3020	5035	5035	6700	6700	5805	16430
625.6	1480	1170	1170	3810	3810	5770	16290
640.7	1660	1680	1680	2000	2000	5770	16050
656.1	1310	1150	1150	5610	5610	5830	17300
671.3	3290	1610	1610	3500	3500	5780	16410
686.6	1250	1490	1490	2630	2630	5750	17140
701.8	1340	1600	1600	1800	1800	5770	17540
717	1630	1350	1350	1870	1870	5810	17310
732.3	2605	1435	1435	2020	2020	5790	18460
747.5	1220	1470	1470	1880	1880	5760	18500
762.8	1270	1280	1280	5210	5210	5800	18430
778.1	2320	1310	1310	13550	13550	5820	18090
793.3	1195	1415	1415	7390	7390	5790	18250
808.6	1030	1180	1180	3390	3390	5790	17380
823.8	1010	1940	1940	1020	1020	5760	17350
839.2	1090	1110	1110	2560	2560	5805	17410
854.3	1010	1235	1235	1320	1320	5825	17340
869.5	1130	1190	1190	3790	3790	5790	17310
884.9	1040	1650	1650	3370	3370	5780	17260
900.1	1320	1330	1330	2320	2320	5770	17170

Run no	62A	62B	62C	62D	62E	62F
t (secs)	M(μNm)	M(μNm)	M(μNm)	M(μNm)	M(μNm)	M(μNm)
0.047	3570	6130	6270	6330	7570	6160
5.109	3910	6490	6335	6790	7460	7720
10.2	3930	6515	6350	6500	7060	8010
15.27	4000	6480	6230	6370	6765	11390
20.36	4050	6390	6020	6150	6710	10750
25.48	4080	6360	5920	6180	6640	10350
30.52	4130	6290	5830	6030	6415	10330
35.64	4145	6235	5780	5880	6315	10750
40.73	4120	6180	5770	5820	6100	9770
45.77	4190	6080	5730	5730	5990	7720
50.86	4190	6040	5590	5700	5980	7200
56	4175	5970	5510	5650	5860	6790
61.05	4210	5885	5460	5540	5735	6370
66.14	4170	5890	5710	6170	5690	6090
71.22	4215	5770	6050	7270	5730	5830
76.3	4210	5770	6400	6140	5650	5620
81.37	4170	5730	6175	6330	5525	9170
86.52	4210	5660	6250	5560	5440	10620
91.53	4185	5660	6265	5420	5490	8040
96.66	4230	5625	5980	5450	8630	7330
101.7	4220	5590	6260	5290	7240	6910
106.8	4180	5565	6180	5320	8705	6620
111.9	4220	5530	5950	5260	6530	6330
117	4185	5410	6050	7100	6270	6060
122.1	4210	5495	5975	6300	6280	6250
127.2	4210	5410	6070	6780	5945	7860
132.2	4160	5400	5990	6760	5830	6820
137.3	4175	5380	5980	6900	5850	6380
142.4	4190	5440	5830	6820	5810	6070
147.5	4185	5360	5900	6760	5670	5790

Cont	62A	62B	62C	62D	62E	62F
t (secs)	M(μNm)	M(μNm)	M(μNm)	M(μNm)	M(μNm)	M(μNm)
152.6	4190	5390	5840	6730	5700	5570
157.7	4175	5270	5850	6720	5730	8100
162.7	4190	5370	5810	6670	5650	10500
167.8	4130	5305	5780	6590	5580	7800
172.9	4205	5340	5790	6410	5725	7180
178	4180	5290	5740	6400	5675	7070
183.1	4160	5270	5730	6460	5650	10770
188.1	4170	5290	5700	6450	8460	8100
193.2	4160	5235	5590	6590	7900	7170
198.3	4180	5290	5750	6470	6990	9130
203.4	4160	5195	5600	6450	8480	9120
208.5	4170	5225	5610	6480	7160	7250
213.6	4155	5160	5630	6520	6430	6740
218.7	4120	5150	5610	6480	6190	6040
223.8	4160	5060	5560	6270	5980	7520
228.8	4140	5085	5560	6490	5890	10110
233.9	4170	5120	5455	6310	5920	7000
239	4155	5070	5470	6310	5810	6510
244.1	4140	5200	5640	6290	5715	6870
249.2	4135	5010	5395	6320	5620	6160
254.3	4110	5125	5540	5670	5730	8620
259.3	4145	4990	5350	5490	5650	7950
264.5	4130	5005	5230	5510	5515	6570
269.5	4100	5120	5050	5450	5535	6370
274.6	4130	5050	5100	5420	5570	9920
279.7	4090	4965	5020	5420	5600	7180
284.8	4140	5060	4970	5360	5575	6800
289.9	4120	5105	4890	5370	5580	6550
295	4085	4940	4770	5360	5660	5800
300	4140		4710			5630

Run no	62G	62H	62I	62H1	62G1	62 F1	62E1
t (secs)	M(μNm)	M(μNm)	M(μNm)	M(μNm)	M(μNm)	M(μNm)	M(μNm)
0.109	8800	9680	3230	4340	7440	12230	8070
5.109	14850	8990	5120	3850	9180	12600	8970
10.19	14520	8390	3780	3080	8580	12220	8960
15.34	14340	1710	2930	2550	8190	11960	8910
20.34	14200	1260	2180	2160	7950	11760	8920
25.44	13890	1040	1730	1830	7730	11570	8910
30.53	13740	1130	1360	1520	7560	11430	8930
35.62	13520	1200	1210	1350	7430	11280	8940
40.69	13380	1310	1130	1290	7340	11080	8940
45.8	13290	1340	1140	1240	7210	10990	8940
50.87	13200	1300	1140	1200	7080	10780	8950
55.97	13030	1180	1120	1300	6950	10650	8970
61.03	12930	1080	1110	1510	6820	10560	9000
66.14	12950	1000	1120	1680	6740	10530	9000
71.25	12790	1000	1150	1760	6680	10510	9010
76.28	12760	990	1180	1790	6580	10540	9040
81.37	12840	1020	1170	1750	6500	10540	9040
86.48	12790	1040	1160	1680	6450	10510	9075
91.58	12720	1040	1170	1630	6410	10480	9110
96.67	12680	1100	1150	1490	6360	10480	9110
101.7	12490	1040	1110	1440	6330	10500	9125
106.9	12550	1040	1140	1440	6290	10480	9140
111.9	12340	1040	1250	1410	6270	10440	9140
117	12420	990	1350	1390	6270	10450	9150
122.1	13210	1000	1420	1370	6230	10460	9190
127.1	13090	1000	1490	1400	6210	10480	9175
132.3	12140	990	1590	1430	6250	10470	9185
137.4	13750	940	1660	1540	6260	10460	9210

Cont	62G	62H	62I	62H1	62G1	62 F1	62E1
t (secs)	M(µNm)	M(µNm)	M(µNm)	M(µNm)	M(µNm)	M(µNm)	M(µNm)
142.4	12190	950	1500	1660	6300	10500	9200
147.5	11750	930	1300	1780	6400	10490	9220
152.6	13470	950	1250	1790	6360	10510	9225
157.7	11860	1050	1160	1590	6400	10510	9230
162.8	11980	1110	1010	1470	6510	10530	9230
167.8	13300	1260	1110	1350	6480	10540	9260
172.9	11100	1470	1140	1220	6510	10530	9260
178	13490	1520	1170	1230	6560	10550	9240
183.2	13180	1300	1210	1140	6590	10570	9270
188.2	13260	1190	1240	1140	6700	10570	9270
193.2	11260	1100	1040	1010	6700	10590	9260
198.3	10940	1080	1000	1060	6710	10620	9320
203.4	10810	1060	1180	1170	6770	10620	9320
208.5	10630	1070	1140	1350	6850	10620	9300
213.6	10270	1060	1100	1440	6840	10610	9320
218.7	10290	1060	1090	1490	6840	10600	9320
223.8	10200	980	1150	1510	6840	10630	9315
228.9	10180	950	1250	1520	6840	10650	9340
233.9	10150	990	1330	1570	6860	10690	9340
239.1	10150	1020	1120	1640	6810	10690	9330
244.2	10110	1160	990	1670	6820	10670	9345
249.2	10070	1240	940	1730	6830	10690	9370
254.3	9980	1310	920	1700	6860	10670	9340
259.4	9860	1220	1020	1700	6900	10700	9350
264.4	9890	1310	990	12280	6940	10690	9360
269.6	10080	1360	1050	12130	7050	10710	9345
274.6	11430	1380	1080	10310	7040	10720	9355
279.8	11900	1300	930	9410	7090	10710	9370
284.7	10820	1110	1120	8450	7660	10740	9360
289.8	10420	1040	1200	7900	14580	10710	9360
294.9	10120	1010	1090	7550	13400	10740	9380
300	9480	1050	1070	7260	12130	10760	9360

Run no	62F2	62G2	62H2	62.I2
t (secs)	M(μNm)	M(μNm)	M(μNm)	M(μNm)
0.047	12070	11510	10750	16240
5.11	13240	15760	13940	18780
10.19	13070	15180	13620	17930
15.3	13010	14490	13510	17120
20.37	13010	15030	13450	16570
25.49	13010	15240	13450	16220
30.59	13040	14930	13430	15970
35.59	12940	14620	13450	15770
40.73	12770	15400	13480	15700
45.81	12680	14940	13530	15680
50.87	12600	14520	13540	15710
56	12480	15030	13520	15580
61.11	12510	15280	13520	15540
66.17	12570	14840	13590	15430
71.25	12470	14700	13650	15340
76.28	12180	14690	13710	15240
81.41	12000	14470	13750	15160
86.55	12230	15500	13800	15150
91.55	11900	15220	13870	15060
96.66	11560	15290	13920	15060
101.8	12030	14820	13970	14980
106.8	11650	14320	14000	14790
112	11780	14700	14040	14530
117	10720	14830	14070	14430
122.1	10690	14510	14060	14250
127.2	10680	13940	14050	14180
132.3	10720	14910	14020	14060
137.3	10760	13970	14010	13950
142.4	10850	13970	14020	13930

Cont	62F2	62G2	62H2	62.I2
t (secs)	M(µNm)	M(µNm)	M(µNm)	M(µNm)
147.5	10890	15230	14020	13740
152.5	10940	14370	14050	13580
157.7	10950	15450	14060	13460
162.7	10980	14050	14080	13270
167.8	11010	13760	14050	13130
172.9	11000	13750	14030	13030
178	11000	13660	14030	12880
183.1	10990	13680	14000	12740
188.2	11000	13630	13990	12580
193.2	10990	13640	14000	12420
198.3	10990	13750	14030	12270
203.4	11010	13730	14070	12140
208.5	11000	13880	14060	12050
213.6	11000	13810	14080	11920
218.7	11020	13940	14090	11820
223.7	11030	13850	14070	11720
228.8	11040	13930	14030	11590
233.9	11050	13920	14050	11500
239	11070	13940	14080	11400
244.1	11090	15040	14080	11360
249.2	11100	14440	14070	11290
254.3	11120	14250	14030	11180
259.4	11100	14250	14060	11110
264.4	11120	14160	14020	10970
269.5	11130	16150	14020	10770
274.6	11160	14330	14040	10480
279.7	11160	14230	14030	10150
284.8	11160	14180	14060	9960
289.9	11170	14280	14040	9540
295	11190	15110	14060	9585
300		15040	14050	9710

Run no	63A	63B	63C	63D	63E	63F
t (secs)	M(μNm)	M(μNm)	M(μNm)	M(μNm)	M(μNm)	M(μNm)
0.047	3610	6040	6400	7210	7270	10360
5.093	3770	6430	6010	6800	7290	11950
10.2	3790	6425	5860	6585	6840	11850
15.28	3860	6370	5750	6430	6635	11800
20.36	3950	6370	5680	6300	6470	11780
25.47	3950	6315	5590	6225	6200	11770
30.51	3970	6250	5565	6150	6110	11770
35.61	4030	6180	5460	6110	5985	11750
40.7	4020	6140	5440	6020	5740	11760
45.76	4005	6060	5390	5980	5530	11740
50.91	4070	6010	5350	5850	7880	11740
55.95	4045	5950	5255	5850	8190	11740
61.06	4060	5845	5220	5820	8425	11730
66.12	4085	5790	5100	5710	9190	11740
71.2	4030	5755	5045	5595	7570	11740
76.34	4065	5680	4930	5620	7320	11760
81.37	4060	5700	4870	5570	7815	11760
86.47	4090	5610	4670	5510	8740	11780
91.58	4060	5580	4780	5410	8880	11790
96.64	4040	5520	5795	5320	8550	11790
101.7	4065	5490	5610	5290	8385	11820
106.8	4050	5445	6090	5150	8590	11820
111.9	4065	5480	6160	5070	8680	11840
117	4060	5470	5900	5140	7190	11850
122.1	4025	5385	6080	6580	6740	11850
127.1	4060	5390	6030	6990	6615	11870
132.3	4050	5265	6035	7580	6390	11860
137.3	4060	5350	6040	6950	6390	11890
142.4	4050	5310	5980	7310	6120	11900

Cont	63A	63B	63C	63D	63E	63F
t (secs)	M(μNm)	M(μNm)	M(μNm)	M(μNm)	M(μNm)	M(μNm)
147.5	4015	5310	5880	7250	5595	11910
152.6	4030	5330	5880	7000	5500	11920
157.7	4050	5175	6035	7145	5470	11910
162.7	4070	5250	5950	6610	5440	11950
167.8	4040	5195	5920	7190	5390	11950
172.9	4000	5180	6005	6120	5430	11970
178	4060	5160	5770	5960	5400	11990
183.1	4010	5100	5820	5850	5430	11990
188.2	4045	5190	5710	5790	5390	12040
193.2	4040	5120	5850	5720	5420	12040
198.3	4020	5180	5580	5660	5440	12080
203.4	4025	4990	5710	5595	5455	12090
208.5	4000	5070	5595	5470	5530	12100
213.6	4010	4950	5680	5440	5550	12130
218.7	4010	4990	5550	5215	5520	12150
223.8	4015	5030	5600	5240	5545	12170
228.8	4000	5035	5480	5215	5540	12190
233.9	3975	4940	5135	5200	5540	12350
239	4010	5000	5170	5180	5510	12560
244.1	3980	4875	5600	5160	5460	12780
249.2	4010	4920	5545	5150	5355	12960
254.3	3985	4935	5480	5110	5280	12510
259.4	4000	4910	5545	5055	5200	12340
264.4	3980	4910	5400	5060	5160	12200
269.5	3985	4865	5490	5070	5075	12120
274.6	3980	4900	5530	5050	4995	12060
279.7	3930	4920	5300	5010	4900	12250
284.8	4000	4900	5385	4960	4820	12230
289.8	3980	4870	5520	4950	4740	12450
295	3980	4890	5330	4940	4675	12320
300		4915	5360		4660	12350

Run no	63G	63H	63I	63H1	63G1	63F1	63E1
t (secs)	M(μNm)	M(μNm)	M(μNm)	M(μNm)	M(μNm)	M(μNm)	M(μNm)
0.156	10750	13650	3190	2900	9630	11790	5020
5.219	13940	11490	5510	2930	14310	11390	5490
10.27	13620	9115	4660	2130	14200	11400	5460
15.3	13510	5060	4190	1710	14110	11480	5430
20.41	13450	4950	3740	1260	14070	11720	5420
25.45	13450	1930	3260	1040	14070	11410	5410
30.72	13430	1270	2790	1130	14050	11020	5420
35.61	13450	1130	2400	1200	14010	10830	5440
40.72	13480	1060	2100	1310	14010	11220	5445
45.83	13530	1165	1920	1340	14040	11190	5465
50.87	13540	1020	1820	1300	14020	11220	5490
56.03	13520	1055	1640	1180	14020	11240	5500
61.06	13520	1150	1400	1080	14050	11900	5510
66.12	13590	1130	1310	1000	14030	11210	5520
71.19	13650	1060	1290	1000	14020	11380	5535
76.28	13710	1130	1210	990	14050	11280	5540
81.39	13750	1080	3010	1020	14030	11400	5550
86.59	13800	1120	3980	1040	14020	11780	5560
91.62	13870	1135	3390	1040	14040	11790	5570
96.73	13920	1090	2510	1100	14020	11790	5580
101.7	13970	1090	2110	1040	14000	11820	5590
106.9	14000	1130	1890	1040	14030	11820	5590
111.9	14040	1240	1720	1040	14040	11840	5600
117	14070	1220	1510	990	14010	11850	5600
122.1	14060	1080	1370	1000	14040	11850	5600
127.1	14050	1040	1220	1000	14060	11870	5600
132.3	14020	1050	1110	990	14020	11860	5600
137.3	14010	970	1050	940	14010	11890	5615
142.5	14020	970	1070	950	14030	11900	5620

Cont	63G	63H	63I	63H1	63G1	63F1	63E1
t (secs)	M(μNm)	M(μNm)	M(μNm)	M(μNm)	M(μNm)	M(μNm)	M(μNm)
147.5	14020	870	1070	930	13990	11910	5630
152.5	14050	720	1020	950	14000	11820	5640
157.8	14060	730	1030	1050	14010	11910	5650
162.8	14080	690	1030	1110	14010	11950	5650
167.9	14050	635	1080	1260	13980	11850	5650
172.9	14030	610	1030	1470	13990	11970	5660
178	14030	750	1010	1520	13960	11990	5660
183.2	14000	700	1020	1300	13930	11990	5670
188.2	13990	810	1010	1190	13950	12040	5675
193.2	14000	710	1020	1100	13950	12040	5670
198.3	14030	840	1050	1080	13910	12080	5690
203.5	14070	1020	1020	1060	13930	12090	5690
208.5	14060	1200	1000	1070	13930	12100	5690
213.6	14080	895	970	1060	13890	12130	5700
218.7	14090	1020	930	1060	13880	12150	5690
223.8	14070	690	970	980	13890	12170	5700
228.8	14030	655	1000	950	13870	12190	5700
234	14050	870	970	990	13870	12350	5710
239.1	14080	865	980	1020	13890	12260	5720
244.1	14080	800	980	1160	13890	12280	5710
249.2	14070	790	1040	1240	13860	12280	5710
254.3	14030	1000	920	1310	13890	12275	5710
259.4	14060	890	800	1220	13870	12260	5710
264.4	14020	1015	530	1310	13840	12290	5720
269.5	14020	1000	510	1360	13850	12560	5710
274.6	14040	900	470	1380	13850	12530	5715
279.8	14030	1040	500	1300	13830	12370	5710
284.8	14060	1160	500	1110	13840	12540	5720
289.9	14040	980	480	1040	13840	12280	5720
295	14060	990	490	1010	13800	12610	5720
300	14050	970	500	1050	13800	12380	5720

Run no	63F2	63G2	63H2	63.I2
t (secs)	M(μNm)	M(μNm)	M(μNm)	M(μNm)
0.047	10250	9740	8290	16110
5.11	11830	14190	17720	15840
10.19	11740	14310	17320	15550
15.3	11680	13990	17060	15260
20.37	11670	14180	16880	14990
25.49	11650	13950	16690	14800
30.59	11660	14160	16510	14610
35.59	11630	13890	16310	14450
40.73	11650	14120	16160	14340
45.81	11620	13920	16010	14240
50.87	11630	14130	15900	14190
56	11620	13900	15840	14130
61.11	11620	14160	15740	14080
66.17	11620	13910	15690	14050
71.25	11630	14130	15630	14040
76.28	11640	13930	15610	14020
81.41	11650	14140	15600	13970
86.55	11660	13900	15560	13950
91.55	11680	14150	15510	13920
96.66	11670	13900	15460	13940
101.8	11710	14110	15440	13960
106.8	11700	13910	15420	13940
112	11730	14150	15390	13950
117	11730	13890	15390	13910
122.1	11740	14150	15360	13880
127.2	11750	13940	15330	13940
132.3	11750	14130	15270	13960
137.3	11770	13890	15230	13980
142.4	11790	14140	15280	14020

Cont	63F2	63G2	63H2	63.I2
t (secs)	M(µNm)	M(µNm)	M(µNm)	M(µNm)
147.5	11790	13870	15300	14050
152.5	11810	14110	15280	14100
157.7	11790	13890	15250	14070
162.7	11840	14120	15230	14090
167.8	11830	13860	15210	14110
172.9	11860	14100	15180	14150
178	11870	13840	15160	14180
183.1	11880	14040	15120	14240
188.2	11920	13830	15120	14250
193.2	11930	14060	15100	14240
198.3	11960	13790	15060	14240
203.4	11980	14040	15040	14230
208.5	11980	13810	15030	14290
213.6	12020	14000	15050	14290
218.7	12030	13760	15030	14300
223.7	12060	14000	15030	14350
228.8	12070	13750	14990	14360
233.9	12240	13980	14970	14370
239	12440	13770	14960	14370
244.1	12670	14000	14950	14360
249.2	12840	13740	14920	14380
254.3	13050	14000	14900	14380
259.4	13190	13750	14910	14400
264.4	13350	13950	14910	14380
269.5	13500	13730	14880	14380
274.6	13610	13960	14860	14390
279.7	13730	13710	14820	14370
284.8	13810	13950	14790	14360
289.9	13870	13720	14780	14300
295	13930	13910	14800	14300
300	13950	13680	14780	14240

Run no	64A	64B	64C	64D	64E	64F
t (secs)	M(μNm)	M(μNm)	M(μNm)	M(μNm)	M(μNm)	M(μNm)
0.047	5500	7930	9310	11450	14790	20170
5.109	5600	5790	9290	11790	14570	17360
10.22	5685	7245	9200	11820	14720	19080
15.3	5720	7390	9170	11670	14440	18500
20.36	5735	7365	8945	11680	14360	16960
25.45	5660	7060	9140	11740	14220	16400
30.52	5635	7300	9130	11020	13090	17170
35.66	5590	6805	9030	11170	13240	17410
40.7	5550	7080	9100	11170	12110	16640
45.78	5460	7215	9000	11140	13140	16720
50.92	5395	6950	9160	11060	13300	15630
55.95	5390	7055	8950	11070	11520	17000
61.03	5300	7020	9050	10740	11960	15990
66.11	5315	6860	9030	11740	14050	15020
71.19	5250	7045	8935	11520	11280	19260
76.3	5170	6870	8940	11670	10930	14110
81.39	5220	6850	8870	11460	10840	12110
86.45	5135	6930	9020	10840	10870	12520
91.53	5130	6765	8840	10670	10550	14240
96.64	5150	6800	8885	11250	9900	16550
101.7	5070	6660	8810	11510	10220	18180
106.8	5080	6590	8680	11660	12780	17390
111.9	5045	6600	8930	11740	13190	14940
117	4980	6585	8580	11380	11290	14660
122.1	5000	6500	8650	11610	11250	16240
127.1	4930	6530	8710	11750	12040	16610
132.2	5015	6760	8845	11440	14450	16250
137.4	4950	6490	8630	11420	12990	18000
142.4	4905	6575	8850	11350	12270	17620

Run no	64A	64B	64C	64D	64E	64F
t (secs)	M(μNm)	M(μNm)	M(μNm)	M(μNm)	M(μNm)	M(μNm)
147.5	4930	6650	8790	10330	11700	19210
152.6	4875	6620	8830	10050	12230	16270
157.7	4900	6610	8765	10720	12440	15380
162.7	4870	6700	8890	11130	11670	14960
167.8	4845	6695	8760	10660	12250	17850
172.9	4850	6730	8790	9890	12610	17650
178	4815	6840	8670	10520	12290	17720
183.1	4860	6740	8720	11050	12100	14440
188.2	4815	6680	8810	10870	11760	16580
193.3	4780	6920	8760	9700	12260	14470
198.3	4790	6700	8630	10010	11930	16220
203.4	4720	6840	8540	10560	11320	15760
208.5	4765	6850	8680	11310	11020	15950
213.6	4750	6810	8650	10140	10650	17590
218.7	4740	6950	8630	10170	10800	19410
223.8	4730	6750	8695	10120	11900	18530
228.9	4690	6900	8770	10340	13700	15800
234	4740	6910	8770	10560	14720	15510
239	4690	6885	8850	11310	12070	16450
244.1	4745	6940	8880	10560	11810	14680
249.2	4720	6855	8815	10450	13760	15040
254.3	4695	6980	9000	10530	14010	18180
259.3	4700	6900	8910	10590	14090	17680
264.4	4665	7010	8840	10370	13570	16360
269.5	4750	6890	8940	10610	11920	13050
274.6	4670	6930	8785	10390	11590	17710
279.7	4690	6950	8870	10820	11070	18180
284.8	4680	6975	8980	10380	11450	17030
289.9	4710	7010	8790	10800	12510	17230
294.9	4650	6910	9030	10520	14570	16410
300	4680	6955				17790

Run no	64G	64H	64I	64J
t (secs)	M(μNm)	M(μNm)	M(μNm)	M(μNm)
0.094	8800	10750	11580	12630
5.109	14850	13940	8670	12970
10.22	14520	13620	7510	7820
15.36	14340	13510	6510	5155
20.37	14200	13450	5700	1110
25.53	13890	13450	4980	1155
30.53	13740	13430	4510	1160
35.59	13520	13450	3880	1150
40.7	13380	13480	3580	1260
45.8	13290	13530	3365	980
50.89	13200	13540	3200	1265
55.95	13030	13520	2900	1190
61.03	12930	13520	2540	1340
66.19	12950	13590	2200	1220
71.23	12790	13650	2115	1220
76.31	12760	13710	1950	1190
81.42	12840	13750	1800	1210
86.48	12790	13800	1710	1305
91.56	12720	13870	1630	1300
96.73	12680	13920	1575	1270
101.8	12490	13970	1520	1240
106.8	12550	14000	1490	1320
112	12340	14040	1520	1240
117	12420	14070	1440	1220
122	13210	14060	1400	1250
127.2	13090	14050	1350	1140
132.2	12140	14020	1325	1170
137.3	13750	14010	1290	1225

Cont	64G	64H	64I	64J
t (secs)	M(μNm)	M(μNm)	M(μNm)	M(μNm)
142.4	12190	14020	1290	1190
147.5	11750	14020	1290	1205
152.6	13470	14050	1310	1180
157.7	11860	14060	1300	1160
162.7	11980	14080	1370	1270
167.8	13300	14050	1255	1250
172.9	11100	14030	1280	1230
178	13490	14030	1230	1230
183.1	13180	14000	1220	1240
188.1	13260	13990	1290	1270
193.3	11260	14000	1240	1300
198.3	10940	14030	1320	1195
203.4	10810	14070	1120	1150
208.5	10630	14060	1170	1165
213.6	10270	14080	950	1090
218.7	10290	14090	625	1040
223.7	10200	14070	720	1050
228.9	10180	14030	800	1080
234	10150	14050	680	1075
239.1	10150	14080	700	1070
244.2	10110	14080	605	1060
249.2	10070	14070	670	1110
254.2	9980	14030	630	1120
259.3	9860	14060	680	1055
264.4	9890	14020	730	1100
269.5	10080	14020	710	1115
274.7	11430	14040	720	1170
279.7	11900	14030	750	1070
284.8	10820	14060	650	1020
289.9	10420	14040	690	1000
294.9	10120	14060	750	980
300.1	9480	14050	650	960

Run no	65	66	67
t (secs)	M(μNm)	M(μNm)	M(μNm)
0.125	9920	21160	7900
15.39	16250	9710	17560
30.58	17070	1050	18050
45.8	15900	1040	17190
61.12	15270	860	17490
76.34	16080	975	16640
91.55	15720	855	17350
106.8	15330	900	17170
122.1	9120	1130	17320
137.3	15090	1060	16790
152.6	8930	2810	11650
167.9	13240	840	12760
183.2	15150	990	12180
198.5	9170	910	12840
213.6	9960	1485	9670
228.9	11470	1080	11790
244.2	9310	2070	13730
259.4	10250	2610	12930
274.6	12360	975	10230
289.8	9450	1265	10000
305.1	10730	1160	10210
320.4	11610	1110	10590
335.6	9630	3190	11180
350.9	10930	970	10460
366.1	12240	930	9870
381.4	9820	2230	14820
396.7	13870	1010	11790
411.9	10860	965	13390

Cont	65	66	67
t (secs)	M (μNm)	M (μNm)	M (μNm)
427.2	9930	1100	14970
442.4	9870	1170	11380
457.7	12790	1170	9770
472.9	11570	1110	16140
488.2	11060	980	12970
503.5	10440	860	11830
518.8	9510	970	10790
534	15150	800	16440
549.3	12910	875	13690
564.5	11710	980	16550
579.7	10870	1060	14440
595	14600	1085	12580
610.2	13770	900	16770
625.5	13500	1020	15050
640.7	13530	990	15750
655.9	13380	1040	15520
671.2	13260	1145	17250
686.5	12970	1060	17110
701.7	12450	1100	17070
717	11880	760	16790
732.3	14870	1065	16740
747.5	16100	1040	15680
762.7	14480	1010	16760
778	13470	1190	17250
793.3	13080	880	17380
808.5	12560	1060	16790
823.9	12140	1120	18030
839.1	15090	880	17830
854.3	15380	1080	17810
869.6	14240	1185	17630
884.7	13480	1280	17270
900	13260	1160	19960

Run no	68A	68B	68C	68D	68E
t(sec)	M (μNm)	M (μNm)	M (μNm)	M (μNm)	M (μNm)
0.156	3930	6310	6100	8430	10570
5.219	4090	6000	6775	8620	11520
10.27	4110	6290	6750	8225	11230
15.3	4125	6260	6655	8175	11060
20.41	4170	6200	6600	8250	10910
25.45	4160	6100	6500	8425	10860
30.72	4205	6000	6580	8140	10620
35.61	4200	5980	6550	8290	10880
40.72	4200	5910	6570	8410	10870
45.83	4180	5920	6560	8380	10770
50.87	4170	5820	6610	8440	10830
56.03	4190	5745	6560	8555	10820
61.06	4170	5830	6620	8640	10690
66.12	4150	5640	6565	8440	10680
71.19	4160	5690	6640	8450	10680
76.28	4100	5690	6630	8530	10960
81.39	4120	5630	6625	8530	10780
86.59	4130	5580	6580	8475	10520
91.62	4090	5530	6575	8690	10510
96.73	4090	5560	6480	8530	10410
101.7	4110	5535	6450	8475	10820
106.9	4105	5500	6590	8560	10830
111.9	4080	5460	6580	8600	10860
117	4070	5435	6555	8530	10910
122.1	4100	5450	6460	8370	11170
127.1	4055	5405	6480	8600	11070
132.3	4040	5430	6670	8560	10760
137.3	4060	5405	6500	8400	11180

Cont	68A	68B	68C	68D	68E
t(sec)	M (μNm)	M (μNm)	M (μNm)	M (μNm)	M (μNm)
142.5	4045	5385	6435	8550	10810
147.5	4060	5460	6450	8490	11150
152.5	4045	5400	6450	8500	11070
157.8	3990	5380	6505	8330	11140
162.8	4040	5330	6490	8290	10890
167.9	4030	5390	6480	8270	10900
172.9	4000	5295	6400	8340	10940
178	4040	5375	6330	8510	10830
183.2	4000	5290	6410	8520	11040
188.2	4030	5385	6390	8545	10880
193.2	4020	5250	6385	8450	10970
198.3	3995	5330	6320	8400	10990
203.5	3990	5250	6370	8335	10830
208.5	3985	5240	6400	8280	10810
213.6	4030	5175	6390	8440	10960
218.7	4005	5190	6340	8500	10960
223.8	3970	5180	6320	8460	10800
228.8	3990	5210	6480	8315	10650
234	3960	5200	6375	8240	11080
239.1	3990	5190	6310	8520	10630
244.1	3975	5240	6325	8320	10890
249.2	4000	5240	6350	8710	10970
254.3	3960	5140	6270	8440	10890
259.4	3950	5190	6355	8520	10770
264.4	3990	5140	6400	8525	10830
269.5	3970	5160	6295	8450	10750
274.6	3975	5120	6360	8455	11100
279.8	3950	5210	6330	8570	10970
284.8	3920	5125	6245	8500	10850
289.9	3990	5030	6400	8375	10880
295	3945	5150	6325	8420	10660
300	3945	5150	6490	8460	11110

Run no	68F	68G	68H	68I	68J
t(sec)	M (μNm)	M (μNm)	M (μNm)	M (μNm)	M (μNm)
0.156	13870	9920	7810	15390	14470
5.219	14430	11950	15490	15790	21640
10.27	13540	12890	13950	14770	20090
15.3	13850	14680	12660	13870	18220
20.41	13930	13730	12130	12820	16410
25.45	13500	13840	11320	11550	14900
30.72	13370	13290	10010	10370	13740
35.61	14120	13060	12090	9140	12480
40.72	13650	13360	11460	7970	10970
45.83	13830	13760	11080	7440	9840
50.87	14130	12810	10750	9600	8325
56.03	14060	13130	10400	8290	7070
61.06	13690	11200	10140	7765	6135
66.12	14030	10870	9800	7360	4910
71.19	13920	14190	9430	6815	3200
76.28	14180	12840	9110	5880	1650
81.39	13950	11200	9160	5425	1310
86.59	13540	14290	8990	5380	1330
91.62	13810	11550	8850	3860	1410
96.73	13300	10960	8830	1540	1390
101.7	13780	11040	8670	1130	1345
106.9	13010	10860	8470	1005	1350
111.9	13730	10920	8450	1010	1310
117	13100	11060	8450	1000	1340
122.1	13600	11360	8330	1030	1350
127.1	12610	11090	8170	1000	1320
132.3	12380	11010	8460	1045	1320
137.3	13520	11140	8370	1080	1340
142.5	13100	11450	8350	1045	1360

Cont	68F	68G	68H	68I	68J
t(sec)	M (μNm)	M (μNm)	M (μNm)	M (μNm)	M (μNm)
147.5	12690	11330	8350	1040	1325
152.5	13520	11200	8200	1065	1360
157.8	12800	11260	8290	1060	1330
162.8	13680	11480	8330	1160	1380
167.9	12880	12650	8040	1090	1360
172.9	13610	12180	8850	4920	1340
178	13380	11540	8770	3170	1260
183.2	13200	11490	8120	1660	1360
188.2	13160	11210	6970	1190	1330
193.2	13310	11450	5920	1160	1320
198.3	12610	11790	6050	1090	1325
203.5	12560	12070	9240	1040	1340
208.5	12530	11870	9250	1190	1350
213.6	12370	11560	9140	1350	1420
218.7	12540	11540	9030	1240	1370
223.8	12280	11670	8860	1000	1465
228.8	11980	11680	8780	1095	2180
234	11980	11790	8800	1080	1725
239.1	11750	13890	8880	1150	2230
244.1	11650	12190	9030	1160	1690
249.2	11590	11260	9180	1210	1770
254.3	11500	11270	9410	1240	1200
259.4	11210	11080	9600	1220	1225
264.4	11270	10820	9740	1120	1430
269.5	10920	10920	10010	1160	1680
274.6	10990	11860	10130	1200	1390
279.8	10750	11250	10350	1120	1140
284.8	10720	13080	10590	1060	1260
289.9	10690	11200	10820	1060	1040
295	10610	11730	10910	1070	1695
300	10400	10730	11030	1065	1870

Run no	69	70	76	75
t (sec)	M μNm	M μNm	M(μNm)	M(μNm)
0.141	12170	9920	17450	9840
15.45	2250	16250	18300	2650
30.56	2310	17070	12010	2660
45.81	3070	15900	15230	3700
61.19	3680	15270	12830	3430
76.37	1180	16080	15270	2660
91.62	1340	15720	3350	2850
106.8	5950	15330	1220	4140
122.1	2440	9120	2690	3470
137.4	2520	15090	5035	3420
152.7	2500	8930	14930	3310
167.8	1590	13240	910	3030
183.2	1090	15150	960	2650
198.3	2440	9170	1015	4410
213.6	1370	9960	7380	2960
228.9	2950	11470	2000	3480
244.2	2250	9310	1385	3810
259.4	1930	10250	6250	3510
274.6	1070	12360	880	3160
290	1420	9450	2770	2870
305.1	3430	10730	4000	6310
320.4	2990	11610	2170	4020
335.6	3100	9630	10690	3940
351	2900	10930	8270	3660
366.2	5290	12240	950	3260
381.4	4670	9820	8090	4330
396.6	5610	13870	7720	3210
411.9	1230	10860	2940	3650

Cont	69	70	76	75
t (sec)	M (μNm)	M (μNm)	M (μNm)	M (μNm)
427.1	3950	9930	3520	3710
442.5	3390	9870	6380	3720
457.7	3320	12790	3835	4460
473.1	3230	11570	6980	8470
488.2	1120	11060	4720	4720
503.4	1620	10440	6640	3380
518.7	1650	9510	12490	5800
534	2940	15150	3200	2490
549.2	2750	12910	7970	2530
564.6	1420	11710	6585	2410
579.7	1410	10870	970	3590
595	2400	14600	3950	4090
610.2	2270	13770	1170	2720
625.5	1300	13500	1955	5310
640.7	1150	13530	1790	2350
656	890	13380	2320	5630
671.2	1010	13260	11730	2850
686.6	1920	12970	1750	3920
701.7	1440	12450	1060	4230
717	2060	11880	4710	5930
732.2	1430	14870	4675	2460
747.5	1360	16100	2380	3110
762.7	2900	14480	2170	5080
778	880	13470	2290	2460
793.4	1010	13080	6515	4350
808.5	1270	12560	3510	4150
823.8	1070	12140	1310	1850
839	1830	15090	1025	1610
854.3	1400	15380	990	1650
869.7	1530	14240	12110	2730
884.8	1830	13480	5400	3200
900.1	2010	13260	7015	2470

Run no	71A	71B	71C	71D	71E
t (sec)	M μNm	M μNm	M μNm	M μNm	M μNm
0.047	3580	6050	6440	8220	10300
5.094	3990	5730	6760	8120	11100
10.2	4060	6095	6705	8070	10900
15.31	4050	6100	6770	7870	10750
20.34	4050	5940	6790	7960	11060
25.45	4135	5930	6800	7775	10870
30.53	4100	5890	6780	7970	10980
35.62	4065	5915	6720	7980	11000
40.72	4090	5800	6740	8220	11090
45.8	4050	5905	6750	8360	10680
50.89	4080	5670	6750	7970	10810
56	4055	5785	6740	7900	10640
61.06	4030	5660	6690	7880	10550
66.14	4020	5790	6670	8130	10960
71.22	3980	5680	6720	8430	10790
76.3	4020	5740	6785	8220	10410
81.39	3985	5645	6770	7945	10830
86.45	3970	5710	6680	8260	10930
91.55	3975	5600	6680	8330	10530
96.66	3950	5590	6670	8515	11070
101.7	3980	5580	6650	8430	10890
106.8	3950	5615	6660	8480	10950
111.9	3900	5530	6655	8390	10900
117	3940	5530	6650	8320	10470
122	3910	5620	6650	8420	10630
127.2	3885	5460	6625	8365	10820
132.3	3890	5520	6550	8510	11100
137.3	3875	5430	6560	8530	10800
142.4	3910	5465	6500	8490	11050

cont	71A	71B	71C	71D	71E
147.5	3905	5350	6500	8530	11080
152.6	3880	5400	6485	8590	10730
157.7	3860	5300	6470	8595	11060
162.8	3840	5400	6505	8550	10790
167.8	3880	5350	6430	8555	11110
172.9	3860	5360	6510	8590	10930
178	3820	5340	6405	8540	10960
183.1	3860	5330	6380	8520	10940
188.1	3830	5360	6510	8670	11030
193.2	3840	5260	6370	8550	10710
198.3	3830	5320	6330	8450	10600
203.4	3815	5305	6410	8500	10690
208.5	3850	5370	6420	8490	10530
213.6	3825	5305	6380	8455	10720
218.7	3820	5430	6370	8400	10640
223.7	3830	5280	6370	8360	10690
228.8	3810	5380	6340	8320	10450
233.9	3830	5290	6280	8370	10660
239	3825	5375	6235	8370	10400
244.1	3850	5340	6240	8475	10900
249.2	3820	5410	6280	8440	10520
254.3	3790	5345	6285	8520	10670
259.3	3805	5390	6220	8605	10720
264.4	3770	5355	6190	8550	10510
269.5	3810	5360	6140	8600	10400
274.6	3820	5390	6250	8455	10520
279.7	3800	5370	6210	8650	10470
284.8	3790	5410	6380	8520	10190
289.9	3780	5430	6245	8595	10010
295	3825	5390	6190	8460	10180
300	3810	5390	6200	8545	10130

Run no	71F	71G	71H	71I	71J	71K	72A	72B
t (sec)	M µNm	M µNm	M µNm	M µNm	M µNm	M µNm	M µNm	M µNm
0.047	11560	10590	12060	10750	7890	15000	17450	14750
5.094	15170	18250	17810	13940	14820	18090	18300	3580
10.2	14690	17680	17120	13620	12380	16320	12010	2760
15.31	14680	16670	16470	13510	10760	15040	15230	3385
20.34	14950	15830	18280	13450	9000	14120	12830	2110
25.45	14880	14930	17190	13450	8830	13190	15270	1590
30.53	14800	14510	16080	13430	13410	12270	3350	2655
35.62	14680	13990	16070	13450	12870	11280	1220	4855
40.72	14840	14940	17670	13480	13780	10400	2690	1670
45.8	14700	16620	16940	13530	13300	9300	5035	1200
50.89	14520	16460	15120	13540	12230	8410	14930	1300
56	14890	16430	15370	13520	12210	7770	910	2265
61.06	14530	15650	17310	13520	10490	6810	960	2320
66.14	14390	15290	16090	13590	12210	6195	1015	4520
71.22	13960	15430	13910	13650	12400	4830	7380	2130
76.3	13960	15080	14900	13710	5590	3260	2000	3160
81.39	14030	15430	17020	13750	1430	2280	1385	2480
86.45	14270	15050	16550	13800	970	1670	6250	4955
91.55	13760	15170	15850	13870	950	1195	880	2500
96.66	14160	14330	13610	13920	930	1300	2770	2130
101.7	14240	14320	13590	13970	3730	1210	4000	1290
106.8	13540	15700	13280	14000	5740	1175	2170	1540
111.9	13970	13190	13460	14040	2560	1150	10690	1055
117	14030	12650	13580	14070	1010	1225	8270	1760
122	13890	12110	14420	14060	960	1240	950	2690
127.2	13350	11780	14420	14050	960	1190	8090	3210
132.3	13250	11500	13670	14020	1000	1090	7720	1170
137.3	13240	11330	13750	14010	1000	1000	2940	1670
142.4	13100	11370	14080	14020	980	1065	3520	1220

Run no	71F	71G	71H	71I	71J	71K	72A	72B
t (sec)	M µNm	M µNm	M µNm	M µNm	M µNm	M µNm	M µNm	M µNm
147.5	12880	14060	13800	14020	1160	1000	6380	3625
152.6	12850	16890	13980	14050	8720	1070	3835	1400
157.7	12880	16950	14360	14060	10870	915	6980	1460
162.8	12710	15940	14500	14080	10100	990	4720	1270
167.8	12650	16120	14520	14050	10720	975	6640	1310
172.9	12480	16350	13890	14030	3630	915	12490	1910
178	12610	14670	14390	14030	2390	950	3200	1370
183.1	12320	14090	14100	14000	1170	925	7970	1435
188.1	12200	13770	14210	13990	940	930	6585	2665
193.2	12390	13550	14200	14000	1000	880	970	1620
198.3	11950	13390	13580	14030	990	930	3950	1120
203.4	12310	13340	14060	14070	1970	900	1170	1220
208.5	11850	13160	13450	14060	5140	955	1955	1125
213.6	11870	12950	12010	14080	3070	890	1790	2270
218.7	12220	15910	11420	14090	1560	1480	2320	1160
223.7	11660	17350	11010	14070	1060	1760	11730	4395
228.8	12030	16060	10490	14030	3670	1720	1750	1135
233.9	11770	14980	10000	14050	7230	2500	1060	1920
239	11690	14710	9690	14080	2000	1795	4710	1110
244.1	11960	14470	9390	14080	890	1490	4675	1650
249.2	11860	14450	9010	14070	840	4795	2380	1360
254.3	11890	14380	11130	14030	780	4280	2170	1340
259.3	12100	14210	10760	14060	890	3160	2290	1500
264.4	11770	14400	10990	14020	1800	2155	6515	1035
269.5	12240	14380	12130	14020	5280	1430	3510	4380
274.6	12020	14410	13260	14040	8480	1150	1310	980
279.7	11730	14280	14650	14030	5120	1060	1025	1870
284.8	12220	14090	16210	14060	2460	1050	990	2490
289.9	11940	13990	15490	14040	1810	1090	12110	1170
295	12000	15240	14370	14060	2120	1080	5400	1650
300	12780	17600	13090	14050	1570	1110	7015	1200

Run no	73A	73B	73C	73D	73E	73F	73G
t_seg in	M µNm	M µNm	M µNm	M µNm	M µNm	M µNm	M µNm
0.047	3780	5830	5590	8120	8870	9060	8970
5.094	3885	5405	5880	8225	9570	12970	15080
10.2	3870	5880	6230	8190	9190	12760	14370
15.31	3940	5770	6100	7890	8970	12560	13820
20.34	4000	5700	6160	7890	9580	12370	13640
25.45	4030	5740	6070	7880	9370	12080	13320
30.53	4010	5665	5950	7770	9050	12550	13090
35.62	3990	5650	6025	7670	9080	12510	12880
40.72	4030	5620	6060	7640	9170	11740	12650
45.8	3990	5660	5960	7670	9150	12100	12750
50.89	4020	5570	6000	7755	9070	11980	14500
56	3980	5550	6000	7760	9010	11330	14640
61.06	3930	5500	5980	7650	9000	11270	13340
66.14	3980	5475	5930	7620	8950	12530	13140
71.22	3950	5480	5900	7570	9040	11320	12720
76.3	3900	5425	5975	7490	9030	11610	12310
81.39	3950	5470	5860	7445	8860	11820	12050
86.45	3945	5350	5890	7470	8700	10920	11960
91.55	3860	5370	5975	7390	8720	11990	11740
96.66	3885	5370	5760	7340	8770	10760	11450
101.7	3890	5330	5675	7300	8830	11080	11250
106.8	3845	5300	5740	7300	8720	11330	11090
111.9	3860	5265	5760	7275	8780	12060	10990
117	3820	5280	5700	7240	8810	11140	10910
122	3860	5250	5610	7305	8740	10490	10990
127.2	3820	5240	5640	7320	8730	10490	10910
132.3	3840	5190	5640	7330	8810	10480	11020
137.3	3830	5195	5605	7160	8870	10530	12840
142.4	3795	5220	5530	7070	8820	10570	14320

Cont	73A	73B	73C	73D	73E	73F	73G
t seg in	M µNm	M µNm	M µNm	M µNm	M µNm	M µNm	M µNm
147.5	3810	5180	5550	7020	8980	10640	14470
152.6	3780	5190	5540	7075	8910	10690	14240
157.7	3820	5120	5540	7150	8780	10730	14630
162.8	3790	5140	5530	7070	8690	10750	14550
167.8	3740	5190	5525	6765	8840	10820	12410
172.9	3770	5115	5570	6750	8920	10850	12200
178	3770	5110	5530	6900	8700	10820	12140
183.1	3780	5070	5450	6925	8730	10750	12110
188.1	3760	5095	5460	6890	8830	10760	11990
193.2	3740	5100	5465	6980	8810	10810	12080
198.3	3730	5105	5430	6960	8890	10930	12140
203.4	3730	5100	5450	6940	8940	10980	12160
208.5	3780	5120	5420	6820	8950	11040	12240
213.6	3750	5050	5420	6820	9100	11030	12360
218.7	3695	5090	5400	6840	9110	11050	12340
223.7	3770	5045	5250	6840	9180	11070	12420
228.8	3730	5090	5235	6775	9390	11070	12400
233.9	3670	5045	5500	6820	9460	11090	12500
239	3690	5060	5650	6770	9520	11100	12550
244.1	3670	5030	5655	6765	9470	11160	12570
249.2	3700	5015	5510	6730	9490	11180	12580
254.3	3700	5080	5185	6845	9550	11150	12590
259.3	3700	5040	5900	6755	9550	11130	12670
264.4	3675	5050	5970	6810	9480	11140	12720
269.5	3660	5040	5540	6765	9520	11250	12740
274.6	3680	5050	5980	6840	9540	11290	12810
279.7	3660	5060	5845	6910	9560	11320	12760
284.8	3680	5050	5700	7005	9470	11310	12750
289.9	3690	5020	6030	7090	9450	11300	12830
295	3680	5025	5820	7130	9480	11290	12890
300	3680	5025	5840	7110	9530	11290	12890

Run no	73H	73I	73J	73K	74A	74B	74C
t(sec)	M µNm	M µNm	M µNm	M µNm	M µNm	M µNm	M µNm
0.047	8170	7930	15640	16760	8900	18140	7150
5.094	17770	17170	16660	14690	20530	18330	13380
10.2	16740	16290	15870	11580	15890	16760	13440
15.31	16000	15580	15320	10730	20850	15180	13820
20.34	15430	15040	14880	10160	20730	13760	12510
25.45	15060	14570	14490	9600	14320	12070	13450
30.53	14900	14290	14120	9045	20080	10690	10770
35.62	14830	14110	13710	8670	19660	4040	9160
40.72	14770	13970	13510	8295	18610	3755	8700
45.8	14750	13820	13270	7610	18320	6130	10300
50.89	14710	13780	13110	7265	18950	4550	5700
56	14610	13740	12970	6980	19400	3260	8230
61.06	14540	13670	12850	6950	18770	4250	7810
66.14	14460	13540	12710	7340	17430	1630	7450
71.22	14420	13460	12550	7650	17110	14840	7290
76.3	14370	13430	12380	7705	18520	13710	6930
81.39	14360	13370	12210	7610	16700	11830	6690
86.45	14250	13350	11970	7190	16390	9750	7330
91.55	14210	13340	11800	6170	16180	9850	6810
96.66	14120	13240	11590	4340	15690	9740	3730
101.7	14040	13230	11330	2645	15360	9335	3890
106.8	13980	13190	10900	1660	14780	8990	1870
111.9	13920	13160	10580	1080	14360	8800	1140
117	13840	13110	10080	960	17470	8270	910
122	13720	13070	9620	980	16910	8050	800
127.2	13540	13100	9315	1000	15280	7900	980
132.3	13350	13080	10760	990	16310	7330	3910
137.3	13210	13070	15600	965	17020	4355	2500
142.4	13050	13060	16060	980	16370	2190	1530

Cont	73H	73I	73J	73K	74A	74B	74C
t(sec)	M µNm	M µNm	M µNm	M µNm	M µNm	M µNm	M µNm
147.5	12980	13090	15720	1000	13560	1230	1340
152.6	12940	13180	11220	1000	13000	780	2350
157.7	12820	13230	9885	990	14210	730	3250
162.8	12680	13330	8650	950	16220	750	1930
167.8	12550	13410	8370	980	15230	790	1810
172.9	12530	13490	8175	1010	13110	780	1670
178	12460	13620	8040	920	14970	800	1530
183.1	12380	13600	7885	940	15810	770	1410
188.1	12320	13630	7630	950	15250	770	1330
193.2	12290	13670	7165	960	14220	780	1320
198.3	12250	13700	6410	945	11430	2755	1290
203.4	12210	13710	5680	970	12520	6130	1260
208.5	12160	13660	5665	990	15830	4550	1350
213.6	12120	13600	6230	960	15880	7260	1360
218.7	12010	13570	6715	970	13750	6250	1650
223.7	11910	13440	6750	990	11900	7630	2060
228.8	11920	13350	6575	900	10640	6840	1640
233.9	11900	13400	6230	890	10920	4710	1630
239	11850	13270	5770	860	10590	3830	3450
244.1	11820	13210	4855	660	10230	3620	2630
249.2	11900	13320	3400	760	15530	1590	2110
254.3	11940	13340	1905	630	13120	450	1690
259.3	11920	13310	920	590	10910	490	1890
264.4	11890	13260	880	640	10100	5530	1770
269.5	11880	13390	890	590	11490	660	1810
274.6	11830	13500	880	580	10030	580	1880
279.7	11830	13550	865	610	14810	665	1810
284.8	11820	13570	880	600	13390	600	1800
289.9	11800	13570	905	510	10970	540	1910
295	11760	13590	890	560	12930	615	1880
300	11760	13570	910	560	14550	750	1980

Run no	77A	77B	77C	77D
t (sec)	M(μNm)	M(μNm)	M(μNm)	M(μNm)
0.078	4270	6260	7240	8240
5.141	4230	6750	5980	8645
10.19	4235	6790	6640	8340
15.33	4320	6795	6300	8840
20.41	4355	6640	6655	8525
25.44	4390	6580	6560	8120
30.52	4380	6550	6780	8755
35.59	4350	6470	6610	8860
40.69	4400	6370	6885	8430
45.8	4410	6360	6750	8550
50.86	4410	6250	6810	8485
55.94	4395	6300	6760	8900
61.03	4380	6320	6700	8905
66.12	4410	6130	6835	8855
71.23	4400	6100	6685	8910
76.31	4355	6120	6720	8720
81.37	4380	6040	6745	9020
86.45	4405	5955	6700	8810
91.53	4410	5970	6720	8835
96.62	4375	5920	6670	8660
101.7	4350	5840	6720	8720
106.8	4400	5850	6695	8750
111.9	4365	5800	6690	8690
117	4380	5800	6720	8780
122.1	4375	5780	6670	8895
127.2	4310	5710	6650	8690
132.2	4355	5820	6790	8720
137.3	4360	5735	6750	8810
142.4	4330	5700	6695	8690

Cont	77A	77B	77C	77D
t (sec)	M(μNm)	M(μNm)	M(μNm)	M(μNm)
147.5	4320	5685	6630	8550
152.5	4310	5690	6620	8580
157.7	4350	5660	6590	8500
162.7	4295	5680	6660	8365
167.8	4325	5610	6680	8370
172.9	4320	5675	6610	8530
178	4260	5710	6690	8505
183.1	4310	5660	6655	8520
188.1	4285	5730	6630	8640
193.3	4330	5600	6625	8605
198.3	4315	5690	6560	8290
203.4	4310	5590	6660	8400
208.5	4275	5660	6650	8470
213.6	4250	5590	6700	8340
218.7	4305	5705	6780	8320
223.7	4250	5570	6720	8360
228.8	4295	5680	6760	8370
233.9	4290	5570	6750	8330
239	4240	5620	6660	8310
244.1	4280	5530	6585	8710
249.2	4250	5580	6600	8340
254.2	4280	5520	6570	8435
259.3	4280	5585	6535	8440
264.5	4245	5440	6580	8560
269.5	4250	5550	6585	8605
274.6	4240	5400	6760	8490
279.7	4300	5500	6630	8440
284.8	4250	5440	6615	8425
289.8	4260	5550	6610	8550
295	4280	5445	6610	8810
300	4220	5510	6620	8610

Run no	77E	77F	77G	77H	77I
t (sec)	M (μNm)	M (μNm)	M (μNm)	M (μNm)	M (μNm)
0.078	10510	7990	9510	10280	7680
5.141	10830	14060	10320	13690	13180
10.19	10730	12890	9680	12800	11350
15.33	10840	13160	9700	11870	9800
20.41	10980	12820	9360	11030	7960
25.44	10640	12210	9060	10030	11000
30.52	10630	12370	9360	8930	9920
35.59	10910	12040	9510	10460	9330
40.69	10670	11660	9350	10930	8670
45.8	11250	11260	9090	10430	8370
50.86	10820	11330	8760	11360	9840
55.94	11100	11480	10600	9660	12890
61.03	10540	11310	9930	11360	10900
66.12	10950	10250	9130	10720	10010
71.23	10380	10420	9180	8960	9730
76.31	11030	10420	9600	11170	6200
81.37	10580	7850	9030	7020	4810
86.45	11060	8160	8950	12320	4510
91.53	10610	10510	8700	9540	2050
96.62	10670	10520	8530	12350	1010
101.7	10640	8040	8910	12380	2680
106.8	10700	9410	8530	12470	1650
111.9	10410	10480	7010	13160	980
117	10840	8230	6720	13480	1020
122.1	10560	8320	6980	13080	980
127.2	10270	9640	7010	13090	980
132.2	10930	8920	6790	13230	1040
137.3	10400	7640	6660	13440	960
142.4	10900	10580	6590	13140	950

Cont	77E	77F	77G	77H	77I
t (sec)	M (μNm)	M (μNm)	M (μNm)	M (μNm)	M (μNm)
147.5	10410	9690	7010	13110	960
152.5	10750	10610	8070	13370	970
157.7	10310	10590	8900	13480	920
162.7	10370	10760	7090	13020	950
167.8	10150	10850	6040	12920	950
172.9	10120	10600	7960	13370	920
178	10180	10500	7700	13460	960
183.1	10390	10640	7850	13090	890
188.1	10160	10470	8680	13360	930
193.3	10330	10610	7750	13570	930
198.3	10510	10370	8440	13050	930
203.4	10540	10530	8330	13640	960
208.5	10480	10270	7810	12780	940
213.6	10430	10120	8120	12970	930
218.7	10500	10210	7730	12520	920
223.7	10260	9990	8780	11920	920
228.8	10200	9920	8420	9820	950
233.9	10300	9660	8350	5480	940
239	10230	9670	7305	1750	890
244.1	10130	9450	7100	850	930
249.2	10180	9360	7120	910	960
254.2	10030	9350	7810	1020	950
259.3	10240	9110	7230	1620	910
264.5	10220	9180	9450	2170	920
269.5	10160	8940	6240	1070	890
274.6	10180	8890	6630	820	890
279.7	10400	8680	6490	800	890
284.8	10350	8960	6000	810	880
289.8	10170	8770	6430	820	790
295	10140	8750	8030	830	700
300	10140	8740	6150	830	700

Run no	80A	80B	80C	80D	80E
t_(sec)	M(μNm)	M(μNm)	M(μNm)	M(μNm)	M(μNm)
0.078	3730	5760	6800	8710	11780
5.141	3875	5260	5880	7665	13300
10.19	3850	5455	6430	7580	13170
15.33	3850	5700	6400	7705	13060
20.41	3885	5905	6160	7560	13160
25.44	3880	5770	6290	7350	12930
30.52	3900	5660	6165	7660	12860
35.59	3920	5720	6230	7560	12820
40.69	3910	5800	6165	7900	12590
45.8	3910	5770	6140	8350	12560
50.86	3920	5705	6090	7940	12560
55.94	3920	5660	6125	8200	12560
61.03	3910	5600	6110	8380	12630
66.12	3920	5650	6065	8035	12630
71.23	3890	5680	6105	8690	12540
76.31	3875	5595	6090	8735	12670
81.37	3880	5550	6080	8900	12720
86.45	3860	5520	6030	9310	12870
91.53	3880	5550	6025	9235	12660
96.62	3890	5530	6030	9490	12690
101.7	3870	5500	6090	9405	12600
106.8	3850	5490	5995	9130	12680
111.9	3830	5470	6020	9005	12590
117	3815	5410	5970	8940	12680
122.1	3830	5440	6000	9040	12550
127.2	3800	5400	5990	9230	12570
132.2	3810	5330	5990	9090	12950
137.3	3760	5350	6000	9165	12630
142.4	3750	5400	6005	9180	12700

Cont	80A	80B	80C	80D	80E
t_(sec)	M(μNm)	M(μNm)	M(μNm)	M(μNm)	M(μNm)
147.5	3740	5400	6025	9145	12560
152.5	3720	5265	5880	9190	12630
157.7	3725	5240	5950	9110	12600
162.7	3720	5270	5920	9205	12670
167.8	3730	5255	5910	9110	12920
172.9	3720	5270	5880	9290	12670
178	3740	5320	5950	9240	12770
183.1	3740	5240	5890	9405	12880
188.1	3725	5230	5830	9270	12780
193.3	3740	5185	5900	9410	12730
198.3	3730	5200	5790	9270	12700
203.4	3700	5220	5820	9350	12780
208.5	3690	5130	5860	9390	12750
213.6	3670	5120	5830	9390	12810
218.7	3690	5015	5860	9480	12580
223.7	3670	5080	5805	9400	12750
228.8	3670	5050	5830	9420	12580
233.9	3670	5100	5765	9460	12630
239	3660	5180	5770	9430	12610
244.1	3660	5115	5830	9505	12650
249.2	3630	5000	5790	9470	12510
254.2	3645	5100	5820	9480	12580
259.3	3610	5140	5785	9610	12610
264.5	3590	5050	5820	9410	12560
269.5	3615	5010	5740	9540	12510
274.6	3630	5090	5750	9610	12610
279.7	3620	5030	5800	9430	12380
284.8	3615	4995	5805	9680	12420
289.8	3630	4950	5810	9475	12490
295	3630	4990	5720	9620	12300
300	3620	4970	5790	9600	12300

Run no	80F	80G	80H	80I	80J
t (secs)	M (µNm)	M in µNm	M in µNm	M in µNm	M in µNm
0.078	10010	9070	8300	8100	17970
5.141	16110	19280	17670	15400	17080
10.19	16150	18360	18020	15170	15370
15.33	15880	17500	17560	13540	15160
20.41	15860	16680	16760	11860	14670
25.44	15900	16440	16170	10810	14770
30.52	15760	16590	15350	9680	12080
35.59	15670	16400	14990	8930	10620
40.69	15470	14460	14300	8160	9630
45.8	15620	16820	14670	11060	8510
50.86	16180	16640	15510	11050	7340
55.94	15890	15220	15500	12100	5845
61.03	16160	12650	15370	14090	8400
66.12	15440	11870	15000	13980	7505
71.23	15220	13940	14580	13700	4870
76.31	16080	13560	14320	13910	3030
81.37	15890	13490	14180	13830	1410
86.45	15110	13150	13780	10440	1160
91.53	14850	13380	13430	12010	1180
96.62	16090	13120	13250	11810	1160
101.7	16620	13080	10810	13510	1180
106.8	16720	12730	12470	9340	1170
111.9	16400	12080	11490	8160	1160
117	15480	11610	9370	6920	1220
122.1	15700	11470	13030	5780	1170
127.2	16400	11180	12990	5000	1235
132.2	15270	11910	12640	4020	1130
137.3	16330	13660	11310	2860	1160
142.4	16660	13850	11270	2080	1115

Cont	80F	80G	80H	80I	80J
t (secs)	M (µNm)	M in µNm	M in µNm	M in µNm	M in µNm
147.5	16920	12690	11040	1540	1120
152.5	16050	12280	8730	1360	1060
157.7	15870	12270	12160	1250	1080
162.7	16190	13580	13410	1210	1010
167.8	16630	13980	13280	1250	835
172.9	16290	13050	10640	1290	970
178	16070	12710	7710	1320	840
183.1	15680	12320	6670	1270	750
188.1	16720	12110	8100	1240	815
193.3	15750	11770	8160	1230	740
198.3	15610	11490	7800	1190	690
203.4	16420	14620	9380	1150	790
208.5	16820	17350	11380	1150	730
213.6	15750	14930	10190	1150	670
218.7	15900	13970	10440	1170	660
223.7	15430	13330	10060	1130	730
228.8	15390	12810	11680	1140	750
233.9	16220	12350	12250	1130	880
239	15260	13190	9820	1150	870
244.1	16070	15700	13250	1140	890
249.2	15180	16470	9160	1130	835
254.2	14950	16440	8990	1130	830
259.3	15780	14090	10180	1100	1010
264.5	14860	13490	10400	1110	970
269.5	15560	13020	10140	1100	1040
274.6	15230	12560	9620	1080	1060
279.7	15150	12170	9180	1120	1080
284.8	14970	12640	8120	1090	1240
289.8	15170	13770	8230	1080	1220
295	15010	15000	8170	1080	1230
300	14390	13390	8520	1100	1110

Run no	83A	83B	83C	83D	83E	83F	83G
t(sec)	M (µNm)	M (µNm)	M (µNm)	M (µNm)	M (µNm)	M (µNm)	M (µNm)
0.078	3940	5660	6260	8600	12470	13860	15380
5.141	4020	5770	6050	8960	13210	15120	20320
10.19	3990	6150	5990	8635	13170	14750	19580
15.33	4090	6055	5945	8550	12830	14610	18950
20.41	4110	5970	5780	8650	12780	14570	18270
25.44	4040	5925	6300	8825	12490	15320	17410
30.52	4105	6040	6450	9190	12460	15000	17140
35.59	4070	5910	6260	8850	12410	14090	16350
40.69	4070	5960	6360	9260	12270	13290	16190
45.8	4070	5780	6340	8680	12190	15050	17060
50.86	4040	5855	6305	9230	12080	14580	17900
55.94	4030	5650	6410	8980	12170	13960	17320
61.03	3990	5715	6480	9070	12310	15950	18250
66.12	4030	5575	6410	9260	11990	14230	18560
71.23	3990	5650	6360	9260	12080	13990	17380
76.31	4005	5590	6450	9210	12050	15770	16350
81.37	3990	5600	6430	9350	11900	14770	15810
86.45	3920	5530	6300	9375	11820	13420	14160
91.53	3960	5470	6485	9270	11790	15850	13500
96.62	3975	5450	6470	9330	11670	15260	13740
101.7	3930	5330	6560	9510	11630	15780	17000
106.8	3930	5330	6510	9410	11540	15350	16250
111.9	3930	5275	6550	9530	11660	14240	15080
117	3930	5300	6520	9480	11390	16670	14270
122.1	3915	5205	6480	9550	11630	15430	16100
127.2	3880	5365	6430	9495	11260	14760	19790
132.2	3885	5210	6550	9540	11300	16050	18340
137.3	3840	5210	6535	9540	11290	16280	18060
142.4	3905	5170	6530	9695	11240	15490	18220

Cont	**83A**	83B	83C	83D	83E	83F	83G
t(sec)	M (µNm)	M (µNm)	M (µNm)	M (µNm)	M (µNm)	M (µNm)	M (µNm)
147.5	3880	5150	6520	9590	11350	15920	15780
152.5	3845	5060	6540	9730	11440	16390	14860
157.7	3850	5140	6570	9680	11390	16400	14980
162.7	3820	5180	6605	9770	11440	15500	17530
167.8	3850	5130	6560	9710	11340	16920	16290
172.9	3830	5200	6600	9835	11280	15760	19010
178	3785	5190	6625	9590	11590	16420	16260
183.1	3830	5140	6550	9720	11330	15640	15060
188.1	3830	5200	6595	9650	11070	16720	15860
193.3	3800	5180	6645	9720	11200	15730	17720
198.3	3760	5225	6600	9780	11180	15570	15630
203.4	3770	5050	6620	9710	11060	16470	14400
208.5	3820	5220	6620	9810	11300	15550	14150
213.6	3800	5040	6615	9750	11290	16830	13630
218.7	3780	5180	6600	9715	11170	16420	16920
223.7	3820	5070	6600	9750	11320	15980	15340
228.8	3780	5190	6570	9650	11110	15700	14400
233.9	3775	5030	6610	9755	11210	16370	16440
239	3740	5100	6635	9690	10960	16080	16650
244.1	3795	5060	6695	9575	10840	16220	14640
249.2	3780	5055	6740	9830	11010	15880	13220
254.2	3750	5100	6735	9790	11010	16980	13150
259.3	3770	5125	6720	9660	10890	16480	14130
264.5	3750	5030	6720	9670	11000	16500	15510
269.5	3800	5100	6700	9920	10970	17290	14750
274.6	3740	4980	6680	9935	11090	17280	13740
279.7	3790	5020	6730	9870	11000	17230	13020
284.8	3760	5095	6740	10050	10860	17550	13850
289.8	3765	4980	6740	9980	10790	17270	13810
295	3770	5155	6765	9930	10660	16800	13620
300	3725	5000	6680	10070	10660	15970	13620

Run no	83H	83I	83J	83K	84A	84B	84C	84D
t(sec)	M(μNm)	M(μNm)	M(μNm)	M(μNm)	M(μNm)	M(μNm)	M(μNm)	M(μNm)
0.078	10820	9810	7890	16630	9100	9280	6460	13650
5.141	15570	14690	14820	18320	10420	8030	11840	11490
10.19	15370	14360	12380	16650	9740	7560	9700	9115
15.33	13240	14140	10760	15050	9320	8070	8210	5060
20.41	13040	13960	9000	13440	9375	8025	10780	4950
25.44	14370	14090	8830	11900	9250	9045	10220	1930
30.52	13250	12460	13410	10240	9400	9025	7390	1270
35.59	12420	12060	12870	11870	9350	7040	6800	1130
40.69	13770	10610	13780	10200	9630	8125	5300	1060
45.8	11680	13840	13300	13840	9635	7795	4220	1165
50.86	12980	13250	12230	11960	9630	8700	2500	1020
55.94	12700	11480	12210	11230	9210	7500	1580	1055
61.03	11170	13430	10490	12900	9540	7530	1280	1150
66.12	11800	10820	12210	8810	9250	9165	1930	1130
71.23	12010	10810	12400	2425	9310	8550	1720	1060
76.31	11050	12730	5590	1030	9450	8830	1410	1130
81.37	11860	11770	1430	950	8990	8680	1250	1080
86.45	9810	10860	970	940	9240	8170	1090	1120
91.53	11520	8250	950	980	8750	8320	1040	1135
96.62	11540	8440	930	975	9030	8010	1000	1090
101.7	10300	12010	3730	1000	8960	7990	980	1090
106.8	11640	10950	5740	1930	8915	6720	990	1130
111.9	8840	12390	2560	2350	8920	6160	3840	1240
117	11050	9620	1010	1060	8820	6410	5620	1220
122.1	11310	10430	960	1110	8730	6370	4430	1080
127.2	10010	13440	960	1120	9010	5810	2770	1040
132.2	10570	9630	1000	2280	8735	6270	1610	1050
137.3	8170	9650	1000	2200	9035	5710	1130	970
142.4	9480	8860	980	7650	8520	5600	3100	970

Cont	83H	83I	83J	83K	84A	84B	84C	84D
t(sec)	M(μNm)	M(μNm)	M(μNm)	M(μNm)	M(μNm)	M(μNm)	M(μNm)	M(μNm)
147.5	11190	8660	1160	6240	8960	5990	3290	870
152.5	8460	8170	8720	2970	8510	6025	2140	720
157.7	11030	7660	10870	1405	8700	5320	1440	730
162.7	10900	7580	10100	4180	8960	6375	1130	690
167.8	8010	7610	10720	1750	8710	8165	1070	635
172.9	11750	8260	3630	1080	8650	7915	4840	610
178	10020	8710	2390	1080	8645	8245	3530	750
183.1	9050	6380	1170	1100	8710	8400	1820	700
188.1	12290	7370	940	1380	8790	7335	1280	810
193.3	7520	7110	1000	1890	8810	6485	1080	710
198.3	6960	6830	990	2430	8600	6020	1030	840
203.4	6510	8430	1970	2380	8650	6050	1080	1020
208.5	6080	8010	5140	2360	8330	6280	2580	1200
213.6	5330	8350	3070	1850	8380	6280	4580	895
218.7	4960	9070	1560	1590	8190	7080	2960	1020
223.7	4380	8480	1060	2030	8115	8530	1610	690
228.8	3950	7550	3670	2045	7900	7670	1200	655
233.9	3110	9230	7230	1690	7760	7630	3080	870
239	1840	10170	2000	1710	7820	8075	1610	865
244.1	940	8960	890	1670	7625	7500	1120	800
249.2	970	6790	840	2170	7445	6770	1170	790
254.2	8100	8930	780	2335	7530	5525	1200	1000
259.3	8300	9780	890	2410	7240	5780	1230	890
264.5	7690	10620	1800	1960	7290	6020	1270	1015
269.5	5780	9460	5280	1860	7295	5970	1250	1000
274.6	5630	7660	8480	1980	7275	5835	1190	900
279.7	8870	9200	5120	1770	7210	6010	1200	1040
284.8	7980	12740	2460	1910	7060	8000	1330	1160
289.8	10650	14130	1810	1815	7110	6705	1410	980
295	10210	12700	2120	1700	6970	8480	1470	990
300	8070	10180	1570	1650	6865	5475	1250	990

Run no	87A	87B	87C	87D	87E	87F
t in s	M(µNm)	M(µNm)	M(µNm)	M(µNm)	M(µNm)	M(µNm)
1.156	4500	8030	10710	10500	12480	13880
6.25	5380	8740	11350	12470	12540	11330
11.31	5370	8900	11310	12850	12620	9360
16.37	5385	9055	11320	12810	12330	7870
21.51	5450	9090	11280	12810	12420	8590
26.58	5485	9120	11250	12400	12290	7950
31.64	5500	9220	11220	12520	11810	6830
36.7	5485	9200	11160	12450	10290	5350
41.81	5480	9230	11190	12520	10460	6590
46.92	5525	9290	11150	12090	9975	8640
51.97	5490	9255	11090	12050	9680	9140
57.05	5490	9290	11070	12020	9330	9800
62.17	5520	9280	10980	12050	9150	9900
67.26	5460	9290	10980	12090	8630	10000
72.34	5500	9300	10940	11850	8750	9110
77.39	5480	9315	10920	11930	8460	7660
82.51	5430	9300	10890	11350	8120	7900
87.58	5490	9320	10890	11390	7525	9690
92.64	5475	9325	10810	11890	7535	9830
97.8	5450	9290	10780	11670	7380	10670
102.8	5460	9315	10720	11490	7130	12660
107.9	5440	9300	10680	10700	6235	11180
113	5480	9305	10670	11400	7055	10550
118.1	5435	9310	10630	11410	7070	10540
123.2	5430	9290	10640	11490	6470	10700
128.3	5465	9285	10620	11730	6420	11870
133.4	5440	9310	10630	11420	6150	10350
138.4	5430	9275	10560	11030	6575	10910

Cont	87A	87B	87C	87D	87E	87F
t in s	M(µNm)	M(µNm)	M(µNm)	M(µNm)	M(µNm)	M(µNm)
143.5	5440	9290	10520	10840	6580	11620
148.6	5400	9290	10500	11230	6550	11430
153.7	5470	9235	10530	11200	6170	10500
158.8	5425	9260	10450	11230	5900	10970
163.9	5380	9265	10470	11250	6220	10360
168.9	5430	9220	10430	10910	6640	9920
174	5400	9255	10360	11220	6740	10680
179.1	5440	9230	10310	11390	6560	9800
184.2	5430	9230	10350	11290	6480	9130
189.3	5430	9260	10330	11410	6690	8050
194.4	5400	9210	10340	11240	6830	10320
199.5	5390	9210	10350	11050	6350	12000
204.5	5440	9220	10270	11360	6475	12070
209.6	5380	9190	10210	11200	6660	12170
214.7	5435	9220	10050	11160	6240	11020
219.8	5410	9240	10020	11210	6050	11060
224.9	5410	9190	10150	11180	6810	10040
230	5410	9190	10360	11230	6315	9320
235	5410	9195	10300	11210	6360	10540
240.1	5380	9160	10160	10760	6120	10380
245.2	5360	9170	10170	11460	5910	10220
250.3	5435	9150	10180	10790	7610	10000
255.4	5380	9220	10170	11210	6880	9290
260.5	5360	9210	10220	11030	6340	9630
265.5	5400	9190	10140	11130	6140	8860
270.6	5350	9190	10150	11400	5715	8430
275.7	5410	9190	10120	11160	5130	8380
280.9	5395	9200	10150	10910	4860	7900
285.9	5350	9230	10080	10670	7510	10340
291	5370	9200	10060	11040	6545	8610
296.1	5345	9185	10040	11010	6200	9520
301.1	5390	9190	10130	10810	5810	10760

Run no	87G	87H	88A	88B	88C
t(sec)	M(μNm)	M(μNm)	M(μNm)	M(μNm)	M(μNm)
1.156	17950	13810	16650	11430	14470
6.25	18820	18530	17500	16910	15370
11.31	11650	7170	15880	10400	3640
16.37	12080	3160	12510	5020	3170
21.51	11550	2180	12790	4140	3440
26.58	9600	2730	13610	5060	3620
31.64	8660	2800	14610	8450	3300
36.7	6070	2590	13180	4980	3630
41.81	4390	3220	10610	4830	3700
46.92	2745	2940	11160	4910	2760
51.97	2540	4300	10250	3890	3410
57.05	2230	2780	9010	4040	3010
62.17	2495	4240	9145	4030	2200
67.26	2460	2060	9855	3260	2020
72.34	2475	2530	10410	4410	2530
77.39	2350	2350	9935	4200	2690
82.51	2320	1860	9770	4370	2950
87.58	2330	1860	10000	4480	3330
92.64	2580	1980	11160	3070	2670
97.8	2370	2660	12920	2260	2690
102.8	2370	2140	11050	2430	3250
107.9	2690	3160	9585	3920	3040
113	2760	3700	10130	6340	2600
118.1	2530	3370	10300	6550	3150
123.2	2365	4420	10070	3740	3930
128.3	2450	3830	9900	2480	2990
133.4	2470	2550	9760	3520	2900
138.4	2615	2240	9670	3970	2480

Cont	87G	87H	88A	88B	88C
t(sec)	M(µNm)	M(µNm)	M(µNm)	M(µNm)	M(µNm)
143.5	2405	2600	9520	3900	2750
148.6	2770	3460	9710	6130	2710
153.7	2820	3100	9855	6750	2180
158.8	2470	3400	9960	5120	1880
163.9	2530	3270	10060	3610	1750
168.9	2375	3750	10060	3920	2170
174	2070	3450	10110	3560	2770
179.1	2870	4840	10150	4080	2920
184.2	2630	3370	10120	3270	2940
189.3	2370	2660	10210	4060	2890
194.4	2360	2770	10170	4690	2920
199.5	2590	2290	10170	8040	3450
204.5	2490	3010	10170	8990	3940
209.6	2270	3480	10140	10490	2430
214.7	2520	2400	10090	10070	2040
219.8	2570	3420	9900	9100	2670
224.9	2390	2700	9760	5480	2080
230	2350	3830	9670	6860	3030
235	2740	3660	9520	9940	3870
240.1	4210	2910	9710	4030	2340
245.2	2900	2360	9855	3230	1780
250.3	2460	2080	9960	2360	2180
255.4	2360	3120	9405	2590	1860
260.5	2790	3260	9730	3490	1470
265.5	2805	2790	9510	6490	1540
270.6	2660	2440	9955	11530	2300
275.7	3200	2700	9515	12400	2510
280.9	3395	3300	9940	11180	2100
285.9	3320	2580	9560	12560	2450
291	3000	2230	9660	12250	2910
296.1	2580	2750	9095	11710	2740
301.1	2470	2640	9240	12300	2260

Run no	89	90
t (secs)	M(μNm)	M(μNm)
0.156	17130	19360
15.3	3880	2860
30.56	3740	2660
45.83	3670	2735
61.11	3930	2450
76.33	2500	2620
91.53	2900	2450
106.8	2490	4340
122.1	3910	3900
137.4	3530	2960
152.6	3260	4010
167.9	4000	4490
183.1	3680	3600
198.4	3290	3570
213.6	2040	3980
228.8	2170	3480
244.1	2530	2120
259.4	5530	3780
274.6	3390	3135
289.9	3320	2230
305.2	4160	3350
320.3	3260	2650
335.6	3150	4180
350.9	2490	2610
366.1	2850	3745
381.4	2610	2140
396.6	2450	6300
411.9	3490	4350
427.2	3470	2385
442.4	2390	3690
457.7	3740	2660
472.9	2360	1835
488.1	4680	4345
503.4	3290	1910

518.7	2760	3940
533.9	4250	3750
549.2	3260	3545
564.5	4060	3770
579.7	3320	4635
594.9	3020	3385
610.3	2260	3740
625.5	4030	4390
640.7	4050	1910
656	3980	1745
671.2	5510	5110
686.5	2530	1750
701.8	4620	4415
717	3340	2660
732.2	3180	2580
747.5	3130	2250
762.7	2970	1840
778	4960	1880
793.3	4590	4520
808.5	4680	3845
823.7	4620	3540
839	3680	2660
854.3	4950	2240
869.6	4750	4645
884.8	3770	3420
900.1	3620	2070

Run no	91A	91B	91C	91D	91E
t(sec)	M(μNm)	M(μNm)	M(μNm)	M(μNm)	M(μNm)
1.125	5910	11790	14880	17700	20150
6.203	6450	13340	15760	18980	22200
11.31	6440	13810	15700	18900	22280
16.37	6460	14020	15690	18820	21770
21.45	6505	14100	15660	18790	21070
26.58	6440	14110	15640	18750	20620
31.61	6505	14130	15660	18670	20280
36.69	6460	14170	15680	18610	19860
41.81	6445	14150	15690	18580	19530
46.87	6440	14170	15700	18530	19480
52	6410	14160	15700	18560	19310
57.06	6410	14180	15700	18560	18680
62.11	6380	14130	15670	18620	18530
67.26	6430	14090	15670	18530	18110
72.26	6360	14110	15650	18550	17850
77.36	6385	14110	15650	18640	17830
82.45	6370	14140	15680	18670	17890
87.58	6310	14110	15710	18660	18090
92.67	6340	14100	15710	18650	17330
97.72	6325	14090	15700	18660	17070
102.8	6360	14070	15680	18660	16810
107.9	6320	14090	15680	18640	15950
113	6310	14090	15660	18640	15620
118	6320	14100	15670	18640	15910
123.2	6275	14150	15680	18620	15800
128.2	6340	14160	15710	18390	16240
133.3	6305	14150	15710	18170	16350
138.4	6340	14090	15730	17830	15460

Run no	91A	91B	91C	91D	91E
143.5	6310	14090	15710	17710	13280
148.6	6340	14110	15700	17690	11930
153.7	6295	14110	15710	17970	10560
158.7	6320	14100	15710	18120	9150
163.8	6300	14130	15720	18250	7700
168.9	6230	14120	15730	18190	6680
174	6295	14110	15740	18080	6340
179.1	6275	14110	15750	18080	6010
184.2	6280	14180	15740	18040	6285
189.2	6295	14200	15730	17930	5775
194.3	6260	14230	15690	17760	5340
199.4	6265	14200	15690	17630	4910
204.5	6250	14200	15690	17730	4670
209.6	6260	14190	15700	17660	4220
214.7	6240	14190	15710	17560	4005
219.7	6235	14180	15770	17500	3860
224.8	6290	14150	15770	17280	3600
229.9	6210	14170	15730	17120	3440
235	6270	14180	15730	17070	3340
240.1	6240	14240	15730	17090	3920
245.2	6230	14230	15720	17020	3910
250.2	6230	14190	15730	16950	3780
255.3	6215	14170	15760	16730	3525
260.4	6240	14200	15770	17850	3245
265.5	6210	14200	15770	18100	2890
270.6	6280	14210	15740	18040	2880
275.7	6220	14240	15730	18010	3150
280.8	6190	14250	15720	17950	3150
285.8	6240	14250	15720	18140	2940
291	6220	14200	15700	18180	2750
296	6210	14200	15720	17780	2790
301.1	6245			17680	2780

Run no	91F	92A	92B	92C
t(sec)	M(μNm)	M(μNm	M(μNm	M(μNm
1.125	12760	16960	21120	12760
6.203	5070	20310	22880	5070
11.31	4360	19580	17620	4360
16.37	4150	18380	18860	4150
21.45	3810	17630	15650	3810
26.58	3875	17110	10460	3875
31.61	3445	17180	8480	3445
36.69	3200	20560	7820	3200
41.81	3200	18800	6560	3200
46.87	2940	19940	5890	2940
52	2910	18640	5120	2910
57.06	2670	17790	5080	2670
62.11	2510	17110	4230	2510
67.26	2250	16740	3730	2250
72.26	2160	19520	3800	2160
77.36	2120	19230	3620	2120
82.45	2160	17890	2370	2160
87.58	2370	17040	2010	2370
92.67	2675	16450	1810	2675
97.72	2925	15970	1725	2925
102.8	3050	16160	1720	3050
107.9	3040	19670	1610	3040
113	3180	17290	1600	3180
118	3380	16470	2400	3380
123.2	3790	19690	2610	3790
128.2	5000	18500	2770	5000
133.3	5795	16300	3210	5795
138.4	5530	15230	2845	5530

Cont	91F	92A	92B	92C
t(sec)	M(µNm)	M(µNm	M(µNm	M(µNm
143.5	5100	16220	2590	5100
148.6	4760	19980	2370	4760
153.7	4130	17400	2455	4130
158.7	3680	18580	2480	3680
163.8	3590	16270	2955	3590
168.9	3490	18110	1450	3490
174	3570	15960	1340	3570
179.1	3460	15270	1280	3460
184.2	3900	14190	1270	3900
189.2	3850	13280	1300	3850
194.3	3420	19260	1230	3420
199.4	3370	20550	2570	3370
204.5	3490	17360	2250	3490
209.6	3320	15910	2570	3320
214.7	3360	14700	2660	3360
219.7	3190	13640	2250	3190
224.8	3210	12820	1025	3210
229.9	3505	15540	2820	3505
235	3490	15250	1020	3490
240.1	3310	19460	1420	3310
245.2	3580	17590	1250	3580
250.2	3420	19710	1450	3420
255.3	3150	17250	1740	3150
260.4	2980	16980	1210	2980
265.5	2880	16770	2330	2880
270.6	2680	17110	1320	2680
275.7	2810	17730	1190	2810
280.8	2550	15200	3120	2550
285.8	2540	17990	1020	2540
291	2660	16170	1350	2660
296	2315	14240	1200	2315
301.1		13190	1400	